Hülse, D

# Effect of ocean euxinia on the efficiency of the biological carbon pump and its feedbacks on global biogeochemical cycles and climate during OAE2

**Dominik Hülse**

"A dissertation submitted to the University of Bristol in accordance with the requirements of the degree of Master of Science by advanced study in "Climate Change Science and Policy" in the Faculty of Science".

School of Geographical Sciences, September 12, 2013

Word count: 11,812

**Abstract**

The Cenomanian-Turonian oceanic anoxic event (OAE2) is characterised by severe disturbances in the global carbon, oxygen and sulfur cycles of the ocean. In this "greenhouse" climate with extreme atmospheric $CO_2$ concentrations, there were episodes of oxygen depletion in the deep ocean associated with the occurrence of hydrogen sulfide ($H_2S$) in the photic zone and enhanced organic carbon burial in sediments (black shale formation). Over the past decades a new mechanism has been increasingly invoked to explain the increased carbon burial under these extreme environmental conditions - sulphurization. Sulphurization is a process process whereby hydrogen sulfide reacts with organic matter to form new molecules that are more resistant to bacterial degradation. Various studies indicate that organic matter sulphurization under euxinic environmental conditions could be a key mechanism for black shale formation and an important emergency instrument for Earth's recovery from these extreme climate events. In this study, I conducted a series of numerical experiments to analyse the impacts of organic matter sulphurization on global biogeochemical cycles in association with OAE2. The model employed is an Earth System model of intermediate complexity (GENIE) which represents the main ocean dynamics and biogeochemistry of the Cretaceous climate and successfully reproduces patterns of bottom water anoxia and photic zone euxinia for before and during OAE2. The results suggest that sulphurization of organic matter has the potential to be an important emergency recovery mechanism from the "greenhouse" world of OAE2 and that it is also important for the enhanced sequestration of organic carbon in marine sediments. In order to quantify the importance of OM sulphurization for the generation of black shales we implemented a new numerical representation of the sediments which includes a mechanistic description of organic carbon preservation. The new model is successfully tested for different bottom water oxygen concentrations and organic matter compositions.

# Acknowledgements

I would like to thank my two Supervisors Sandra Arndt and Andy Ridgwell for giving me the opportunity to work on such an interesting topic, for their great scientific support and especially for taking me out for drinks when I needed it. I definitely owe Nicolas Goossen from the Université Libre de Bruxelles a couple of beers with whom we implemented the Sediment Model and who helped with sediment questions. Also a big "Thank You" to all the helpful members of BRIDGE which I constantly bothered with annoying questions (especially to Fanny Monteiro and Sarah Greene) and to the girls from the School Office. Finally thanks to Alexander for introducing me to the power of Shell scripting and for hosting me when various stomach bugs entered my house.

**Author's declaration**

I declare that the work in this dissertation was carried out in accordance with the requirements of the University's Regulations and Code of Practice for Taught Postgraduate Programmes and that it has not been submitted for any other academic award. Except where indicated by specific reference in the text, this work is my own work. Work done in collaboration with, or with the assistance of others, is indicated as such. I have identified all material in this dissertation which is not my own work through appropriate referencing and acknowledgement. Where I have quoted from the work of others, I have included the source in the references/bibliography. Any views expressed in the dissertation are those of the author.

SIGNED: ..... DATE: .....

(Signature of student)

# Contents

# List of Figures

# List of Tables

# 1 Introduction

## 1.1 The Global Carbon cycle and Climate

Accepting the Gaia theory (i.e. considering our Planet as a living System, Lovelock (2003)) means attributing particular functions to our Earth System for self-regulating its physical or "physiological" properties or in other words its climate system. A major role in this context plays the global carbon cycle (Falkowski et al., 2000) (Figure 1.1). It has long been recognized that atmospheric $CO_2$ concentrations and the average surface temperature are highly correlated (Hansen et al., 1981; Mitchell et al., 1995). Carbon dioxide is continuously exchanged between atmosphere, ocean, terrestrial and sedimental ecosystems and the rate of oceanic and terrestrial absorption and emission determines the overall change of atmospheric $CO_2$. Especially the oceanic carbon reservoir is of great importance as it is the largest pool in the short term carbon cycle (e.g about 60 times larger than the atmospheric reservoir (compare Figure 1.1 and (Brovkin et al., 2002; Solomon et al., 2007))). The ocean is already a sink for around 30% of all anthropogenic $CO_2$ emissions (Sabine et al., 2004) and has the long-term potential to absorb about 70% of all the $CO_2$ released from fossil fuel burning (Archer et al., 1997). Additionally the climate sysytem has shown to be highly sensitive to the chemical partitioning of carbon in the ocean (Goodwin et al., 2009) (nowadays even more as in the last 400 million years) which adds another degree of complexity. The relatively constraint domain of atmospheric $CO_2$ during the last glacial-interglacial cycles suggests strong feedbacks within the climate system defining the strengths of the different reservoirs as carbon sinks (Sigman and Boyle, 2000). Yet, rapid anthropogenic greenhouse gas emissions (such as $CO_2$ and $CH_4$) since the Industrial Revolution have changed the carbon cycle significantly (compare red fluxes and pool sizes in Figure 1.1) and ice core records show that the current atmospheric concentrations of $CO_2$ and $CH_4$ are unprecedented within the last 420,000 years (Petit et al., 1999; Crowley, 2000). Therefore finding analoga in the distant geological past with similar massive releases of greenhouse gases to the atmosphere and analyzing and understanding how the Earth System recovered from these "greenhouse" climates is crucial if we want to make reasonable predictions for how the climate system will respond to current extreme variations (Falkowski et al., 2000).

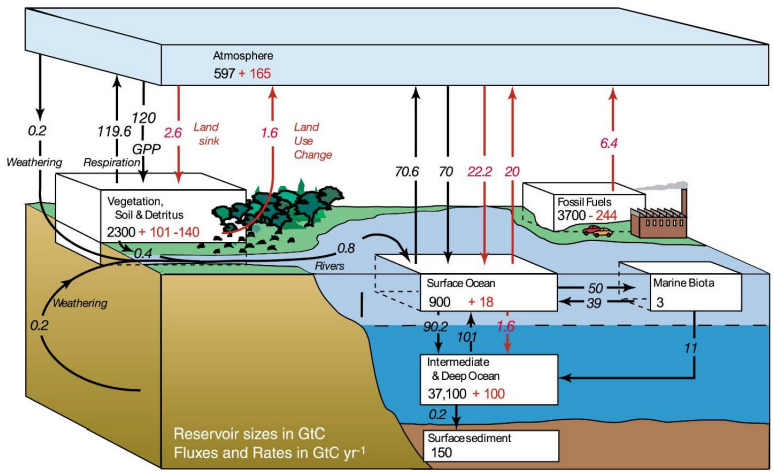


Figure 1.1: The global short term carbon cycle for the 1990s, showing the main annual fluxes in GtC $yr^{-1}$: pre-industrial 'natural' fluxes in black and 'anthropogenic' fluxes in red. Atmospheric carbon content and all cumulative fluxes since 1750 are as of end 1994. (Adapted from (Solomon et al., 2007).)

In general, the Earth System has two (emergency) modes of recovery in order to "heal" itself from extreme global temperatures and elevated atmospheric $CO_2$. Firstly, silicate rock weathering on land is a powerful regulatory mechanism which is enhanced in a warmer and wetter climate driven by higher atmospheric $CO_2$ concentrations. Silicate weathering controls climate by consuming atmospheric $CO_2$, which gets eventually buried as carbonates ($CaCO_3$) in ocean sediments (Kump et al., 2000; Ridgwell and Zeebe, 2005). This represents a negative feedback loop (Berner, 1999) and helps to regulate the atmospheric $CO_2$ concentrations over hundreds of thousands of years (Berner and Caldeira, 1997). These long-term processes have been comparably well studied and are often included in long-term fate studies of anthropogenic $CO_2$ released to the atmosphere (e.g. Ridgwell and Hargreaves (2007)).

A second, more direct and also very efficient way of removing $CO_2$ from the atmosphere is by burying carbon in oceanic sediments in the form of organic matter (OM). The magnitude of this carbon sink is strongly correlated with the efficiency and functioning of the so-called "biological carbon pump" (Volk and Hoffert, 1985) (see Section 1.2). This complex set of interrelated processes describes the vertical transport of OM from surface waters to the sediments and is still not fully understood Sarmiento et al. (2004); Ridgwell (2011).

## 1.2 The biological carbon pump

Figure 1.2 gives a schematic of the main processes that constitute the biological pump in the ocean. In general it includes four interrelated biogeochemical and physical components: primary production, export of organic carbon from surface waters, flux to depth and sedimentation. The pump begins in the euphotic (or epipelagic) zone ($\sim$ 0-200 m) where carbon dioxide enters the surface ocean and immediately reacts with water to form carbonic acid ($H_2CO_3$), bicarbonate ($HCO_3^-$) and carbonate ($CO_3^{2-}$). Carbon dioxide, carbonic acid, bicarbonate and carbonate are collectively known as dissolved inorganic carbon (DIC): $[DIC = (CO_2(aq) + H_2CO_3) + HCO_3^- + CO_3^{2-}]$. In the sunlit surface ocean, primary production (PP) converts large amounts of DIC through photosynthesis to $O_2$, particulate organic carbon (POC) and particulate inorganic carbon (PIC). In context of today's global carbon cycle, the marine biosphere is responsible for roughly half of the annual photosynthetic absorption of $CO_2$ from the atmosphere (Field et al., 1998). The majority of the POC is directly degraded by metabolic processes in the surface ocean into DIC, dissolved organic carbon (DOC) and nutrients. The remaining POC (about 15-20% (Honjo et al., 2008)) escapes degradation and is transferred, together with PIC and DOC, below the euphotic zone, often called the export production of carbon (EP). Further heterothrophic degradation occurs at mesopelagic depths ($\sim$ 200-1000 m), predominantly through the consumption of heterotrophs and overall just a small fraction of POC resulting from PP reaches the deep ocean and is ultimately buried in the sediments.

In today's, well oxidized ocean, only a small fraction of the organic matter produced in the surface layer escapes heterothrophic degradation in the ocean and the sediments and is ultimately buried and preserved in the deep sediment (e.g. (Emerson and Hedges, 1988; Middelburg and Meysman, 2007)). However, it has been shown that certain environmental conditions greatly influence the preservation of organic carbon in the ocean and the sediments (e.g. (Middelburg et al., 1993; Arndt et al., 2013b)) and that the relative fraction of the deposited organic carbon that is ultimately buried can range from 0 to 100 % (Canfield, 1994). But which factors control the degradation and preservation of organic matter in the ocean and the sediments and, thus, the efficiency of the biological carbon pump?

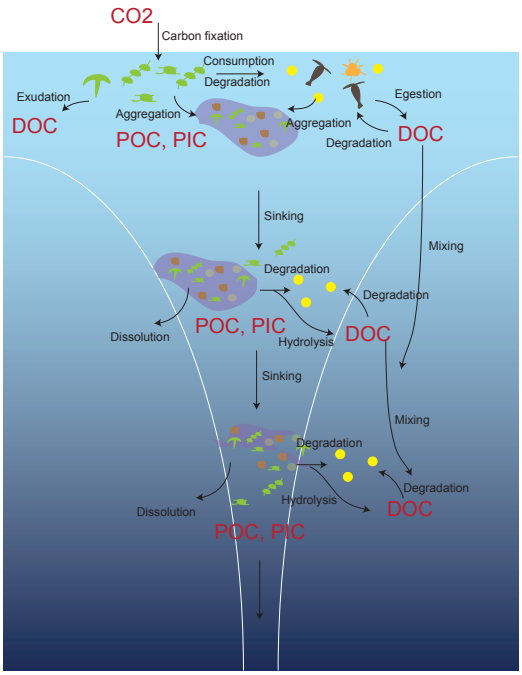


Figure 1.2: Schematic of the main processes constituting the ocean's biological pump.

## 1.3 Controls on Organic matter degradation/preservation

Depending upon depths where the sinking organic carbon is regenerated, the ocean's interior and the marine sediments are a sink for $CO_2$ for months to thousands and millions of years. In general, the greater the depths where the POC is degraded, the longer it takes for the $CO_2$ to return to the atmospheric carbon cycle (compare Figure 1.3a). Without this carbon pump, today's $CO_2$ concentration in the atmosphere would be almost twice as high as current levels (Sarmiento and Toggweiler, 1984). But, as already mentioned, these numbers just hold for the modern ocean and the biological pump and in particular its organic part has been shown to work more or less efficient in the Past (Sigman and Haug, 2003).

Table 1: Mass of carbon (C, in grams) in todays major exogenic Earth reservoirs. (Adapted from (Mackenzie et al., 2004).)

| | |
|---|---|
| Sediments | $7.78 \times 10^{22}$ |
| Carbonates | $6.53 \times 10^{22}$ |
| Organic matter | $1.25 \times 10^{22}$ |
| Ocean | $3.85 \times 10^{19}$ |
| Atmosphere | $7.85 \times 10^{17}$ |

The Earth's sediments store more than $10^7$ gigatonnes of organic carbon of marine origin (Mackenzie et al., 1993) and are therefore essential for understanding the global carbon cycle and climate Berner et al. (1989); Siegenthaler and Sarmiento (1993); Archer (1994); Mackenzie et al. (2004); Ridgwell and Zeebe (2005). Among the exogenic reservoirs (i.e. sediments, hydrosphere, biosphere and atmosphere), the sediments are by far the largest carbon pool, involving carbonates and organic matter (Mackenzie et al., 2004) (compare Table 1). Global degradation of organic matter in the ocean

and the sediment is donor controlled and includes among others the following major contributions: (1) photosynthetically produced OM in the sunlit euphotic zone (the main constituent); (2) riverine transport of dissolved and particulate OM derived from terrestrial weathering and/or photosynthesis; and (3) chemoautotrophically produced OM (Figure 1.3b). But depart from that, degradation of OM is also affected by various other chemical, biological and physical processes (Arndt et al., 2013b), as summarized in Figure 1.4.

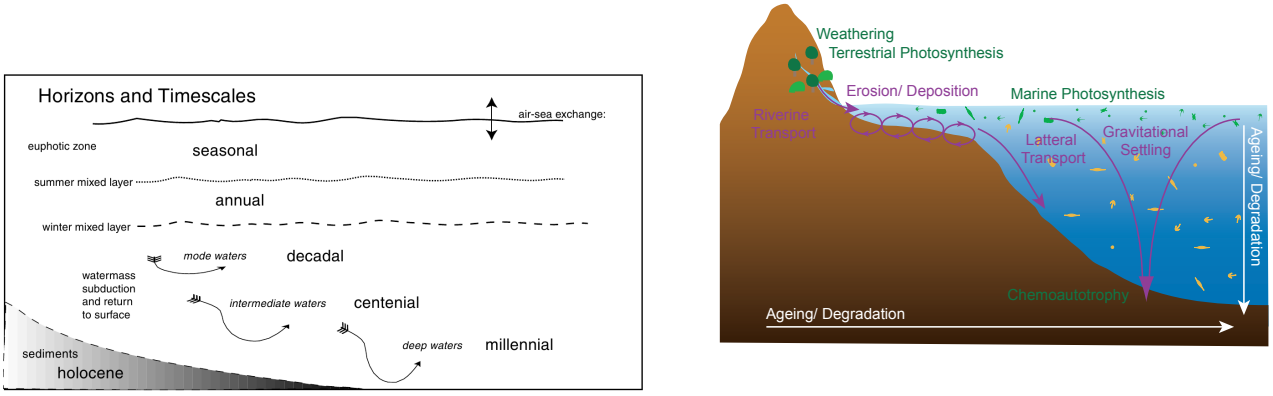


(a) (b)

Figure 1.3: **(a)** Depth horizons in the ocean, important for the remove of carbon from contact with the atmosphere an a wide range of timescales. In general, the greater the depths at which sinking organic carbon is degraded, the longer it takes for the $CO_2$ to return to the atmospheric carbon cycle. Adapted from Boyd and Trull (2007).
**(b):** Sources (green), transport (purple) and transformation (white) processes that determine the supply of organic matter to marine sediments. (From Arndt et al. (2013b))

It is a widely accepted fact that feedback mechanisms acting between the ocean, land and atmosphere have come to limit the aggregation of organic carbon in sediments worldwide (Reimers, 1998). In order to understand these interrelations I need to introduce some basic concepts of organic matter degradation. In general, organisms obtain energy by degradation of OM, a process during which an electron gets transferred from an electron donor (e.g. organic matter) to an electron acceptor (e.g. oxygen, nitrate, iron, manganese, sulfate, or OM itself in the case of methane fermentation) (Martens et al., 1992; Sarmiento and Gruber, 2006). See Table 2 for a summary of the reactions and the energy released due to the different electron acceptors. The general understanding is, that these reactions do not occur simultaneously, but rather tend to follow the progression from higher to lower energy gain (Froelich et al., 1979) (compare Table 2). Figure 1.5 shows a typical vertical profile of different chemical species in marine sediments, which also mirrors the sequencing of the degradation reactions. Aerobic respiration takes place in the first part of the sediments as indicated by the decrease of $O_2$ concentration in this area. As aerobic degradation of OM produces nitrate ($NO_3^-$) its concentration increases in the first part of the sediments and it decreases as denitrification takes over. Additionally, when oxygen runs out, $MnO_2$, the insoluble form of manganese gets reduced to form soluble $Mn(OH)_2$ which is then used as an oxidant and therefore dissolved $Mn^{2+}$ is produced in the sediment column. In a similar way one can explain the appearance of ammonia ($NH_3$, the product of iron reduction), hydrogen sulfide ($H_2S$ or $S^{2-}$, resulting from sulfate reduction) and methane ($CH_4$, coming from methanogenesis) (e.g. Hulth et al., 1999; Sarmiento and Gruber, 2006). Furthermore, vertical profiles

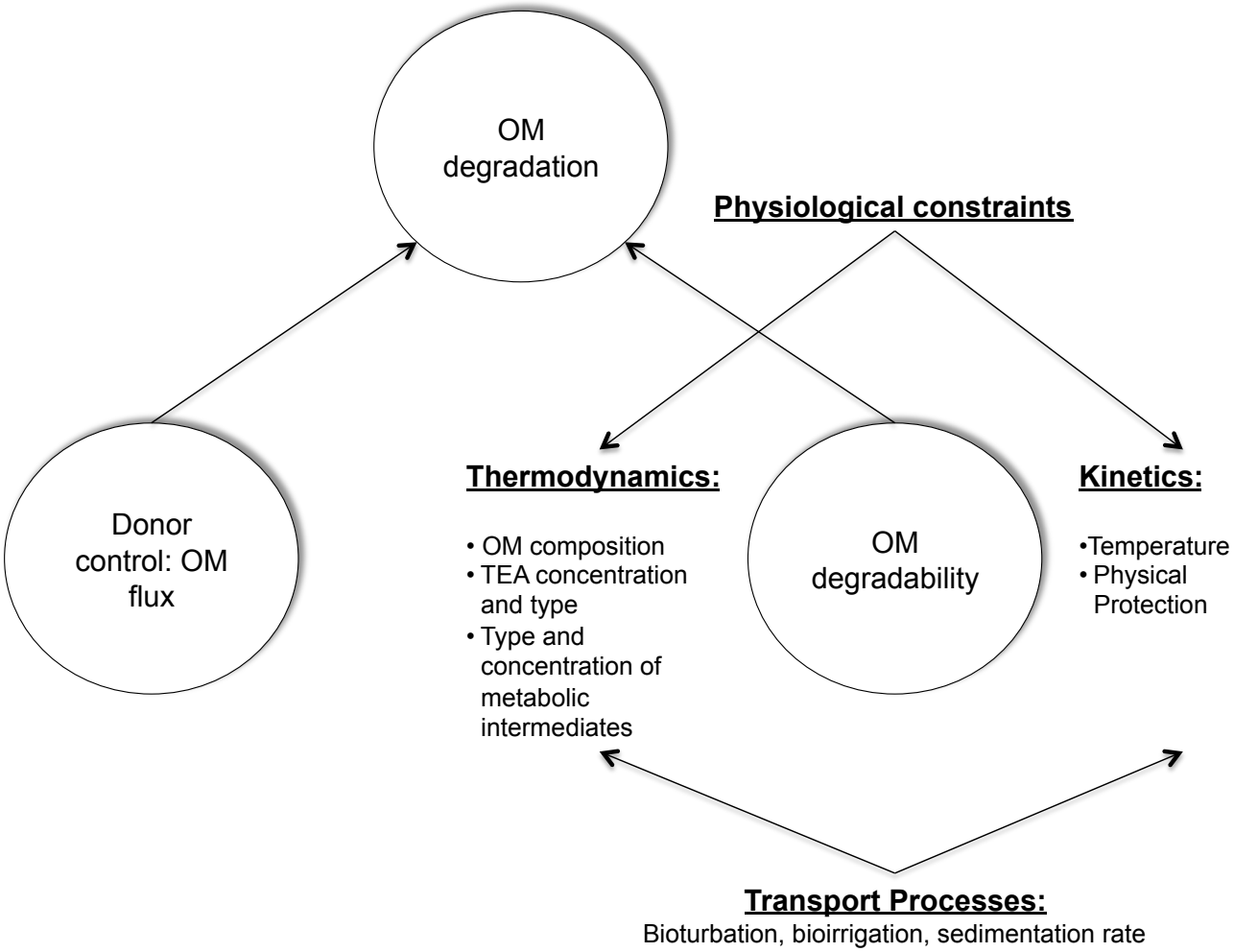


Figure 1.4: Schematic illustration of the main controls of organic matter degradation in marine sediments. The degradation of organic matter in marine sediments is sustained by the flux of organic matter to the sediment-water interface and, therefore, donor controlled. During burial, the consumption of this flux is determined by the degradability of organic matter in the sediment. It is thus thermodynamically and/or kinetically controlled through the different abilities of the physiological groups that compete for the common substrate. In addition, transport processes, such as bioturbation, bioirrigation and sedimentation rate exert an indirect control on the degradation reaction mainly through their influence on organic matter, terminal electron acceptor (TEA) and metabolic intermediate concentrations. Copied from Arndt et al. (2013b).

of sulfide and ammonia show a decrease above the sulfate reduction zone (Hulth et al., 1999) (or above the iron reduction zone respectively (Reimers et al., 1992), due to a variety of oxidation reactions. Therefore, as argued by Canfield (1993), the overall water to sediment flux is a good proxy for the total carbon oxidation rate. Table 2 also summarizes estimates for the fraction each degradation pathway accounts for in terms of total organic carbon degradation. This highlights that oxygen is by far the most important oxidant (65%), followed by sulfate (17.9%), the process of methane fermentation (9.8%) and nitrate (6.5%). Note, that these values are for todays, well-oxidized ocean, meaning that anaerobic respiration is even more important for the anoxic/euxinic conditions during OAEs (compare Section 1.4).

Table 2: Organic matter degradation reactions, its free energy changes and their contribution to global oxidation rate. (Adapted from (Sarmiento and Gruber, 2006).)

| Reaction | Oxidant | Free Energy Change kJ $mol^{-1}$ of sucrose | % of global organic C oxidation |
|---|---|---|---|
| Aerobic respiration | $O_2$ | -476 | 65.0% |
| Denitrification | $HNO_3$ | -452 | 6.5% |
| Manganese reduction | $MnO_2$ | -388 | $\sim$ 0.6% |
| Iron reduction | $FeO_3$ | -187 | $\sim$ 0.3% |
| Sulfate reduction | $H_2SO_4$ | -82 | 17.9% |
| Methane fermentation (methanogenesis) | $H_2O$ | -71 | 9.8% |

Many studies suggested, that the time OM is exposed to oxygen in the sediments is one important factor for how much organic carbon gets buried (e.g. Demaison and Moore, 1980; Paropkari et al., 1992; Hartnett et al., 1998). Which makes sense, considering the lower free energy gains through anaerobic degradation ((LaRowe and Van Cappellen, 2011) and as discussed above), the need for more complex bacterial consortia, reduced bioturbation and grazing or the presence of non-hydrolyzable substrates that resist fermentative breakdown, in anoxic environments (Canfield, 1994; Hedges and Keil, 1995). But reality is by far more complex, which can already be seen as the relationship of oxygen exposure and the efficiency of organic carbon burial is clearly nonlinear (Hartnett et al., 1998). One approach to explain this is that specific classes of organic substrates are limited specifically to aerobic bacterial degradation (Hartnett et al., 1998) and that the degradation of these compounds eventually limit carbon burial. But as Reimers (1998) argue, this might just be true for the well oxidized and/or bioturbated environments but once oxygen exposure gets reduced the secondary electron acceptors (i.e. nitrate, iron, manganese, sulfate and the organic compounds reduced via methanogenesis) are becoming more important for preservation. Additionally, a number of studies showed in anoxic surface sediments similar OM degradation rates as under oxic conditions (Henrichs and Reeburgh, 1987). This may help to explain observations that degradation efficiency is not constant (Canfield and Thamdrup, 2005) and the great variability in burial efficiency (Arthur et al., 1985; Canfield, 1994; Hartnett et al., 1998; Blair and Aller, 2012). Therefore, it is very likely that two benthic areas show very different burial efficiencies even though they receive the same amount of annual organic carbon flux and exhibit the same bottom-water oxygen concentration (Reimers, 1998).

As stated by Werne et al. (2008) “sulphurization of organic matter is a globally significant biogeochemical process” which affects the resistance of OM to bacterial mineralization and therefore en-

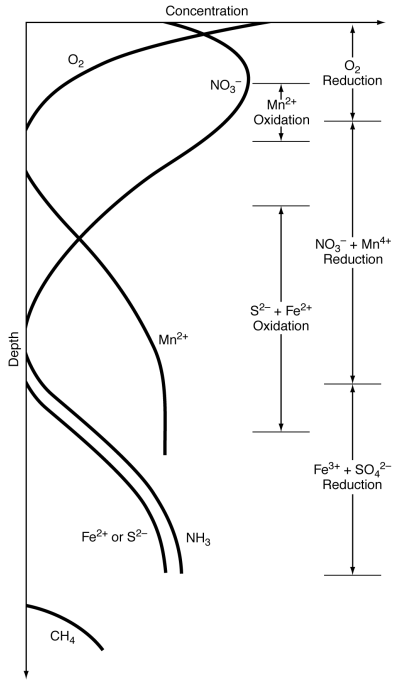


Figure 1.5: Schematic vertical profiles of reactants and products of degradation reactions in sediments, reduction zones where the various reactions of Table 2 occur and zones where the soluble products of reduction reactions are reoxidized as they diffuse upwards. Adapted from Sarmiento and Gruber (2006).

hances the preservation or organic carbon. During sulphurization, reduced inorganic sulphur species (e.g. $H_2S$) react with organic matter through their functional groups, resulting in the formation of a "sulphur cross-linked insoluble macromolecular network of carbohydrate skeletons" (Sinninghe Damsté et al., 1989a; Sinninghe Damsté and De Leeuw, 1990; Werne et al., 2000) which is less prone to bacterial degradation (Toth and Lerman, 1977; Sinninghe Damsté et al., 1989b; Sinninghe Damsté and Köster, 1998; Moodley et al., 2005).

Especially OAEs (see Section 1.4) are characterized by enhanced sequestration of organic carbon indicated by thick layers of laminated organic carbon-rich black-shales (e.g. Stein et al., 1986). Hence, these significant carbon depositions highlight the central importance of efficient organic carbon burial for the Earth's recovery mode from these extreme climate events. Although our general understanding of carbon burial has been advanced through the analysis of black shales (Arthur et al., 1987; Meyers et al., 2001), via diagenetic modelling (Berner, 1980; Middelburg, 1989; Boudreau and Ruddick, 1991; Tromp et al., 1995; Wallmann et al., 2006) as well as from modern day observations (Emerson and Hedges, 1988; Tyson and Pearson, 1991), and primary production, sedimentation/dilution and microbial degradation have been identified as the major drivers for carbon burial in sediments, the relative importance of each of these processes, especially under extreme conditions in the distant geological past, is difficult to asses (Johnson Ibach, 1982; Pedersen and Calvert, 1990; Sageman et al., 2003; Burdige, 2007). As already mentioned, enhanced sequestration of OM in sediments is traditionally related to water column anoxia or an anoxic depositional environment (Demaison and Moore, 1980; Emerson, 1985) but several newer studies showed that a direct, unambiguous relationship between both parameters does not exist (Henrichs and Reeburgh, 1987; Tyson, 2001). Over the past decades, organic matter sulphurization has been more and more proposed to explain increased burial under

anoxic and/or euxinic conditions (Sinninghe Damsté and Köster, 1998; Kolonic et al., 2002; Hebting et al., 2006; Arndt et al., 2009) as prevailing during OAE2. Therefore investigating the patterns of organic carbon burial under the anoxic and euxinic ocean environments during OAEs could shed some light on the importance on this process.

## 1.4 Oceanic anoxic events (OAE)

Oceanic anoxic events (OAEs) represent severe disturbances in the global and, in particular, the ocean carbon cycle and were common during the Cretaceous period (Schlanger et al., 1976; de Graciansky et al., 1984; Schlanger et al., 1987; Jenkyns, 2010).

In the "greenhouse world" of the Cenomanian-Turonian boundary event (OAE2, Bonarelli event, $\sim 93.5\ Ma$) dysoxic or even anoxic bottom waters where widespread on a global scale (de Graciansky et al., 1984; Sarmiento et al., 1988; Arthur and Sageman, 1994) and reconstructions of atmospheric $CO_2$ show concentrations at its onset in the range of 500-3300 ppmv (Bice et al., 2006; Damsté et al., 2010). Furthermore, reconstructions of sea-surface temperature (SST) suggest strong warming, reaching $33 - 42°$ in mid- and tropical latitudes (Bice et al., 2006; Forster et al., 2007) and more than 20° in Arctic regions (Jenkyns et al., 2004) (compare Figure 2.2c for the predicted SST using GENIE). In addition an increased accumulation of organic carbon-rich black shales (Stein et al., 1986) and a positive excursion in the $\delta^{13}$ record is observed for this event (Schlanger et al., 1976; Scholle and Arthur, 1980; Sinninghe Damsté and Köster, 1998). Although OAEs have been described more than 30 years ago (Schlanger et al., 1976), the mechanisms triggering widespread ocean anoxia and enhanced organic carbon burial are still topics of intense debate (Arthur and Sageman, 1994; Meyer and Kump, 2008; Jenkyns, 2010). In the past, two scenarios are commonly considered: Either a decreased oxygen supply to the deeper ocean due to slower ocean circulation (Erbacher et al., 2001) leading to enhanced organic carbon preservation (Demaison and Moore, 1980; Schlanger et al., 1987; Arthur and Sageman, 1994); an increased oxygen demand due to an elevated surface productivity (Sarmiento et al., 1988; Pedersen and Calvert, 1990; Handoh and Lenton, 2003; Monteiro et al., 2012); or a combination of both (Erbacher et al., 2001; Wilson and Norris, 2001). Increasing temperatures, caused by massive volcanism (Kuroda et al., 2007) are believed to have increased the potential of ocean anoxia (Wagner et al., 2007) due to a decrease in oxygen solubility in seawater. On the other hand, warmer temperatures could also have influenced the productivity of marine phytoplankton in a positive way (Eppley, 1985). Recently it has been suggested that increased phosphate ($PO_4^{3-}$) inputs from intensified continental weathering could have played a key role in stimulating primary productivity Handoh and Lenton (2003); Jenkyns (2010); Ozaki et al. (2011); Pogge von Strandmann et al. (2013). This idea has been tested and verified by Monteiro et al. (2012) using the 3-D Earth System model GENIE.

But also other nutrient cycles experienced major disturbances during OAE2 and might have been important for the enhanced organic carbon burial. Various studies found that the black shales formed during this event (and also other OAEs) contain biomarkers derived from the green sulfur bacteria, a biomarker characteristic for photic zone euxinia, as it requires both light and free hydrogen sulfide ($H_2S$) (Sinninghe Damsté and Köster, 1998; Kuypers et al., 2002). And, as described in Section 1.3, it is well known that euxinic conditions significantly increase the resistance of organic matter to microbial degradation.

But how exactly did the Earth recover from such extreme conditions? How important are the

different processes? And might humans even force a return to Cretaceous climate as Hay concluded to be *"likely unless humanity can organize an effective campaign to stop CO2 emissions to the atmosphere and remove some of the excess CO2 already introduced."* (Hay, 2011)

## 1.5 General structure

Having all these complex and interrelated processes responsible for the degradation of OM in the ocean and marine sediments in mind and considering its feedbacks with the global carbon cycle and climate due to the immense size of carbon stored in the sediments, a mechanistic description of organic carbon preservation in marine sediments and its coupling to a 3-D Earth System model in order to study the global long-term sedimentary carbon sink and its impacts on the Earth climate system is urgently needed to advance our understanding of past and future climate change. Even though various studies highlight the potential importance of OM sulphurization for the formation of ancient, organic-carbon rich sediments (Sinninghe Damsté et al., 1998; Kolonic et al., 2002; Arndt et al., 2009) and for regulating atmospheric $CO_2$ concentrations and climate, this idea still lacks a quantitative analysis and needs to be tested. This can be attributed to the fact that a fully coupled 3-D atmosphere-ocean-sediment model representation, capable to reproduce the widespread oceanic euxinia, quantify the enhanced benthic carbon burial and calculate its impact on atmospheric $CO_2$ concentrations currently does not exist because of the high computational costs of simulating all essential redox reactions controlling carbon burial and sediment-water interface fluxes of various chemical species.

Therefore, I investigate the hypothesis, that under extreme environmental conditions, **sulphurization could be an important emergency recovery mechanism** from a "greenhouse" world and I start analyzing its significants and feedbacks on global biogeochemical cycles during OAE2. In order to do so, I utilize the Earth System model GENIE (Ridgwell et al., 2007), which, as a model of Intermediate Complexity, is well designed for this investigation because it can be run for hundreds of thousand years needed to equilibrate the ocean biogeochemistry, and it is able to represent the main ocean characteristics and biogeochemical cycles of the Late Cretaceous (more information on GENIE in Section 2.1). I implemented a representation for OM sulphurization in the GENIE model (see Section 2.1.1) and, together with colleagues, developed a new diagenetic model that includes a mechanistic description of organic carbon preservation in marine sediments (compare Section 2.2). Using these new tools, I analyze the global biogeochemical impacts of OM sulphurization with the new GENIE version in a representation without sediments. Additionally, I test the new stand-alone benthic model for different bottom water oxygen concentrations and organic matter composition and investigate the magnitude of carbon burial and the impacts on the sediment profiles and sediment-water interface flux for various species.

The dissertation is laid out as follows: Section 2 provides a description of the Earth System model GENIE employed for this study and reports on the modifications I made in order to model OM sulphurization. Later in Section 2, our new benthic model is described. Section 3 presents and discusses the results of the GENIE experiments and reports on the sediment model evaluation. In Section 4 I give an outlook on further development paths before Section 5 concludes this dissertation, summarising the main results.

# 2 Model Description

To quantitatively test the hypotheses discussed in Section 1, computer models are powerful tools because they resolve the underlying process interplay and allow a direct comparison with the geological record (Randall et al., 2007). Especially during the last decades a number of coupled, multi-dimensional climate models have emerged and many modelling advances have occurred due to the increasing computer power (Solomon et al., 2007, Chap. 8). But anyway, the Earth System and specifically the carbon cycle is driven by such diverse, coupled biogeochemical processes which are still not fully understood that a computer model will never be a perfect representation of the reality and it's important to be aware of their limitations (Stone and Risbey, 1990; Räisänen, 2007; Christensen et al., 2007). For further improvement, the functionalities of the Earth System need to be parameterized based on a more mechanistic understanding of the underlying processes. Likewise, in order to help answering the question *"World where are you heading?"* (Zeebe, 2011) we need to test them against comparable extreme scenarios in the distant past as *"state-of-the-art climate models are largely untested against actual occurrences of abrupt change"* (Valdes, 2011) and therefore might not be able to simulate sudden climate change when a so-called "tipping point" is crossed.

In order to help answering these questions, I explore the impact of widespread OM sulphurization on biogeochemical cycles and quantitatively assess if OM sulfurization could have been a climate cooling mechanisms during OAE2. Therefore, I use the Earth System model GENIE of intermediate complexity (2.1) and extend it with a representation for sulphurization of organic matter (2.1.1). Furthermore, to eventually include the important burial of organic carbon in marine sediments into GENIE we developed a new benthic model which is described in Section 2.2.

## 2.1 GENIE

A version of the "Grid ENabled Integrated Earth system model" (GENIE) (Ridgwell et al., 2007; Ridgwell and Hargreaves, 2007) is used to test the hypothesis. GENIE is a model of Intermediate Complexity and couples a frictional-geostrophic 3D-ocean model to the the fast energy-moisture balance 2D-atmosphere model "C-GOLDSTEIN" of Edwards and Marsh (2005). The 3-D ocean circulation based C-GOLDSTEIN model has been extended with the marine "BIOGEochemistry Model" (BIOGEM) (Ridgwell et al., 2007) and later with the "SEDiment GEochemistry Model" (SEDGEM) (Ridgwell and Hargreaves, 2007) to help explore the role of ocean biogeochemistry and marine sediments within the global carbon cycle and in regulating atmospheric $CO_2$ concentrations on multimillenial timescales. The conceptual relationship of BIOGEM and SEDGEM with the climate component of the GENIE Earth system model is illustrated in Figure 2.1.

The ocean model is implemented on a 36×36 equal-area horizontal grid and 16 z-coordinate levels in the vertical similar to GENIE-16 (e.g. in (Cao et al., 2009)). Here, the GENIE configuration for the Late Cretaceous is employed, using Cenomanian bathymetry and continental configuration as described in Monteiro et al. (2012) and shown in Figure 2.2a. Although GENIE represents the whole terrestrial-atmosphere-ocean(-sediment) carbon cycling it has been shown to simulate more than 1000 years per (2.4 GHz) CPU hour using a desktop PC (Ridgwell and Hargreaves, 2007). Such an efficient 3D Earth System Model is needed for my experiments as it takes about 10,000 years to equilibrate the ocean biogeochemistry. The employed GENIE version simulates the cycling of carbon, phosphorus, oxygen, and sulfur as described by Ridgwell et al. (2007). Despite its lower resolution, GENIE is

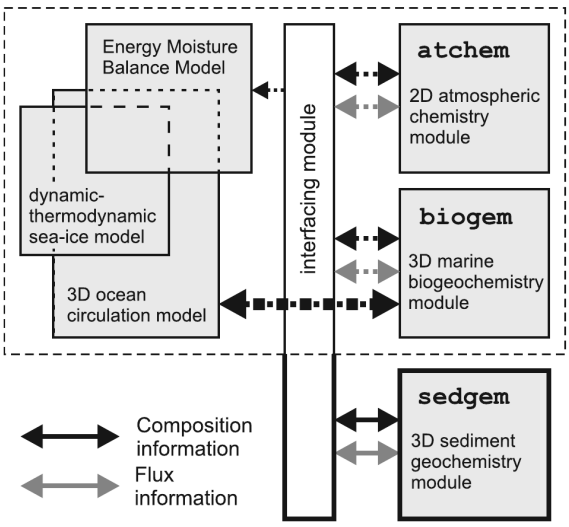


Figure 2.1: Schematic describing the relationship between the different model components comprising the GENIE model. Adapted from Ridgwell and Hargreaves (2007).

able to reproduce the main biogeochemical cycles and 3-D features of ocean dynamics of the Late Cretaceous such as ocean circulation and deep-water formation in the Southern Ocean and North Pacific (Poulsen et al., 2001; Trabucho-Alexandre et al., 2010). Although GENIE already provides a representation of the sediments (SEDGEM), this module is not appropriate for our analysis as it does not include burial of organic matter and the related redox reactions. Therefore, we implemented a new representation of the sediments more appropriate for my analysis (compare Section 2.2).

### 2.1.1 GENIE modification: Sulphurization of organic matter

GENIE simulates two classes of biodegradable particulate organic carbon (POC), a labile (L-POC) fraction with a shorter degradation length scale (about 589.94 m) and a more refractory fraction (R-POC) which does not degrade during sinking (length scale 1,000,000.0 m). POC transport in a specific water-column ($k$) is simulated by calculating the fractional remineralization in each layer ($kk+1$) and moving the particulate remainder to the layer below ($kk$). In order to simulate the impact of organic matter sulphurization when $H_2S$ is present in a certain grid-cell, we change the partitioning of L-POC and R-POC by converting a specific amount of labile to refractory POC. Therefore we first check weather there is labile POC left at depth $kk+1$ and if $H_2S$ is available in the grid-cell below. If so, and in case L-POC is the limiting species we transform all L-POC to R-POC and adjust the $H_2S$ concentration with the appropriate magnitude (assuming 1 mol $H_2S$ converts 1 mol POC). In case $H_2S$ is the limiting factor, we set the hydrogen sulfide concentration at depth $kk$ to zero and adjust the POC fractionation in an analog way. Figure 2.3 shows the Fortran code for this procedure.

### 2.1.2 Experiment setup

Different sets of numerical experiments are run to investigate the impact of organic sulphurization on the ocean redox state across OAE2, all set up with the Late Cretaceous bathymetry configuration as shown in Figure 2.2a and the reference experiments are simulated without organic matter sulphurization. The pre-OAE2 event experiments are set with modern oceanic phosphate concentration ($1 \times PO_4 = 2.159\ \mu molPkg^{-1}$) and twice the pre-industrial atmospheric $CO_2$ ($2 \times CO_2 = 556\ ppmv$).

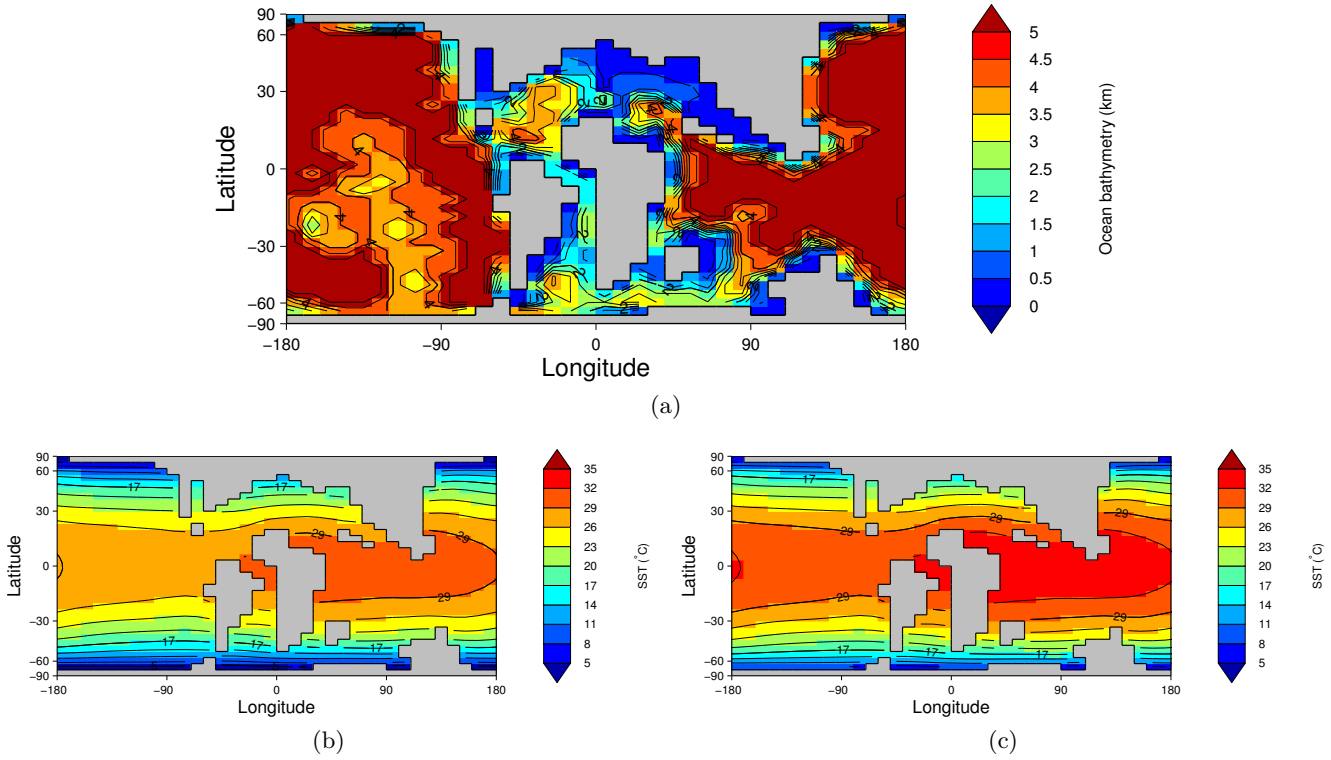


Figure 2.2: Model configuration for the Late Cretaceous. (a) GENIE ocean bathymetry for the Cenomanian rescaled from FOAM (Donnadieu et al., 2006). GENIE annual mean sea-surface temperature (SST) for before (b) and during (c) OAE2.

In the sensitivity experiments (SULPH-PRE, SULPH-PEAK) phosphate and $CO_2$ concentrations are prescribed accordingly and OM sulphurization is modelled as outlined under 2.1.1. Table 3 provides an overview of the described experiments which are run for 10 kyrs to steady state. The main experiments are run without a representation for the sediments and all particulate species are remineralized at the seafloor.

Table 3: Experiment setup for OM sulphurization.

| Exp-Name | Ocean phosphate concentration times pre-industrial | in $\mu molPkg^{-1}$ | Atmospheric $CO_2$ times modern | in ppmv | OM sulphurization |
|---|---|---|---|---|---|
| REF-PRE | $1 \times PO_4$ | 2.159 | $2 \times CO_2$ | 556 | NO |
| REF-PEAK | $2 \times PO_4$ | 4.318 | $4 \times CO_2$ | 1112 | NO |
| SULPH-PRE | $1 \times PO_4$ | 2.159 | $2 \times CO_2$ | 556 | YES |
| SULPH-PEAK | $2 \times PO_4$ | 4.318 | $4 \times CO_2$ | 1112 | YES |

```
! calculate change in partitioning between different POC fractions
l = is2l(is_POC_frac2)

!calculate L-POC in kk to compare magnitude
loc_LPOC_compare_kk = (1-loc_bio_part_TMP(l,kk+1))*loc_bio_part_TMP(is2l(is_POC),kk+1) &
                    & *loc_bio_part_POC_ratio*loc_bio_remin_layerratio
! Check H2S enabled
if (ocn_select(io_H2S)) then
   ! check is POC in grid-cell
   if (loc_bio_part_TMP(l,kk+1) > const_real_nullsmall) then
        ! check H2S in grid-cell
        if (dum_vocn%mk(io2l(io_H2S),kk) > const_real_nullsmall) then
            ! check still labile POC left to convert, i.e. loc_bio_part_TMP(l,kk) < 1
            if(1-loc_bio_part_TMP(l,kk+1) > const_real_nullsmall) then
                ! check whether H2S or labile POC is limiting
                if(dum_vocn%mk(io2l(io_H2S),kk) .LE. loc_LPOC_compare_kk) then
                    ! set H2S concentration to zero
                    loc_bio_remin(io2l(io_H2S),kk) = &
                        & loc_bio_remin(io2l(io_H2S),kk) - dum_vocn%mk(io2l(io_H2S),kk)
                    ! calculate new R-POC and L-POC concentration in kk
                    loc_RPOC = (1.0 - loc_bio_remin_POC_frac2)*loc_bio_part_TMP(l,kk+1) &
                              & *loc_bio_part_POC_ratio + dum_vocn%mk(io2l(io_H2S),kk)
                    loc_LPOC = (1.0 - loc_bio_remin_POC_frac1)*loc_bio_part_TMP(l,kk+1) &
                              * loc_bio_part_POC_ratio - dum_vocn%mk(io2l(io_H2S),kk)
                    loc_bio_part_TMP(l,kk) = loc_RPOC/(loc_RPOC + loc_LPOC)
                else    ! labile POC is limiting
                    loc_bio_part_TMP(l,kk) =  1.0   ! everything refractory
                    loc_bio_remin(io2l(io_H2S),kk) = &
                        & loc_bio_remin(io2l(io_H2S),kk) - loc_LPOC_compare_kk
                end if
            else    ! just refractory in kk=1
                loc_bio_part_TMP(l,kk) =  1.0
            end if
        else    ! NO HS2 -> normal change in partitioning
                loc_bio_part_TMP(l,kk) =  min(1.0,(1.0 - loc_bio_remin_POC_frac2)* &
                                          & loc_bio_part_TMP(l,kk+1)/loc_bio_part_POC_ratio)
        end if
   else     ! NO POC in grid-cell kk+1
        loc_bio_part_TMP(l,kk) = 0.0
   end if
else     ! OLD, NO H2S method
   if (loc_bio_part_TMP(l,kk+1) > const_real_nullsmall) then
        loc_bio_part_TMP(l,kk) =  &
        & (1.0 - loc_bio_remin_POC_frac2)*loc_bio_part_TMP(l,kk+1)/loc_bio_part_POC_ratio
   else
        loc_bio_part_TMP(l,kk) = 0.0
   end if
end if
```

Figure 2.3: Fortran code for Full-Switch OM sulphurization scenario as implemented in GENIE and described under 2.1.1.

## 2.2 SEDIMENT MODEL

Models for early diagenesis are generally based on one-dimensional advection-diffusion-reaction equations for solid and dissolved species in a porous media (Berner, 1980; Boudreau, 1997). The conservation equation explains biological, chemical and physical processes important for organic matter degradation in upper layers of marine sediments as well as secondary reactions describing the oxidation of the products OM mineralization. The general diagenetic equation is given by:

$$\frac{\partial \xi C_i}{\partial t} = -\frac{\partial}{\partial z}\left(-\xi D \frac{\partial C_i}{\partial z} + w \xi C_i\right) + \sum_j \xi REAC_i \quad , \tag{1}$$

where $C_i$ is the concentration of the biogeochemical species $i$, $\xi$ equals the porosity $\phi$ for solute species and $(1-\phi)$ for solid species, hence represents the partitioning of species $i$ into the solute and dissolved phase. The term $z$ is the sediment depth, $t$ denotes the time, $D$ is the diffusion coefficient, $w$ is the advection rate and $\sum_j \xi REAC_i$ represents the sum of production/consumption rates $j$ that affect species $i$. For each species $i$ we employ a boundary condition at the sediment-water interface (SWI) depending on the phase of the species. Which means for solute species we assume the concentration at $z = 0$ in the sediments to equal the bottom water (BW) concentration ($C|_{z=0} = C(BW)$) and a flux for solid species ($F_{C_i} = -D\frac{\partial C_i}{\partial z}|_{z=0} + wC_i|_{z=0}$). The model is based on a three layer approach, distinguishing between the bioturbated ($z_{bio}$), the oxic ($z_{ox}$) and the sulfate reduction zone ($z_{SO4}$) (compare Figure 2.4). An analytical steady-state solution is found for the reaction-transport equation of each chemical species in each layer.

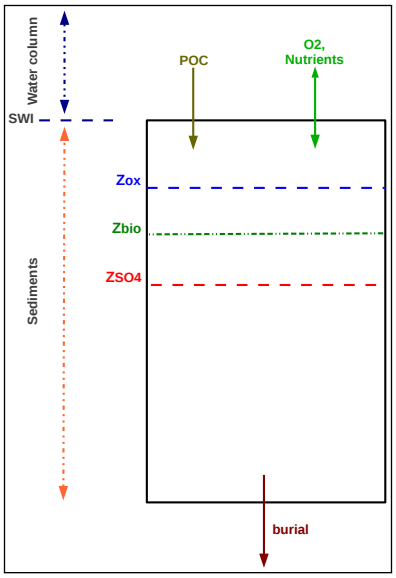


Figure 2.4: Schematic of Sediment-water interface (SWI) showing the case $z_{ox} < z_{bio} < z_{SO_4}$.

### 2.2.1 Organic matter

We follow the approaches given in Lancelot and Billen (1985) and/or Gypens et al. (2008) and consider two classes of biodegradable organic matter in the sediments, characterized by a temperature-dependent first-order degradation constant, which is independent of the water depth. The sediment depth is partitioned into two functional layers: a bioturbated surface zone streching from the sediment surface to the bioturbation depth ($z_{bio}$) where OM concentration is described with the general

advection-diffusion-reaction equation and a non-bioturbated layer below this zone where the concentration just depends on advection-reaction processes (compare Appendix A, Eq. (3) and (4)). The two steady-state solutions (Appendix A, Eq. (5) and (6)) both follow a simple exponential decay and enter the equations for the other biogeochemical species.

### 2.2.2 Oxygen

To describe oxygen concentration the sediments are partitioned into two layers, the oxic layer extending from the BWI to the oxygen penetration depth ($z_{ox}$) and an anoxic layer below this depth, where oxygen concentration is zero (Appendix A, Eq. (26)). For the oxic layer we need to distinguish two cases. Firstly, when ($z_{ox} \leq z_{bio}$) one can describe the oxic layer with one conservation equation (Appendix A, Eq. (9)); second for ($z_{bio} z z_{ox}$) we subdivide the oxic layer into an bioturbated and a non-bioturbated layer (compare Appendix A, Eq. (21) and (22)), which affects the diffusion coefficient employed and the phase of organic carbon (i.e. solid, solute) available for mineralization. In general, below $z_{ox}$, degradation of OM consumes oxygen with a fixed O:C ratio (compare e.g. Appendix A, Eq. (9), 3rd term). (Note: As I didn't include nitrogen in the GENIE simulations, I do not discuss nitrogen related processes in this dissertation, even the sediment model is able to simulate them.) According to this discussion, the consumption of oxygen just takes into account aerobic mineralization of OM but not the $O_2$ consumption during re-oxidation of reduced substances produced in the anoxic layer and diffusing into the oxic zone. To account for this process, we include the related oxygen consumption as a flux to the oxic-anoxic boundary condition for oxygen (see e.g. Appendix A, Oxygen, Case 1, boundary condition 3). The interested reader is referred to Appendix B.2 or Gypens et al. (2008) for further details on the calculation.

### 2.2.3 Sulfate and hydrogen sulfide

For modelling $SO_4$ concentrations we consider 3 different cases: **(0)** The special case, in particular important for the OAE2 conditions, with anoxic bottom waters and without nitrate available for respiration, hence leading to ($z_{ox} = z_{bio} = 0$). Therefore, one conservation equation can describe the dynamics of sulfate over the entire sediment column (Appendix B.3, Eq, (27)). In Case **(1)** we assume bioturbation to extend over the whole oxic layer ($z_{ox} \leq z_{bio}$). Furthermore, we have to distinguish weather $z_{bio}$ is lower or deeper as the nitrate penetration depth $z_{NO_3}$ and we get four different functional layers for either case (compare Appendix B.3, Eq. (29) - (32); (38) - (41) respectively). Note, that we exclude the rare case of $z_{SO_4} < z_{bio}$, which is a reasonable assumption (Regnier et al., 2011). Case **(2)** describes the situation where bioturbation ends above the oxygen penetration depth ($z_{bio} < z_{ox}$), causing again 4 different functional layers to model sulfate concentration (see Appendix B.3, Eq. (46) - (49)). Note that we consider the flux of the reduced substance $H_2S$ coming from the layer $z_{NO_3} \leq z \leq z_{SO_4}$ in the diffusive flux boundary conditions at $z_{ox}$ (see e.g. Appendix B.3, Case 1, boundary condition 3). Additionally, we calculate the sulfate penetration depth $z_{SO_4}$ using the fact that methane produced below $z_{SO_4}$ gets re-oxidized and therefore must equal the diffusive flux of $SO_4$ at this boundary depth.

For hydrogen sulfide we consider the same three cases (i.e. **(0)**: $z_{ox} = z_{bio} = 0$; **(1)**: $z_{ox} \leq z_{bio}$ and **(2)**: $z_{bio} < z_{ox}$). For the special case **(0)** we model two layers: first, above $z_{SO_4}$ hydrogen sulfide obeys a traditional advection-diffusion-reaction equation (Appendix B.4, Eq. (55)), whereas below it is described as a pure advection-diffusion transport (Appendix B.4, Eq. (56)). Case **(1)** distinguishes again two sub-cases, depending on weather the bioturbation depth is above or below $z_{NO_3}$ (Note:

Again we exclude $z_{SO_4} < z_{bio}$.) Eventually, for Case **(1)** and **(2)** we model five different functional layers to calculate hydrogen sulfide profiles (see Appendix B.4, Eq. (59) - (63); (70) - (74) and (80) - (84), respectively).

For a more detailed mathematical description of the differential equations, boundary consitions and general solutions, the interested reader is refered to Appendix B.3 and B.4; or for a more elaborate evaluation of the model to our eventual publication ((Arndt et al., 2013a), in prep).

### 2.2.4 Phosphorus

To model the phosphorus profile in the sediments we take into account the change with depth of phosphate in pore-waters and iron-bond P and thereby mainly follow the description of Caroline P. Slomp et al. (1996) and/or Gypens et al. (2008). Like Caroline P. Slomp et al. (1996), we divide the sediment column into three zones, but in contrast to the original paper we distinguish again the two cases: (1) $z_{bio} \leq z_{NO_3}$ and (2) $z_{NO_3} < z_{bio}$. In the oxic layer, we take into account that $PO_4$ can be adsorbed to iron oxides forming Fe-bound phosphorus (Krom and Berner, 1980; Slomp et al., 1998). Whereas in the anoxic layer, phosphate is produced by mineralization of OM and desorption of $P$ due to the reduction of iron oxides. Additionally, the formation of authigenic phosphorous represents a permanent sink of $PO_4$ (Slomp et al., 1996) in the anoxic layer. For more details on the role of phosphorus in the sediments refer to Tromp et al. (1995); Delaney (1998) and for the mathematical principles of the model see Appendix in (Caroline P. Slomp et al., 1996).

### 2.2.5 Model Parameters and Boundary conditions

Transport of solid species is dictated by sediment accumulation (advection) and bioturbational mixing of the sediments. Sediment accumulation rate ($w$) is the deposition of new material at the sediment-water interface (Berner, 1980). Bioturbation ($D_{bio}$) results from sediment mixing mediated by organisms living at the seafloor Boudreau (1986). Transport of dissolved species depends on molecular diffusion and burrow irrigation. For an overview of the parameters see Table 9 in Appendix B.6. For the internal boundary or continuity conditions at the different layers the reader is referred to the mathematical description in Appendix B.

### 2.2.6 Experiment setup

As a first test the model is applied to three sets with varying composition of organic matter input and/or different bottom water oxygen concentrations. In order to show the different behavior of the model within the three layers, I simulate a very high-oxygen ($300.0 \times 10^{-8}$ $mol\ O_2\ cm^{-3}$) and a dysoxic ($300.0 \times 10^{-8}$ $mol\ O_2\ cm^{-3}$) case with POC equally separated into labile and refractory (Exp 1 and Exp 2). In order to show the impact of OM composition on the burial flux, additionally one one case under anoxic conditions with 99% of the POC reaching the bottom water being refractory is simulated (Exp 3). The experiment setup and the model results are summarized in Table 5 and discussed in Section 3.2. Bottom water (BW) concentrations not mentioned in Table 5 here are constant over the experiments. The total TOC concentration at the SWI is 0.417 $mol/cm^3$ for each experiment and the fraction of labile- and refractory-POC (R-POC) is changed as mentioned above. Hydrogen sulfide concentration for the oxic experiment (Exp 1) is zero as $H_2S$ gets instantly oxidised by oxygen.

Table 4: Reaction parameters

| Parameter/Variable | Unit | Value | Description |
|---|---|---|---|
| **stoichiometric factors** | | | |
| OC | $mol/mol$ | 1.0 | oxygen to carbon ratio |
| $NC_1$ | $mol/mol$ | 0.1509 | nitrogen to carbon ratio refractory fraction |
| $NC_2$ | $mol/mol$ | 0.13333 | nitrogen to carbon ratio labile fraction |
| $SO_4C$ | $mol/mol$ | 0.5 | sulfate to carbon ratio |
| $MC$ | $mol/mol$ | 0.5 | methane to carbon ratio |
| **secondary reaction parameters** | | | |
| $\gamma_{NH_4}$ | - | 1.0 | fraction of $NH_4$ that is oxidised in oxic layer |
| $\gamma_{H_2S}$ | - | 0.8 | fraction of $H_2S$ that is oxidised in oxic layer |
| $\gamma_{CH_4}$ | - | 1.0 | fraction of $CH_4$ that is oxidised at $z_{SO_4}$ |

Table 5: Experiment setup for the evaluation of the sediment model. Bottom water concentrations not mentioned here are the same for each experiment.

| Exp-Name | Bottom water concentrations | | |
|---|---|---|---|
| | R-POC (in %) | $O_2$ ($mol\ cm^{-3}$) | $H_2S$ ($mol\ cm^{-3}$) |
| Exp 1 | 50 | $300.0 \times 10^{-8}$ | 0.0 |
| Exp 2 | 50 | $300.0 \times 10^{-12}$ | $7.2917 \times 10^{-8}$ |
| Exp 3 | 99 | $300.0 \times 10^{-12}$ | $7.2917 \times 10^{-8}$ |

# 3 Model Results and Discussion

## 3.1 GENIE Experiments

The behaviour of different biogeochemical species in the Late Cretaceous ocean before and during OAE2 is reconstructed and simulations with and without OM sulfurization are compared. Modeled dysoxic/anoxic conditions are defined by oxygen concentrations lower than 10 $\mu mol\ O_2\ kg^{-1}$ (Arthur and Sageman, 1994) and photic zone euxinia by the occurrence of free hydrogen sulfide ($H_2S > 0$) in the sub-surface ocean (80-200m). First the impact of organic matter sulphurization on the biological pump is investigated (3.1.1), followed by effects on oceanic biogeochemical cycles (3.1.2) and under Section 3.1.3 implications for atmospheric $CO_2$ concentrations are discussed.

### 3.1.1 Influence of OM sulphurization on the biological carbon pump

The biological pump is responsible for the distribution of organic carbon in the ocean as explained in Section 1.2. The production of organic matter (or POC) in the photic zone of the ocean is limited by (amongst other things) the availability of macronutrients, such as nitrate ($NO_3^-$) and phosphate ($PO_4$) (e.g. Smith, 1984; Howarth, 1988; Falkowski et al., 1998). As the employed GENIE version does not simulate nitrate, the limiting macronutrient for primary productivity in our model is phosphate (Fig. 3.1 and 3.2a). The degradation of organic matter in the water column can be tracked by the value of $\delta^{13}DIC$ (Fig. 3.2b) as lighter DIC is preferentially used during primary productivity (PP) in the upper ocean and is released further down when POC is degraded to DIC. This leads to the general pattern of higher $\delta^{13}DIC$ values in the surface ocean and lower values where OM is degraded. Furthermore, the global patterns of POC flux itself are analysed (Fig. 3.3).

Table 6: Oceanic mean concentrations of biological pump related parameters.

| Exp-Name | Oxygen $\mu mol\ O_2\ kg^{-1}$ | POC $nanomol\ kg^{-1}$ | DIC $mmol\ kg^{-1}$ | surface $PO_4$ $\mu mol\ kg^{-1}$ |
|---|---|---|---|---|
| REF-PRE | 116.50 | 38.94 | 1.955 | 0.1297 |
| REF-PEAK | 41.15 | 87.34 | 2.104 | 0.2160 |
| SULPH-PRE | 128.75 | 30.47 | 2.022 | 0.1005 |
| SULPH-PEAK | 67.03 | 61.01 | 2.402 | 0.1490 |

When considering the surface concentration of $PO_4$ (Fig. 3.1 and Table 6) it is apparent that due to OM sulphurization the values decrease slightly from 0.1297 to 0.1005 $\mu mol\ kg^{-1}$ for the PRE-OAE2 analog (and from 0.2160 to 0.1490 $\mu mol\ kg^{-1}$ for the PEAK-OAE2 analog). But even though the $PO_4$ inventory of the ocean has been doubled for the PEAK-scenarios and the nutrient-rich areas at high latitudes expand (compare Fig. 3.1), the mean surface phosphate concentration increases just slightly compared to the REFERENCE scenarios. The minimal size of this surface $PO_4$ increase can be explained as the enhanced nutrients at the surface are getting utilized by primary productivity and the total affect on the distribution of $PO_4$ reveals when analyzing its vertical profiles. Figure 3.2a for instance visualizes the doubling in the oceanic $PO_4$ inventory for the PEAK OAE2 scenarios compared with the PRE experiments. The impact of higher nutrient concentration enhances global export production (compare with Fig. 3.3) and as result the globally averaged ocean oxygen concentration drops from 116.50 to 41.15 $\mu mol\ O_2 kg^{-1}$ (by about 65 %) for the REFERENCE scenarios (Table 6).

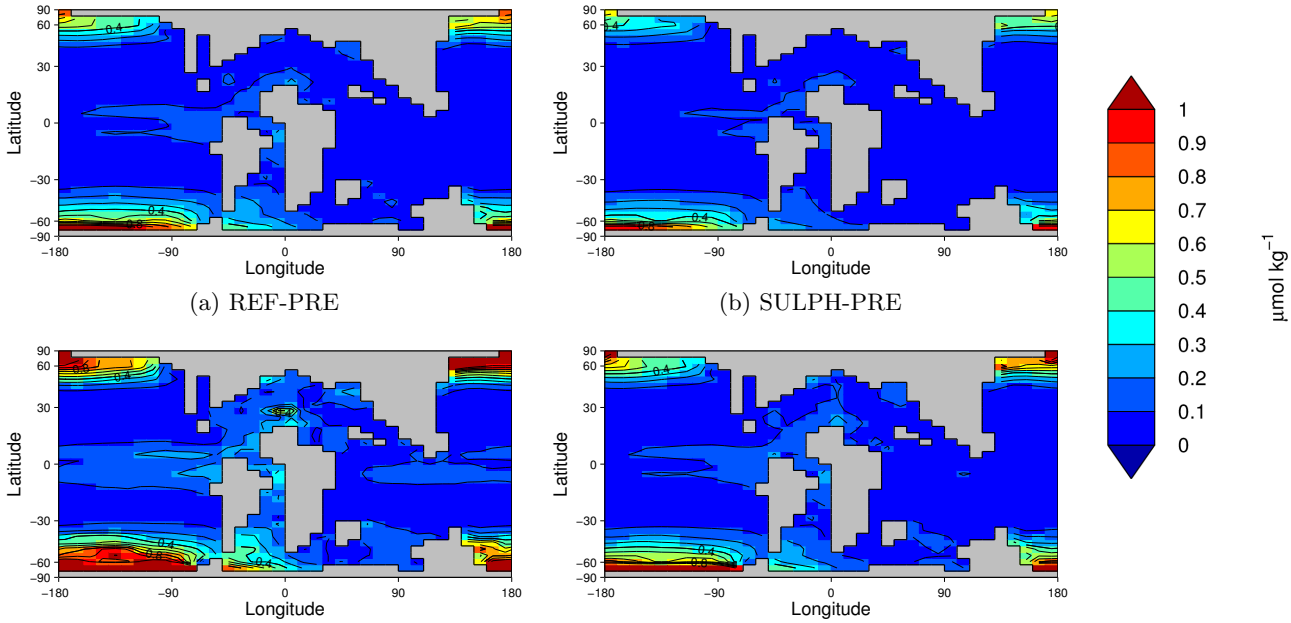


(a) REF-PRE (b) SULPH-PRE

(c) REF-PEAK (d) SULPH-PEAK

Figure 3.1: Surface concentrations of $PO_4$ (in $\mu mol\ kg^{-1}$) for the four scenarios.

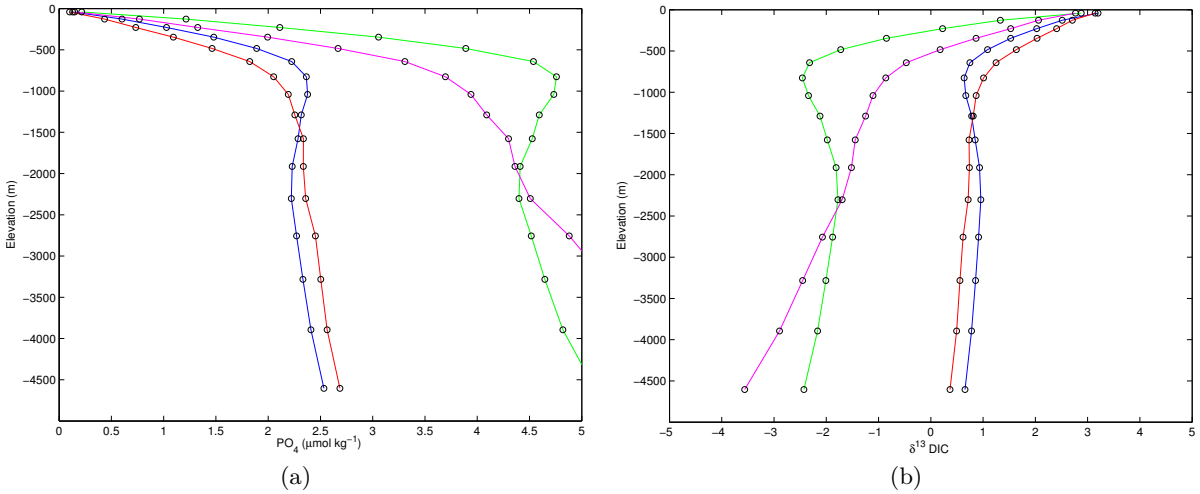


(a) (b)

Figure 3.2: Globally averaged profiles for (a) $PO_4$ and (b) $\delta^{13}$. PRE-REF, REF-PEAK, SULPH-PRE, SULPH-PEAK.

Furthermore, it is evident that especially the deep- and bottom-water phosphate concentrations (i.e. below 2000m) increase for the SULPHURIZATION simulations (Fig. 3.2a). This is because OM is more refractory and the POC flux extends deeper in the ocean (Fig. 3.3b and 3.3d), which can also be seen by the POC degradation patterns mirrored by the $\delta^{13}DIC$ Figure 3.2b. Especially when comparing the PEAK event scenarios one sees that the degradation of OM peaks between 500-1000m for the REFERENCE scenario and at the bottom water for the SULPHURIZATION scenario (compare also the $PO_4$ concentration in Fig. 3.2a). Note that the maximum degradation at the seafloor for the SULPHURIZATION experiments is an artifact due to the model-setup without sediments and is less pronounced when including OM burial in the sediments or simulating no degradation of particulate species at the seafloor (not shown here).

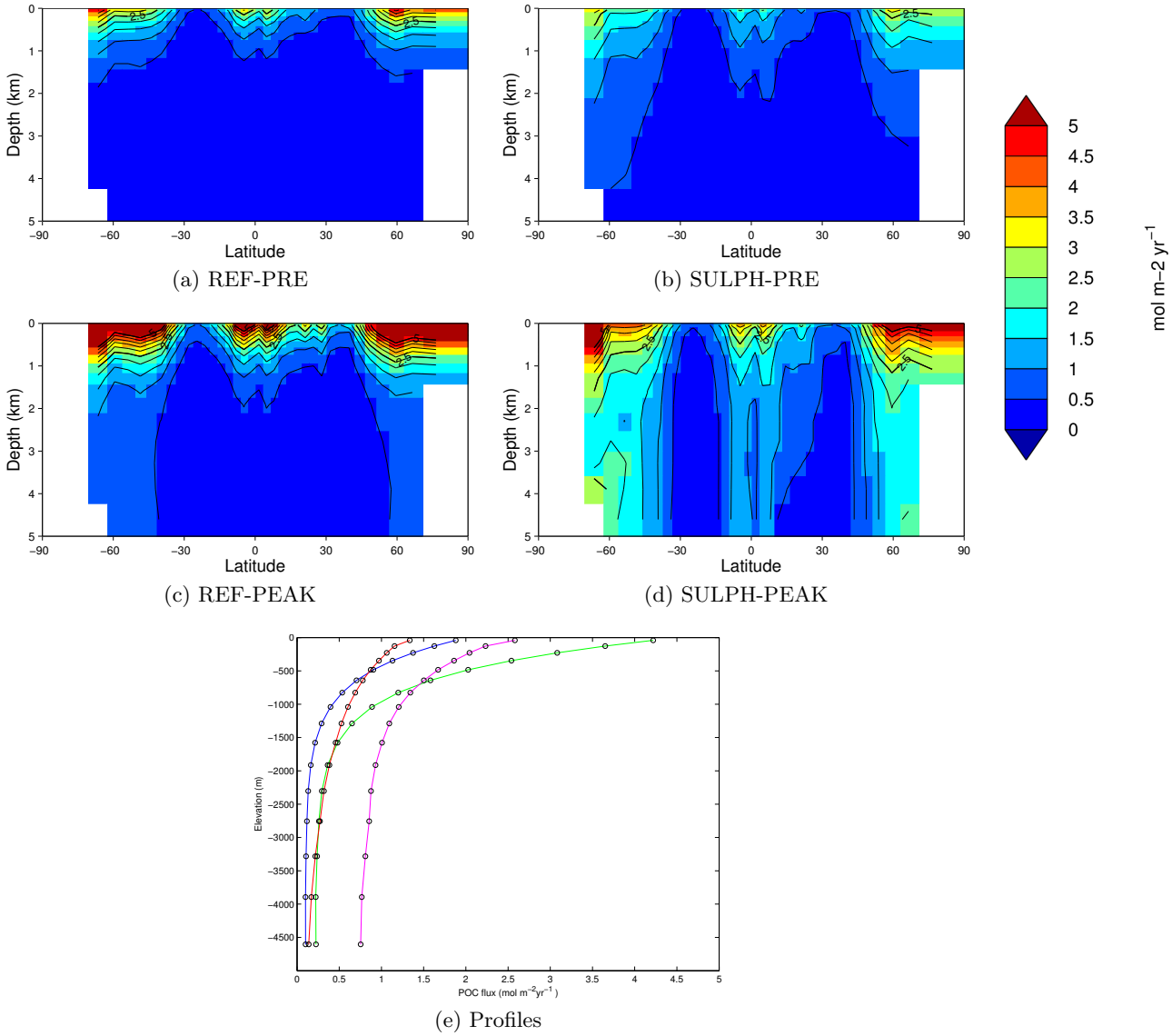


(a) REF-PRE (b) SULPH-PRE

(c) REF-PEAK (d) SULPH-PEAK

(e) Profiles

Figure 3.3: (a)-(d): Vertical distribution of POC flux for the four scenarios (longitudinally averaged). (e): Globally averaged POC flux profiles. PRE-REF, REF-PEAK, SULPH-PRE, SULPH-PEAK. All values in $mol\ m^{-1}yr^{-1}$.

The reduced POC flux in the upper ocean for the SULPHURIZATION experiments (as indicated e.g. by lower mean values in the first 500m in Fig. 3.3e) furthermore illustrates the decrease of primary

productivity, which can be explained by limited nutrient availability due to decreased POC degradation at these depths. The small POC fluxes at lower to mid-latitudes in Figure 3.3d are attributable to the Cretaceous ocean circulation with sinking waters in sub-tropical gyres (Barron and Peterson, 1990; Poulsen et al., 2001). In these downwelling areas less nutrients are transported from the deep to the upper ocean resulting in reduced primary productivity and POC-flux. Note, that Table 6 shows higher mean POC values for the REFERENCE compared to the SULPHURIZATION scenarios. This can be explained by the enhanced refractory POC reservoir in the SULPHURIZATION experiments being degraded at greater depth/at the seafloor; this leads to more DIC storage in the ocean as it is less available for PP in the photic zone. Furthermore, the addition of OM sulphurization to GENIE changes the relationship between oceanic oxygen concentrations and the amount of carbon stored in the ocean. The simplistic view of this relationship - that low oxygen concentrations are correlated to a high DIC inventory - is invalidated as the SULPH-PEAK experiment shows higher mean $O_2$ and also higher DIC values than the REF-PEAK simulation (see Table 6). This modified relationship is caused by the influence of organic matter sulphurization on the oceanic biogeochemical cycles and is discussed in further detail in the following Section 3.1.2.

### 3.1.2 Influence of OM sulphurization on global biogeochemical cycles

In the ocean, the distribution of biogeochemical species such as oxygen and hydrogen sulfide is determined by the gas exchange between the atmosphere and the ocean, the ocean circulation and removal via degradation of organic matter. Temperature (or the atmospheric $CO_2$ concentration) impacts the solubility of these species in seawater (and therefore the air-sea gas exchange); marine productivity is influenced by the nutrient content of the ocean and temperature as well. Additionally, $O_2$ and $H_2S$ concentrations are affected by the oxidant used to degrade organic matter (compare Section 1.3). The impacts of temperature and nutrient inventory of the ocean on oxygen have been analysed by Monteiro et al. (2012). Therefore, the following examination is focused on changes of oxygen and hydrogen sulfide distribution caused by the OM sulphurization simulations for the PRE- and PEAK-OAE2 events.

Table 7: Mean oceanic concentrations of oxygen and hydrogen sulfide and percentage of Dysoxia/Anoxia in bottom waters (BW) and globally.

| Exp-Name | BW Oxygen | | Global Oxygen | | Hydrogen Sulfide | |
|---|---|---|---|---|---|---|
| | concentr. $\mu mol\ kg^{-1}$ | Dysoxia (in %) | concentr $\mu mol\ kg^{-1}$ | Dysoxia (in %) | Photic Zone $\mu mol\ kg^{-1}$ | Global $\mu mol\ kg^{-1}$ |
| REF-PRE | 93.34 | 12.24 | 116.50 | 8.89 | 0.5540 | 5.392 |
| REF-PEAK | 10.77 | 87.47 | 41.15 | 82.42 | 12.8714 | 70.306 |
| SULPH-PRE | 79.15 | 15.94 | 128.75 | 8.00 | 0.0020 | 3.095 |
| SULPH-PEAK | 13.26 | 82.99 | 67.03 | 67.69 | 0.0004 | 38.622 |

When considering bottom water oxygen concentration for the high productive PEAK-OAE2 ocean, one sees that anoxia spreads across the global ocean with about 87 % of the seafloor becoming dysoxic/ anoxic for the REF-PEAK scenario and 83 % for the SULPH-PEAK experiment (Table 7) which is comparable with results presented in Monteiro et al. (2012). Comparing the SULPH- with the REF-experiments shows that BW $O_2$ decreases for the PRE-OAE2 event (from 93.34 to 79.15 $\mu mol\ kg^{-1}$) but increases for the PEAK-OAE2 analog (from 10.77 to 13.26 $\mu mol\ kg^{-1}$).

As already mentioned, the globally averaged oceanic $O_2$ concentration drops by about 65% when comparing REF-PEAK and REF-PRE. Considering the SULPH-scenarios this effect is less pronounced and the global mean concentration decreases only by about 48 % (from 128.75 to 67.03 $\mu mol\ O_2\ kg^{-1}$) (see Table 7). In other words, the REF-PEAK scenario yields about 82% anoxia in the global ocean whereas the SULPH-PEAK experiment produces only about 68% anoxia. This difference can be explained because the sulphurization of OM produces more refractory POC which is mainly degraded at the seafloor. When $O_2$ is exhausted at these depths, further degradation is mediated via sulfate-reduction. Whereas in the REF-PEAK experiment degradation occurs additionally at lower water depths (i.e. above $\sim 2000m$, compare Fig. 3.2b) and therefore oxygen depletion occurs in both parts of the ocean (compare Fig. 3.5c and 3.5d). The organic matter degradation in the deep ocean via sulfate reduction in the SULPH-PEAK simulation is also evidenced by the high $H_2S$ values occurring in deep waters (Fig. 3.7d).

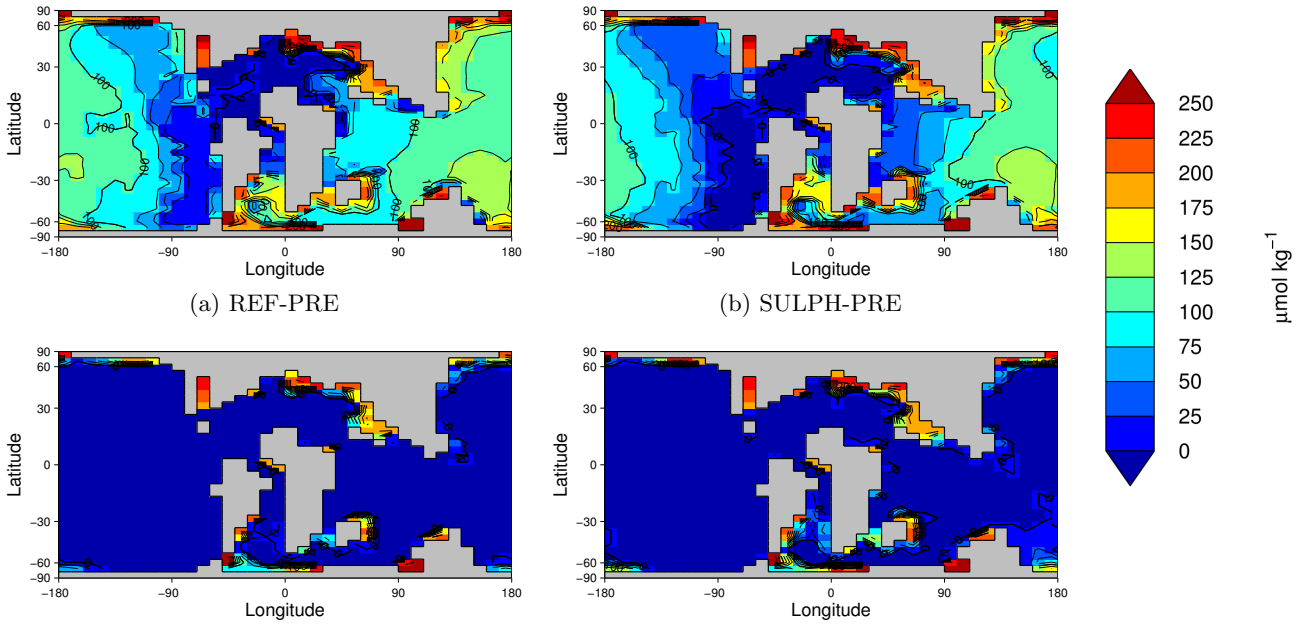


(a) REF-PRE (b) SULPH-PRE

(c) REF-PEAK (d) SULPH-PEAK

Figure 3.4: Bottom water concentrations of $O_2$ (in $\mu mol\ kg^{-1}$) for the four scenarios.

The more steady water column degradation for the SULPH simulations of the pre-OAE2 event (as shown in Fig. 3.2b) is also pictured as the oxygen minimum zone at mesopelagic depths for the REF-PRE experiment (Fig. 3.5a) is reduced in the SULPH-PRE simulation (Fig. 3.5b) and lower oxygen concentrations are spread more equally across the water-column (compare the SULPH-PRE profile in Fig. 3.5e). Again the pronounced anoxic conditions for the deep ocean in the SULPH-simulations are artifacts because all OM is degraded when it reaches the seafloor. Nonetheless, Figures 3.4a and 3.4b show that the bottom water concentrations for the PRE-OAE2 event are decreased slightly due to OM sulphurization (compare also Table 7). As already mentioned this effect is reversed when examining the PEAK-OAE2 simulations and one can spot some areas in Figure 3.4d with slightly elevated oxygen concentrations compared to the REF-PEAK results (Fig. 3.4c). The higher values might have been caused by reduced primary productivity in these areas due to a circulation-induced reduction of nutrient input from other oceanic regions where less organic matter degradation occurs because of OM

sulphurization. Therefore a smaller amount of POC would reach the seafloor. But this assumption needs to be further investigated.

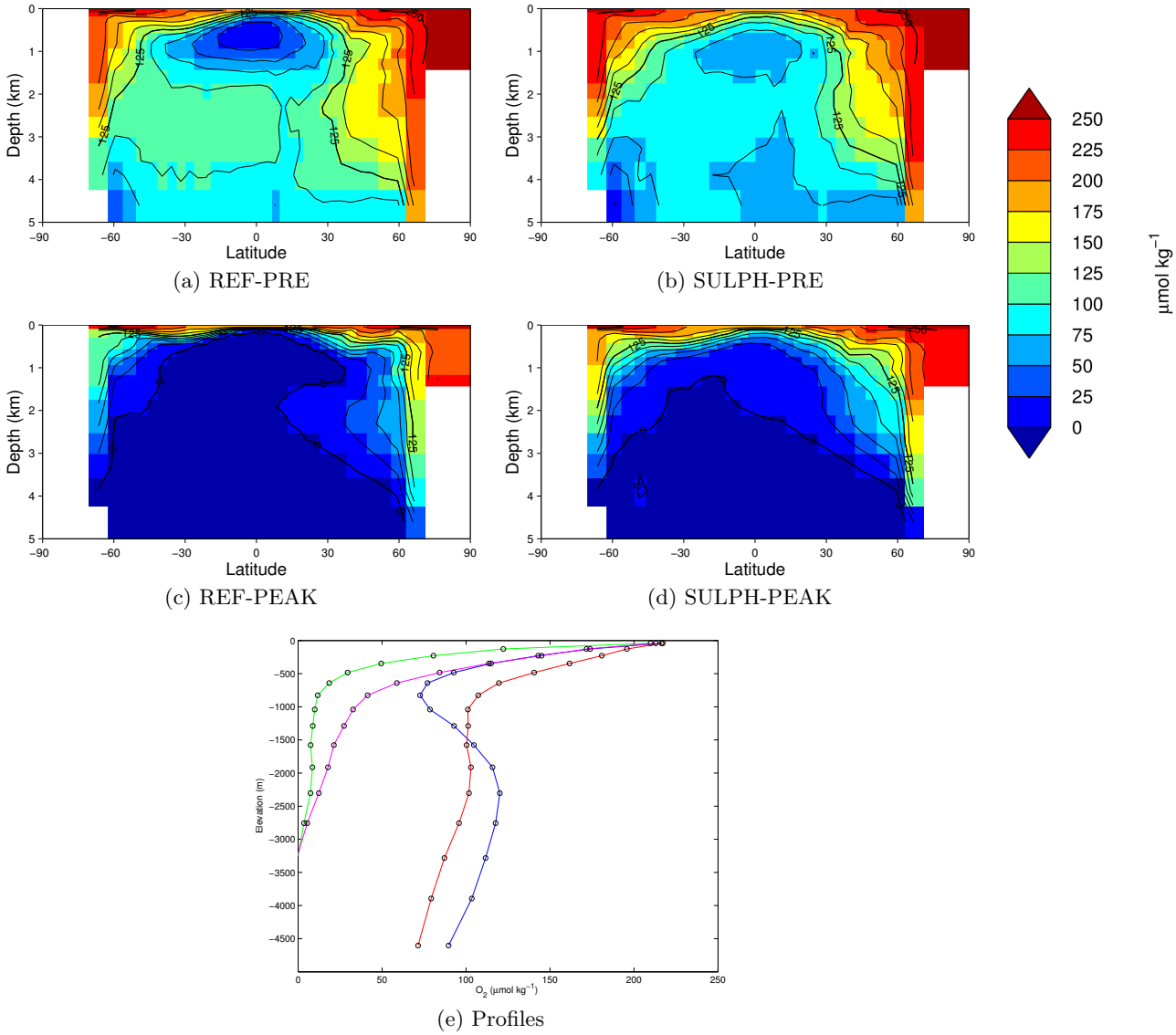


Figure 3.5: (a)-(d): Vertical distribution of $O_2$ for the four scenarios (longitudinally averaged). (e): Globally averaged $O_2$ profiles. PRE-REF, REF-PEAK, SULPH-PRE, SULPH-PEAK. All values in $\mu mol\ kg^{-1}$.

The global mean oceanic $H_2S$ concentration decreases due to OM sulphurization from 5.392 to 3.095 $\mu mol\ kg^{-1}$ at the PRE-OAE2 event and from 70.306 to 38.633 $\mu mol\ kg^{-1}$ for PEAK-OAE2 (compare Table 7). The simulations also indicate that photic zone euxinia already exhisted before OAE2 in the Atlantic and East Pacific Ocean (Fig. 3.6a) and expanded into all equatorial regions and most of the proto-Atlantic Ocean and Tethys Sea during OAE2 (Fig. 3.6b). The SULPH-simulations show no photic zone euxinia (compare Table 7, Figures not included), indicating that $H_2S$ is the limiting factor in the OM sulphurization reaction and is completely consumed at these depths. The significantly high equatorial $H_2S$ concentrations between 500-1500m for the REF-PEAK scenario (see Fig. 3.7c) have two causes: First, the Atlantic ocean is about 1500m deep at these latitudes (Fig. 2.2a) and exhibits pronounced bottom water anoxia (compare Fig. 3.4a), leading to organic matter

degradation via sulfate reduction and therefore the build-up of $H_2S$. Second, the East Pacific ocean shows an oxygen minimum zone in this area causing the production of hydrogen sulfide due to OM degradation (see Fig. 3.9 (a) and (c) in Section 3.1.4).

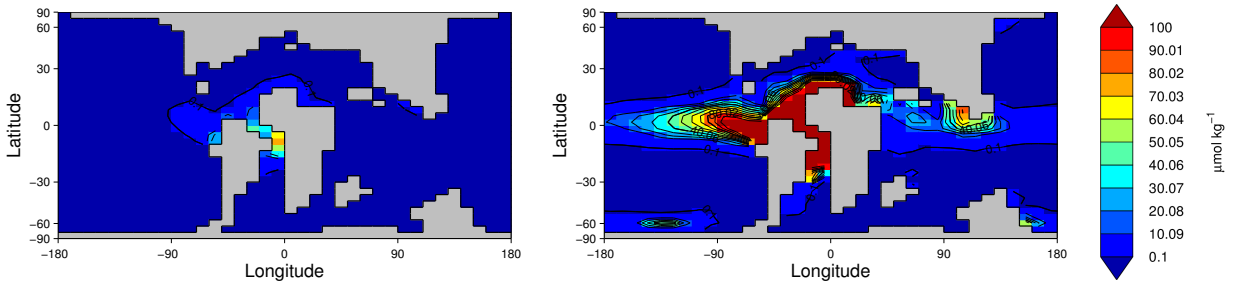


(a) REF-PRE (b) REF-PEAK

Figure 3.6: Photic zone euxinia (in $\mu mol\ H_2S\ kg^{-1}$) for the two reference scenarios. SULPH-scenarios show zero photic zone euxina as all $H_2S$ is used for organic matter sulphurization.

The globally averaged $H_2S$ concentration decreases by about 45 % (from 70.306 to 38.622 $\mu mol\ kg^{-1}$) when comparing the REF-PEAK and SULPH-PEAK scenario (see Table 7) because hydrogen sulfide has been used to make organic matter more refractory by sulphurization. Again, the exaggerated bottom water $H_2S$ concentrations for the SULPH-PEAK scenario (Fig. 3.7d) appears because the employed GENIE-version does not include an appropriate sediment model to represent burial of particulate species.

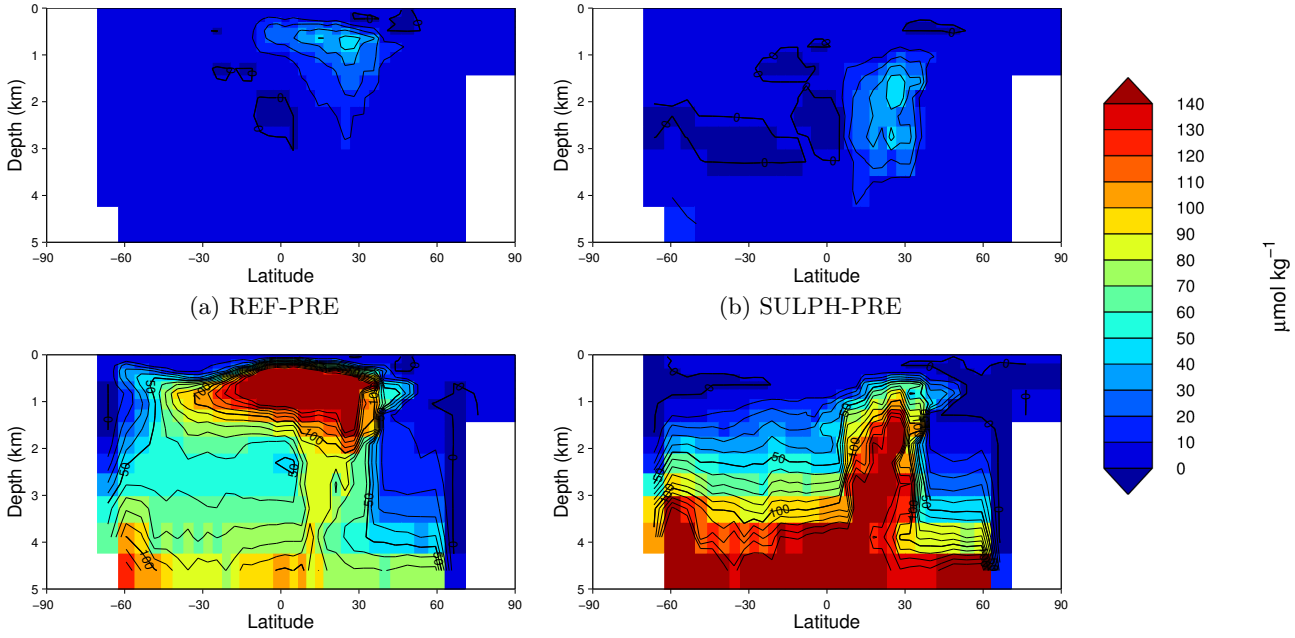


(a) REF-PRE (b) SULPH-PRE

(c) REF-PEAK (d) SULPH-PEAK

Figure 3.7: Vertical distribution of $H_2S$ for the four scenarios (longitudinally averaged). All values in $\mu mol\ kg^{-1}$.

### 3.1.3 Implications for Climate

As discussed in Chapter 1 marine productivity and the functioning and efficiency of the biological pump are closely related to climatic conditions and especially the atmospheric $CO_2$ concentration. Even though, the atmospheric carbon dioxide inventory in our experiments is prescribed (compare Section 2.1.2), potential impacts on its magnitude can be derived from the change in net sea to air $CO_2$ exchange-flux. Figure 3.8 displays the results for the two PEAK-OAE2 scenarios (i.e. REF-PEAK and SUPLH-PEAK), with "cold" colours representing an influx of $CO_2$ to the ocean and "warm" colours a discharge from the ocean. The organic matter sulphurization experiment (Fig. 3.8b) shows out-flux regions at the mid-latitudes of the Pacific and Tethys Ocean and a very concentrated area in the Southern Pacific. In contrast the areas of high $CO_2$ influx are larger and mainly mirror the patterns of photic zone euxina observed for the REF-PEAK scenario (Fig. 3.6b). This is because in regions with photic zone euxina POC becomes more refractory due to sulphurization and therefore gets transported and degraded deeper in the ocean. As a consequence DIC is less concentrated in surface and mesopelagic depths, leading to more $CO_2$ uptake in order to equilibrate with the atmosphere.

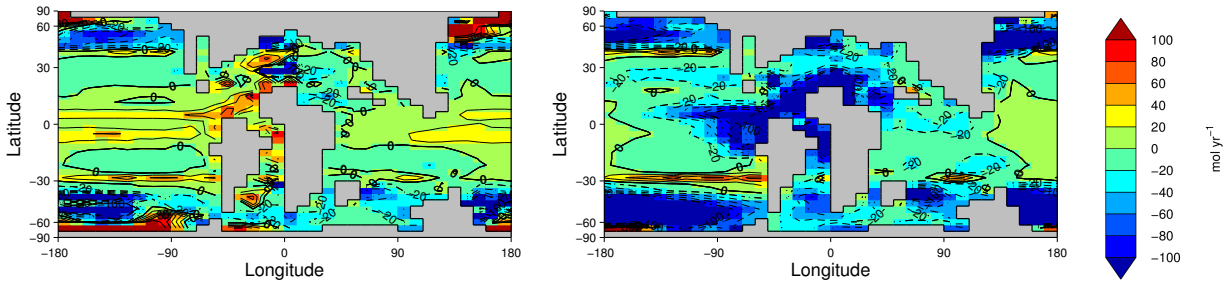


(a) REF-PEAK (b) SULPH-PEAK

Figure 3.8: Net sea to air $CO_2$ exchange for the two PEAK-OAE2 scenarios. The values are plotted with their scale symmetrical around zero, giving red or "warm" colours for positive values (i.e. $CO_2$ flux from the ocean to the atmosphere), and blue or "cold" colours for negative values (i.e. $CO_2$ flux from the atmosphere into the ocean).

### 3.1.4 Case Study: The East Pacific

As a case study, the impact of OM sulphurization in the PEAK-OAE2 simulations is analyzed for a transect through the East Pacific Ocean (between Longitude $-95°$ and $-85°$). This area has been chosen for two reasons: Firstly, it has been shown to exhibit photic zone euxinia and seafloor anoxia during OAE2 for the reference scenarios (see (Monteiro et al., 2012) and Fig. 3.9 (a) and (c) ). Secondly, the mean water depths is about twice as large as in a comparable transect through the Atlantic and therefore makes the investigation of water-column profiles more interesting.

The simulation without OM sulphurization shows that areas characterized by photic zone euxinia did indeed overlie anoxic mesopelagic waters (Fig. 3.9 (a) and (c)) as previously suggested by Sinninghe Damsté and Köster (1998) and modeled in Monteiro et al. (2012). These euxinic intermediate waters develop as $H_2S$ is produced by sulfate reduction under anoxic conditions prevailing in this area (see Fig. 3.9 (a)) and elevated phosphate concentrations (compare Figure 3.9 (g)) display large organic matter degradation at these depths. When simulating sulphurization of organic matter, this

hydrogen sulfide in intermediate waters is almost completely utilized and the new profile shows a clear increase in $H_2S$ concentration with water depth (Fig 3.9 (d)). Accordingly, $PO_4$ rises with depth (Fig. 3.9 (h)), whereas not in such a stratified way as $H_2S$. This is because in the high productivity - low latitudes, POC concentration exceeds $H_2S$ concentrations and therefore not all organic matter gets sulphurized. Hence, the remaining labile fraction gets degraded via oxygen and/or sulfate reduction also in intermediate depths. As for the global analysis, also in the East Pacific Ocean oxygen minimum zones at mesopelagic depths decrease in the SULPH experiment as overall less organic matter gets remineralzed via aerobic respiration. Figure 3.9 (f) shows the extent of POC flux to deeper ocean depths for the equatorial area and latitudes between 40° and 60° South. This is caused by the simultaneous presence of $H_2S$ and POC in the upper ocean as indicated in Figures 3.9 (c) and (e) for the simulation without OM sulphurization. In contrast, deep-water POC transport is not enhanced at latitudes where either no photic zone euxinia or not enough surface water POC is present in the reference scenario.

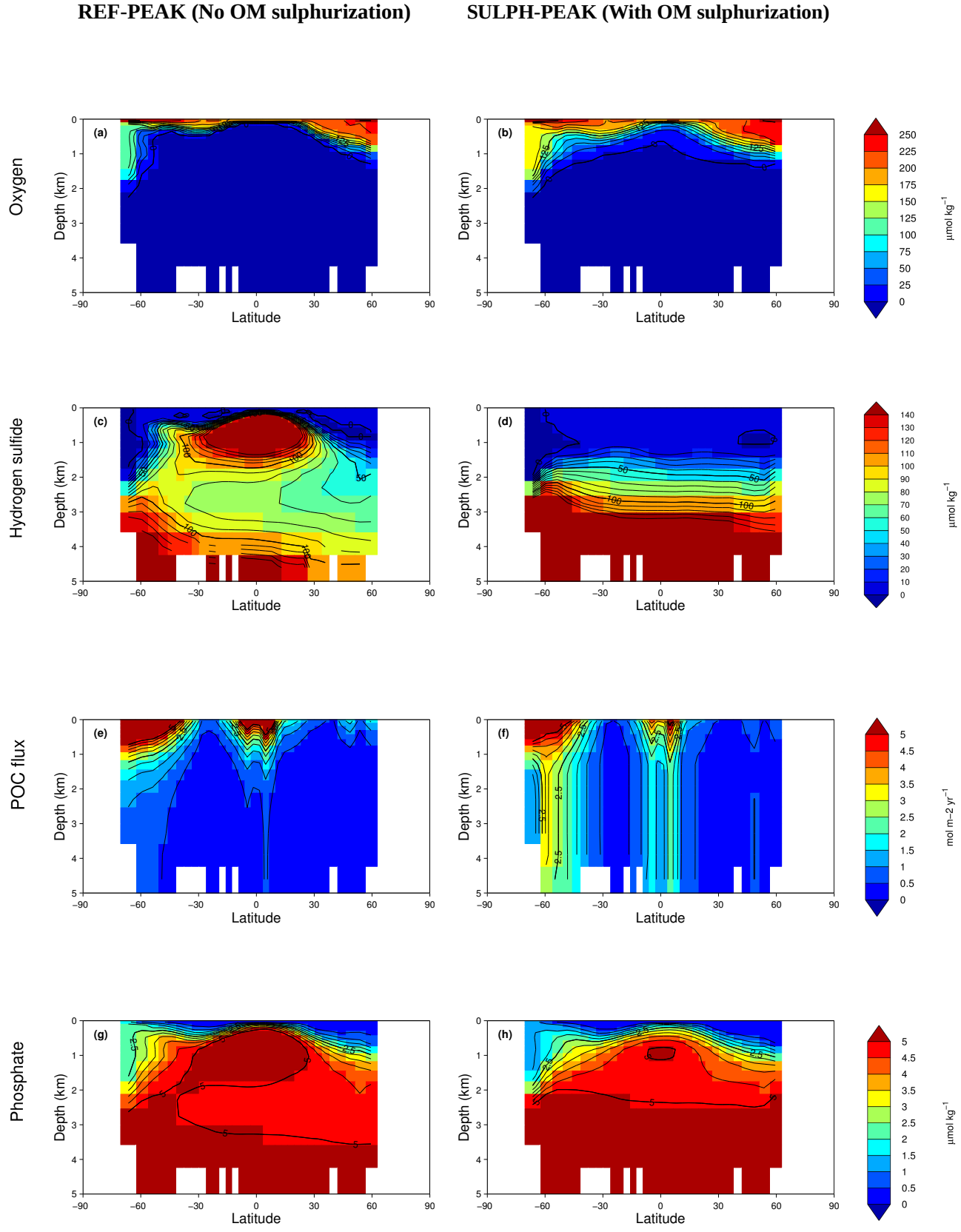


Figure 3.9: Vetical profiles for the East Pacific (−95° to −85° longitude) without organic matter sulphurization (left) and with organic matter sulphurization (right) for the PEAK-OAE2 scenarios. (a, b) Oxygen; (c, d) Hydrogen sulfide; (e, f) POC flux; (g, h) Phosphate.

### 3.2 Sediment model evaluation

To visualise the behaviour of our new model for the three experiments (compare Section 2.2.6) sediment column profiles of TOC and various chemical species (i.e. oxygen, sulfate and hydrogen sulfide) are plotted in Figure 3.10. Table 8 summarises the resulting $O_2$ and $SO_4$ fluxes at the sediment water interface (SWI) and the amount organic carbon buried in the sediments at the lower boundary of 100cm.

Table 8: Experiment results for the sediment model. Carbon-burial is the TOC flux at the lower boundary (100cm). Positive SWI fluxes represents a flux from the water column into the sediments.

| Exp-Name | $z_{ox}$ (in cm) | $z_{SO_4}$ (in cm) | $O_2$-flux at SWI ($mol\ cm^{-3}yr^{-1}$) | $SO_4$-flux at SWI ($mol\ cm^{-3}yr^{-1}$) | Carbon-burial ($mol\ cm^{-3}yr^{-1}$) |
|---|---|---|---|---|---|
| Exp 1 | 2.2 | 5.0 | $3.547 \times 10^{-4}$ | $1.0709 \times 10^{-4}$ | $6.250 \times 10^{-4}$ |
| Exp 2 | $1.98 \times 10^{-4}$ | 3.75 | $3.274 \times 10^{-4}$ | $1.2147 \times 10^{-4}$ | $6.250 \times 10^{-4}$ |
| Exp 3 | $2.69 \times 10^{-4}$ | 3.67 | $2.413 \times 10^{-4}$ | $1.5560 \times 10^{-4}$ | $12.3750 \times 10^{-4}$ |

As organic matter degradation in our model just depends on the reactivity of the two POC fractions and not on the oxidant used, the TOC profiles for Exp 1 and Exp 2 are identical. Also note that the labile fraction is consumed more rapidly as the refractory part. In Exp 3, when changing the POC partitioning to 99% refractory, the profile changes significantly and almost twice as much TOC is buried at the lower sediment boundary (compare Table 5). This indicates that it is mainly the refractory POC part that is buried. Additionally, the oxygen and sulfate penetration depths ($z_{ox}$ and $z_{SO_4}$) change depending on benthic $O_2$ concentrations and POC composition. Caused by the reduction of benthic oxygen (from Exp 1 to Exp 2) $z_{ox}$ is decreased by four orders of magnitude. As a consequence (because sulfate reduction starts earlier in the sediment column) also $z_{SO_4}$ is decreased (from 5.0 to 3.75 cm). When making POC more refractory, oxygen penetrates deeper into the sediments as OM degradation is slower. Note that $z_{SO_4}$ is reduced to 3.67 cm as it is a complex balance between $SO_4$ concentration at the SWI, OM degradation by different pathways and various fluxes (e.g. AOM at $z_{SO_4}$ and $H_2S$ oxidation at $z_{ox}$). These interrelations are not analysed in further detail here. The bioturbation depth $z_{bio}$ is fixed to 2cm in all our experiments. In a more realistic representation it would depend on the depth of the SWI interface as described in Middelburg et al. (1997). The TOC profiles visualise the difference between the bioturbated and non-bioturbated layer. The diffusion-advection transport in the upper layer is clearly more efficient than the pure advection transport in the non-bioturbated layer. TOC concentration above $z_{bio}$ is almost constant as this sediment-part is well mixed and diffusion of OM is more rapid than its consumption (compare also timescales of bioturbation and OM degradation, see references in Table 9).

Oxygen (if present at the SWI) is rapidly consumed in the upper sediments and its penetration depth depends on the BW $O_2$ concentration and the composition of POC at the seafloor as discussed above. Furthermore, $O_2$ is consumed at $z_{ox}$ due to the re-oxidation of reduced substances (here $H_2S$). The water-to-sediment oxygen flux decreases when considering dysoxic conditions (compare Table 8 Exp 2). This is caused because the flux is driven by the $O_2$ concentration gradient between the bottom water and the sediments which is reduced for dysoxic conditions. The flux also decreases when POC gets more refractory as oxygen penetrates deeper into the sediments and therefore the concentration gradient is reduced.

The impact of anaerobic degradation of OM is shown by the $H_2S$ and $SO_4$ profiles in Figure 3.10. Below $z_{ox}$ organic matter gets degraded via sulfate reduction and therefore sulfate is consumed and hydrogen sulfide produced. This is indicated by the change of slope for $SO_4$ at $z_{ox}$ in Exp 1. Simultaneously the concentration of $H_2S$ starts to increase below the oxygen penetration depth. Hydrogen sulfide produced in the anoxic sediment-part diffuses upwards until it gets oxidised at $z_{ox}$. Note that the production of $H_2S$ also depends on the degradability of POC as the different slope for Exp 2 and Exp 3 indicates. The water-to-sediment sulfate flux increases for the dysoxic case (Exp 2) compared with the well oxidised experiment Exp1 (Table 8). This can be explained as aerobic OM degradation is less intense and more OM is degraded via sulfate reduction in the sediments. This causes an increase of the $SO_4$ concentration gradient and therefore an elevated flux from the water column. For Exp 3 the flux increases (compared to Exp2) which is again caused by the complex interplay between $SO_4$ concentration at the SWI, OM degradation by different pathways and various fluxes and is not discussed in further detail here. Note that we assume constant $H_2S$ concentrations below $z_{SO4}$.

The discussion of $PO_4$ profiles is left out as it has been implemented by Nicolas Goossen from the Université Libre de Bruxelles and mainly follows the description of Caroline P. Slomp et al. (1996). For a plot of the corresponding profiles see Figure B.1 in Appendix B.

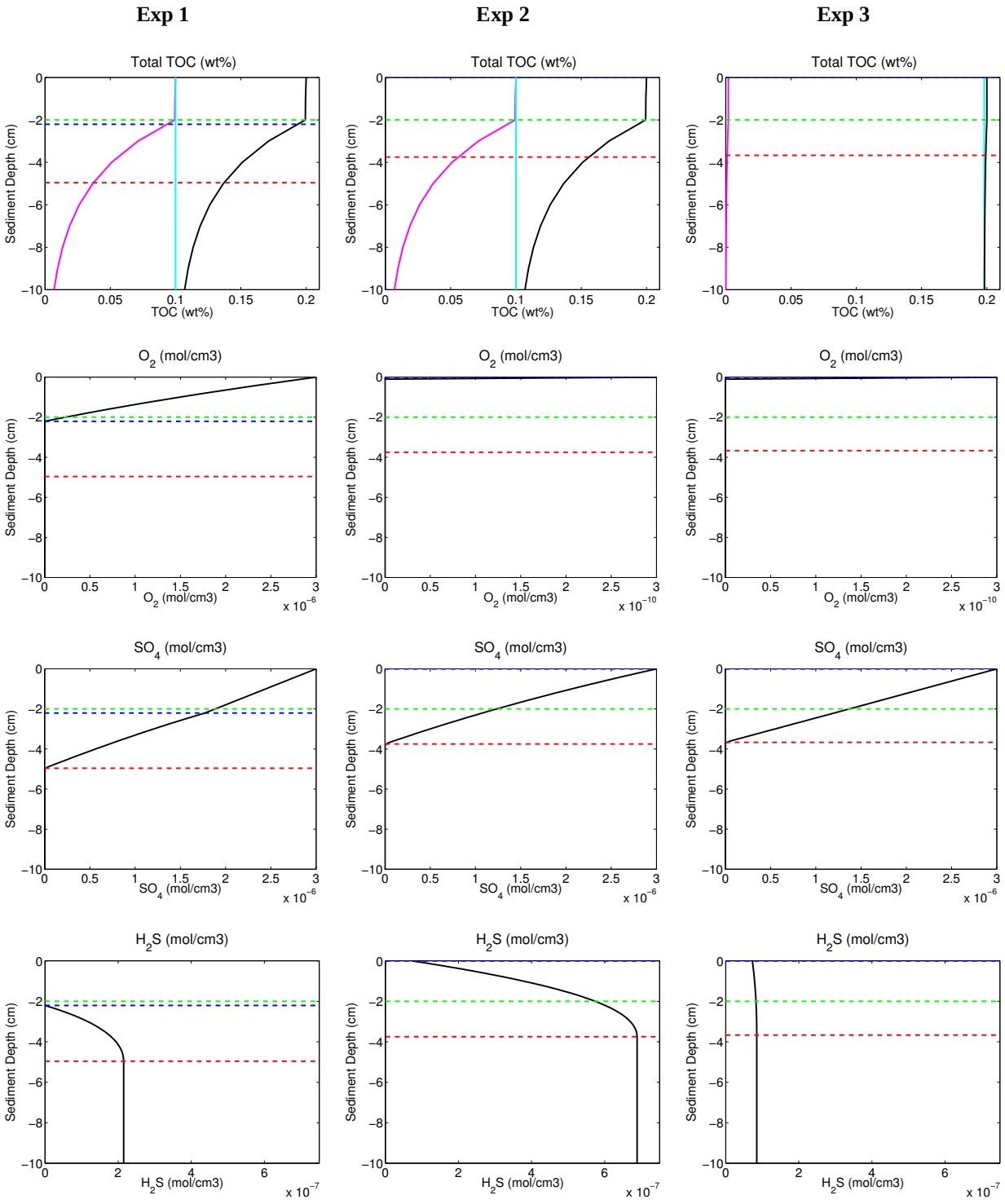


Figure 3.10: Comparison of TOC and nutrient profiles generated by our new analytic model under different organic matter loadings and oxygenation of the overlying bottom water. TOC plots showing labile POC in magenta, refractory in cyan and the sum in black. For the Experiment setup see Table 5. Dashed horizontal lines representing the different penetration depths ($z_{bio}$, $z_{ox}$ and $z_{SO_4}$).

# 4 Further Work

In order to improve the tools presented here two major steps are considered for the future:

## 4.1 Kinetic approach for OM sulphurization

My experiments investigate the extreme case where it is assumed that all labile POC can be converted to refractory POC. The model just checks whether labile POC or $H_2S$ is less abundant, sets the smaller species to zero and adjusts the other concentration appropriately. In reality this process is more complex and the change of POC composition also depends on a rate constant for sulphurization of organic matter ($k_{Sorg}$). Following Dale et al. (2009) the potential labile POC concentration which can be converted ($L\_POC_{pot}$) is calculated in the following way:

$$L\_POC_{pot} = k_{Sorg} \cdot [H_2S] \cdot [L\_POC] \tag{2}$$

where $[H_2S]$ and $[L\_POC]$ represent concentrations in the appropriate grid-cells. Subsequently $L\_POC_{pot}$ needs to be compared with the actual $H_2S$ and labile POC concentration in the grid-cells and the concentrations has to be updated in the appropriate way (as described in Section 2.1.1). For the rate constant for sulphurization of organic matter Dale et al. (2009) evaluated a value of 0.2 $M^{-1}yr{-}1$ for OM in the sediments which can act as a first start for a sensitivity analysis. The Fortran code for this procedure is given in Figure 4.1.

## 4.2 Integration of the sediment model into GENIE

In order to eventually analyse the feedbacks of organic carbon preservation in marine sediments with oceanic biogeochemical cycles and climate on a global scale our new sediment model will be coupled to the three-dimensional Earth System model GENIE. Therefore, GENIE's benthic concentrations of chemical species and the water-to-sediment flux of POC (and its composition) are delivered to the sediment model. Additionally, the seafloor depth will be handed over in order to describe bioturbation and sediment accumulation rate as a function of depth. These processes will be modelled as described in Middelburg et al. (1997) and/or Thullner et al. (2009). The benthic model calculates burial of POC at the lower boundary of the sediments and the resulting SWI interface fluxes and transfers this information back to GENIE for each bottom water grid-cell. This will enable a quantitative analysis of OM sulphurization impact on the formation of black-shales and aid to answer the question if OM sulphurization has a key significance for the recovery of the Earth System from the Cretaceous "greenhouse" world in further detail.

```
! calculate change in partitioning between different fractions
l = is2l(is_POC_frac2)
!calculate L-POC in kk to compare magnitude
loc_LPOC_compare_kk = (1-loc_bio_part_TMP(l,kk+1))*loc_bio_part_TMP(is2l(is_POC),kk+1) &
                    & *loc_bio_part_POC_ratio*loc_bio_remin_layerratio
! Check H2S enabled
if (ocn_select(io_H2S)) then
   ! check is POC in grid-cell
   if (loc_bio_part_TMP(l,kk+1) > const_real_nullsmall) then
        ! check H2S in grid-cell
        if (dum_vocn%mk(io2l(io_H2S),kk) > const_real_nullsmall) then
            ! check still labile POC left to convert, i.e. loc_bio_part_TMP(l,kk) < 1
            if(1-loc_bio_part_TMP(l,kk+1) > const_real_nullsmall) then
                ! calculate potential labile POC to be converted:
                ! R = kSorg*H2S(kk)*LPOC(kk+1)*dum_dtyr
                loc_R_Sorg = loc_kSorg * dum_vocn%mk(io2l(io_H2S),kk) &
                           & * loc_LPOC_compare_kk * dum_dtyr
                ! check, H2S or labile POC is smaller
                if(dum_vocn%mk(io2l(io_H2S),kk) .LE. loc_LPOC_compare_kk) then
                    if(loc_R_Sorg .LE. dum_vocn%mk(io2l(io_H2S),kk))then
                        ! nothing is limiting (all loc_R_Sorg gets converted)
                        loc_bio_remin(io2l(io_H2S),kk) = &
                            & loc_bio_remin(io2l(io_H2S),kk) - loc_R_Sorg
                        ! calculate new R-POC and L-POC concentration in kk
                        loc_RPOC = (1.0 - loc_bio_remin_POC_frac2)*loc_bio_part_TMP(l,kk+1) &
                                   & *loc_bio_part_POC_ratio + loc_R_Sorg
                        loc_LPOC = (1.0 - loc_bio_remin_POC_frac1)*loc_bio_part_TMP(l,kk+1) &
                                   & *loc_bio_part_POC_ratio - loc_R_Sorg
                        loc_bio_part_TMP(l,kk) = loc_RPOC/(loc_RPOC + loc_LPOC)
                    else    !H2S is LIMITING
                        ! set H2S concentration to "zero"
                        loc_bio_remin(io2l(io_H2S),kk) = &
                            & loc_bio_remin(io2l(io_H2S),kk) - dum_vocn%mk(io2l(io_H2S),kk)
                        ! calculate new R-POC and L-POC concentration in kk
                        loc_RPOC = (1.0 - loc_bio_remin_POC_frac2)*loc_bio_part_TMP(l,kk+1) &
                                   & *loc_bio_part_POC_ratio + dum_vocn%mk(io2l(io_H2S),kk)
                        loc_LPOC = (1.0 - loc_bio_remin_POC_frac1)*loc_bio_part_TMP(l,kk+1) &
                                   & *loc_bio_part_POC_ratio - dum_vocn%mk(io2l(io_H2S),kk)
                        loc_bio_part_TMP(l,kk) = loc_RPOC/(loc_RPOC + loc_LPOC)
                    end if
                else    ! l-POC < H2S
                    if(loc_R_Sorg .LE. loc_LPOC_compare_kk)then
                        ! nothing is limiting (all loc_R_Sorg gets converted)
                        loc_bio_remin(io2l(io_H2S),kk) = &
                            & loc_bio_remin(io2l(io_H2S),kk) - loc_R_Sorg
                        ! calculate new R-POC and L-POC concentration in kk
                        loc_RPOC = (1.0 - loc_bio_remin_POC_frac2)*loc_bio_part_TMP(l,kk+1) &
                                   & *loc_bio_part_POC_ratio + loc_R_Sorg
                        loc_LPOC = (1.0 - loc_bio_remin_POC_frac1)*loc_bio_part_TMP(l,kk+1) &
                                   & *loc_bio_part_POC_ratio - loc_R_Sorg
                        loc_bio_part_TMP(l,kk) = loc_RPOC/(loc_RPOC + loc_LPOC)
                    else    ! labile POC is limiting
                        loc_bio_part_TMP(l,kk) =  1.0   ! everything refractory
                        loc_bio_remin(io2l(io_H2S),kk) = &
                            & loc_bio_remin(io2l(io_H2S),kk) - (loc_LPOC_compare_kk)
                    end if

                end if
            else    ! just refractory in kk+1
                loc_bio_part_TMP(l,kk) =  1.0
            end if
        else    ! NO HS2 -> normal change in partitioning
                loc_bio_part_TMP(l,kk) =  min(1.0,(1.0 - loc_bio_remin_POC_frac2)* &
                                          & loc_bio_part_TMP(l,kk+1)/loc_bio_part_POC_ratio)
        end if
   else ! NO POC in grid-cell kk+1
        loc_bio_part_TMP(l,kk) = 0.0
   end if
else     ! OLD, NO H2S method
   if (loc_bio_part_TMP(l,kk+1) > const_real_nullsmall) then
        loc_bio_part_TMP(l,kk) =  &
        & (1.0 - loc_bio_remin_POC_frac2)*loc_bio_part_TMP(l,kk+1)/loc_bio_part_POC_ratio
   else
        loc_bio_part_TMP(l,kk) = 0.0
   end if
end if
```

Figure 4.1: Fortran code for kinetic version of organic matter sulphurization scenario as implemented in GENIE and described in 4.1.

# 5 Conclusion

I conducted a series of numerical experiments with the Earth System model GENIE to analyse the impacts of organic matter sulphurization on global biogeochemical cycles in association with OAE2. In doing so, I compared oceanic patterns of biogeochemical species and organic carbon before and during the event. The study led to four important results. First, the reference model (without OM sulphurization) successfully reproduced patterns of bottom water anoxia and photic zone euxinia before and during OAE2 as observed and modelled in Monteiro et al. (2012). My reference simulations suggest that bottom water anoxia was a global phenomenon covering 12% of the deep ocean by area before and 87% during OAE2. Overall the mean oceanic oxygen content decreased by about 65% during OAE2. Prior to the event, photic zone euxinia already covered most parts of the lower latitude proto-Atlantic Ocean and some parts of the equatorial East Pacific. Second, the model suggests that sulphurization of organic matter has the potential to be an important emergency recovery mechanism from the "greenhouse" world of OAE2. As a result of OM sulphurization, POC is transported deeper into the ocean, where it eventually gets degraded at the seafloor. This causes an increased storage of organic carbon in the deep ocean and its isolation from the atmospheric carbon cycle for longer timescales. Third, my simulations also indicate that OM sulphurization is important for the enhanced sequestration of organic carbon in marine sediments during OAE2. The modelled organic carbon concentrations at the seafloor are significantly increased by OM sulphurization, which would lead to elevated carbon burial in the sediments. Finally, it has been shown that the lack of an appropriate sediment representation in GENIE acutely hinders an improved analysis of the total effect of organic matter sulphurization. This has two causes: Firstly, the employed GENIE representation degrades all particulate species at the seafloor and therefore benthic chemical concentrations rise to very unrealistic values. Secondly, in order to quantify the importance of OM sulphurization for the generation of organic-carbon rich black-shales and to improve the feedback mechanisms within the global carbon cycle an appropriate representation of the sediments is indispensable. To close this gap we implemented a new numerical encapsulation of the sediments that includes a mechanistic description of organic carbon degradation. The new model has been successfully tested for different bottom water oxygen concentrations and organic matter compositions and highlights the importance of these factors for the preservation of organic carbon in marine sediments.

## References

Archer, D. (1994). Effect of deep-sea sedimentary calcite preservation on atmospheric co2 concentration. *Nature*, 367.

Archer, D., Kheshgi, H., and Maier-Reimer, E. (1997). Multiple timescales for neutralization of fossil fuel CO2. *Geophysical Research Letters*, 24(4):405–408.

Arndt, S., Goossen, N., and Hülse, D. (2013a). A new, efficient steady state diagentic model for global biogeochemical and earth system models. *in preperation*.

Arndt, S., Hetzel, A., and Brumsack, H.-J. (2009). Evolution of organic matter degradation in cretaceous black shales inferred from authigenic barite: A reaction-transport model. *Geochimica et Cosmochimica Acta*, 73(7):2000–2022.

Arndt, S., Joergensen, B., LaRowe, D., Middelburg, J., Pancost, R., and Regnier, P. (2013b). Quantifying the degradation of organic matter in marine sediments: A review and synthesis. *Earth-Science Reviews*, 123:53–86.

Arthur, M., Dean, W., Pollastro, R., Scholle, P., and Claypool, G. (1985). A comparative geochemical study of two transgressive pelagic limestone units, cretaceous western interior basin, us. *Fine-Grained Deposits and Biofacies of the Cretaceous Western Interior Seaway: Evidence of Cyclic Sedimentary Processes: SEPM, Field Trip Guidebook*, (4):16–27.

Arthur, M. A. and Sageman, B. B. (1994). Marine shales: depositional mechanisms and environments of ancient deposits. *Annual Review of Earth and Planetary Sciences*, 22:499–551.

Arthur, M. A., Schlanger, S. O., and Jenkyns, H. C. (1987). The cenomanian-turonian oceanic anoxic event, II. palaeoceanographic controls on organic-matter production and preservation. *Geological Society, London, Special Publications*, 26(1):401–420.

Barron, E. J. and Peterson, W. H. (1990). Mid-cretaceous ocean circulation: Results from model sensitivity studies. *Paleoceanography*, 5(3):319–337.

Berner, R. A. (1980). *Early Diagenesis: A Theoretical Approach*. Princeton University Press.

Berner, R. A. (1999). A new look at the long-term carbon cycle. *GSA Today*, 9(11):1–6.

Berner, R. A. and Caldeira, K. (1997). The need for mass balance and feedback in the geochemical carbon cycle. *Geology*, 25(10):955–956.

Berner, R. A., Canfield, D. E., et al. (1989). A new model for atmospheric oxygen over phanerozoic time. *Am. J. Sci*, 289(4):333–361.

Bice, K. L., Birgel, D., Meyers, P. A., Dahl, K. A., Hinrichs, K. U., and Norris, R. D. (2006). A multiple proxy and model study of cretaceous upper ocean temperatures and atmospheric CO2 concentrations. *Paleoceanography*, 21(2).

Blair, N. E. and Aller, R. C. (2012). The fate of terrestrial organic carbon in the marine environment. *Annual Review of Marine Science*, 4(1):401–423.

Boudreau, B. P. (1986). Mathematics of tracer mixing in sediments; i, spatially-dependent, diffusive mixing. *American Journal of Science*, 286(3):161–198.

Boudreau, B. P. (1997). *Diagenetic models and their implementation*, volume 505. Springer Berlin.

Boudreau, B. P. and Ruddick, B. R. (1991). On a reactive continuum representation of organic matter diagenesis.

Boyd, P. and Trull, T. (2007). Understanding the export of biogenic particles in oceanic waters: Is there consensus? *Progress in Oceanography*, 72(4):276–312.

Brovkin, V., Bendtsen, J., Claussen, M., Ganopolski, A., Kubatzki, C., Petoukhov, V., and Andreev, A. (2002). Carbon cycle, vegetation, and climate dynamics in the holocene: Experiments with the CLIMBER-2 model. *Global Biogeochemical Cycles*, 16(4):86–1–86–20.

Burdige, D. J. (2007). Preservation of organic matter in marine sediments: Controls, mechanisms, and an imbalance in sediment organic carbon budgets? *Chemical Reviews*, 107(2):467–485.

Canfield, D. E. (1993). Organic matter oxidation in marine sediments. *Interactions of C, N, P and S biogeochemical Cycles and Global Change*, 14:333–363.

Canfield, D. E. (1994). Factors influencing organic carbon preservation in marine sediments. *Chemical Geology*, 114(3–4):315–329.

Canfield, D. E. and Thamdrup, B. (2005). *Aquatic Geomicrobiology*. Gulf Professional Publishing.

Cao, L., Eby, M., Ridgwell, A., Caldeira, K., Archer, D., Ishida, A., Joos, F., Matsumoto, K., Mikolajewicz, U., Mouchet, A., Orr, J. C., Plattner, G.-K., Schlitzer, R., Tokos, K., Totterdell, I., Tschumi, T., Yamanaka, Y., and Yool, A. (2009). The role of ocean transport in the uptake of anthropogenic CO2. *Biogeosciences*, 6(3):375–390.

Caroline P. Slomp, Eric H.G. Epping, Willem Helder, and Wim Van Raaphorst (1996). A key role for iron-bound phosphorus in authigenic apatite formation in north atlantic continental platform sediments. *Journal of Marine Research*, 54(6):1179–1205.

Christensen, J. H., Carter, T. R., Rummukainen, M., and Amanatidis, G. (2007). Evaluating the performance and utility of regional climate models: the PRUDENCE project. *Climatic Change*, 81(1):1–6. Cited by 0337.

Crowley, T. J. (2000). Causes of climate change over the past 1000 years. *Science*, 289(5477):270–277.

Dale, A. W., BrÃ$\frac{1}{4}$chert, V., Alperin, M., and Regnier, P. (2009). An integrated sulfur isotope model for namibian shelf sediments. *Geochimica et Cosmochimica Acta*, 73(7):1924–1944.

Damsté, J. S. S., van Bentum, E. C., Reichart, G.-J., Pross, J., and Schouten, S. (2010). A CO2 decrease-driven cooling and increased latitudinal temperature gradient during the mid-cretaceous oceanic anoxic event 2. *Earth and Planetary Science Letters*, 293(1–2):97–103.

de Graciansky, P. C., Deroo, G., Herbin, J. P., Montadert, L., Müller, C., Schaaf, A., and Sigal, J. (1984). Ocean-wide stagnation episode in the late cretaceous. *Nature*, 308(5957):346–349.

Delaney, M. L. (1998). Phosphorus accumulation in marine sediments and the oceanic phosphorus cycle. *Global Biogeochemical Cycles*, 12(4):563–572.

Demaison, G. and Moore, G. (1980). Anoxic environments and oil source bed genesis. *Organic Geochemistry*, 2(1):9–31.

Donnadieu, Y., Pierrehumbert, R., Jacob, R., and Fluteau, F. (2006). Modelling the primary control of paleogeography on cretaceous climate. *Earth and Planetary Science Letters*, 248(1–2):426–437.

Edwards, N. R. and Marsh, R. (2005). Uncertainties due to transport-parameter sensitivity in an efficient 3-d ocean-climate model. *Climate Dynamics*, 24(4):415–433.

Emerson, S. (1985). Organic carbon preservation in marine sediments. *The Carbon Cycle and Atmospheric CO: Natural Variations Archean to Present*, pages 78–87.

Emerson, S. and Hedges, J. I. (1988). Processes controlling the organic carbon content of open ocean sediments. *Paleoceanography*, 3(5):621–634.

Eppley, R. (1985). Citation classic - temperature and phytoplankton growth in the sea. *Current Contents/Agriculture Biology & Environmental Sciences*, (37):1063–1085. WOS:A1985APZ5200001.

Erbacher, J., Huber, B. T., Norris, R. D., and Markey, M. (2001). Increased thermohaline stratification as a possible cause for an ocean anoxic event in the cretaceous period. *Nature*, 409(6818):325–327.

Falkowski, P., Scholes, R. J., Boyle, E., Canadell, J., Canfield, D., Elser, J., Gruber, N., Hibbard, K., Högberg, P., Linder, S., Mackenzie, F. T., Iii, B. M., Pedersen, T., Rosenthal, Y., Seitzinger, S., Smetacek, V., and Steffen, W. (2000). The global carbon cycle: A test of our knowledge of earth as a system. *Science*, 290(5490):291–296.

Falkowski, P. G., Barber, R. T., and Smetacek, V. (1998). Biogeochemical controls and feedbacks on ocean primary production. *Science*, 281(5374):200–206.

Field, C. B., Behrenfeld, M. J., Randerson, J. T., and Falkowski, P. (1998). Primary production of the biosphere: Integrating terrestrial and oceanic components. *Science*, 281(5374):237–240.

Forster, A., Schouten, S., Moriya, K., Wilson, P. A., and Damsté, J. S. S. (2007). Tropical warming and intermittent cooling during the Cenomanian/Turonian oceanic anoxic event 2: Sea surface temperature records from the equatorial atlantic. *Paleoceanography*, 22(1).

Froelich, P., Klinkhammer, G., Bender, M., Luedtke, N., Heath, G., Cullen, D., Dauphin, P., Hammond, D., Hartman, B., and Maynard, V. (1979). Early oxidation of organic matter in pelagic sediments of the eastern equatorial atlantic: suboxic diagenesis. *Geochimica et Cosmochimica Acta*, 43(7):1075–1090.

Goodwin, P., Williams, R. G., Ridgwell, A., and Follows, M. J. (2009). Climate sensitivity to the carbon cycle modulated by past and future changes in ocean chemistry. *Nature Geoscience*, 2(2):145–150.

Gypens, N., Lancelot, C., and Soetaert, K. (2008). Simple parameterisations for describing n and p diagenetic processes: Application in the north sea. *Progress in Oceanography*, 76(1):89–110.

Handoh, I. C. and Lenton, T. M. (2003). Periodic mid-cretaceous oceanic anoxic events linked by oscillations of the phosphorus and oxygen biogeochemical cycles. *Global Biogeochemical Cycles*, 17(4).

Hansen, J., Johnson, D., Lacis, A., Lebedeff, S., Lee, P., Rind, D., and Russell, G. (1981). Climate impact of increasing atmospheric carbon dioxide. *Science*, 213(4511):957–966.

Hartnett, H. E., Keil, R. G., Hedges, J. I., and Devol, A. H. (1998). Influence of oxygen exposure time on organic carbon preservation in continental margin sediments. *Nature*, 391(6667):572–575.

Hay, W. W. (2011). Can humans force a return to a cretaceous climate? *Sedimentary Geology*, 235(1–2):5–26.

Hebting, Y., Schaeffer, P., Behrens, A., Adam, P., Schmitt, G., Schneckenburger, P., Bernasconi, S. M., and Albrecht, P. (2006). Biomarker evidence for a major preservation pathway of sedimentary organic carbon. *Science*, 312(5780):1627–1631.

Hedges, J. I. and Keil, R. G. (1995). Sedimentary organic matter preservation: an assessment and speculative synthesis. *Marine Chemistry*, 49(2–3):81–115.

Henrichs, S. M. and Reeburgh, W. S. (1987). Anaerobic mineralization of marine sediment organic matter: Rates and the role of anaerobic processes in the oceanic carbon economy. *Geomicrobiology Journal*, 5(3–4):191–237.

Honjo, S., Manganini, S. J., Krishfield, R. A., and Francois, R. (2008). Particulate organic carbon fluxes to the ocean interior and factors controlling the biological pump: A synthesis of global sediment trap programs since 1983. *Progress in Oceanography*, 76(3):217–285.

Howarth, R. W. (1988). Nutrient limitation of net primary production in marine ecosystems. *Annual Review of Ecology and Systematics*, 19:89–110.

Hulth, S., Aller, R. C., and Gilbert, F. (1999). Coupled anoxic nitrification/manganese reduction in marine sediments. *Geochimica et Cosmochimica Acta*, 63(1):49–66.

Jenkyns, H. C. (2010). Geochemistry of oceanic anoxic events. *Geochemistry, Geophysics, Geosystems*, 11(3).

Jenkyns, H. C., Forster, A., Schouten, S., and Damsté, J. S. S. (2004). High temperatures in the late cretaceous arctic ocean. *Nature*, 432(7019):888–892.

Johnson Ibach, L. E. (1982). Relationship between sedimentation rate and total organic carbon content in ancient marine sediments. *Am. Assoc. Pet. Geol., Bull.; (United States)*, 66.

Kolonic, S., Sinninghe Damsté, J. S., Böttcher, M. E., Kuypers, M. M. M., Kuhnt, W., Beckmann, B., Scheeder, G., and Wagner, T. (2002). Geochemical characterization of Cenomanian/Turonian black shales from the tarfaya basin (sw morocco). *Journal of Petroleum Geology*, 25(3):325–350.

Krom, M. D. and Berner, R. A. (1980). Adsorption of phosphate in anoxic marine sediments. *Limnol. Oceanogr*, 25(5):797–806.

Kump, L. R., Brantley, S. L., and Arthur, M. A. (2000). Chemical weathering, atmospheric CO2, and climate. *Annual Review of Earth and Planetary Sciences*, 28(1):611–667.

Kuroda, J., Ogawa, N. O., Tanimizu, M., Coffin, M. F., Tokuyama, H., Kitazato, H., and Ohkouchi, N. (2007). Contemporaneous massive subaerial volcanism and late cretaceous oceanic anoxic event 2. *Earth and Planetary Science Letters*, 256(1–2):211–223.

Kuypers, M. M. M., Pancost, R. D., Nijenhuis, I. A., and Sinninghe Damsté, J. S. (2002). Enhanced productivity led to increased organic carbon burial in the euxinic north atlantic basin during the late cenomanian oceanic anoxic event. *Paleoceanography*, 17(4).

Lancelot, C. and Billen, G. (1985). Carbon-nitrogen relationships in nutrient metabolism of coastal marine ecosystems. *Advances in aquatic microbiology*, 3:263–321.

LaRowe, D. E. and Van Cappellen, P. (2011). Degradation of natural organic matter: A thermodynamic analysis. *Geochimica et Cosmochimica Acta*, 75(8):2030–2042.

Lovelock, J. (2003). Gaia: The living earth. *Nature*, 426(6968):769–770.

Mackenzie, F. T., Lerman, A., and Andersson, A. J. (2004). Past and present of sediment and carbon biogeochemical cycling models. *Biogeosciences Discussions*, 1(1):27–85.

Mackenzie, F. T., Ver, L. M., Sabine, C., Lane, M., and Lerman, A. (1993). C, n, p, s global biogeochemical cycles and modeling of global change. *Interactions of C, N, P and S Biogeochemical Cycles and Global Change*, 4:1–61.

Martens, C. S., Haddad, R. I., and Chanton, J. P. (1992). Organic matter accumulation, remineralization, and burial in an anoxic coastal sediment. *Productivity, Accumulation, and Preservation of Organic Matter: Recent and Ancient Sediments*, pages 82–98.

Meyer, K. M. and Kump, L. R. (2008). Oceanic euxinia in earth history: Causes and consequences. *Annual Review of Earth and Planetary Sciences*, 36(1):251–288.

Meyers, S. R., Sageman, B. B., and Hinnov, L. A. (2001). Integrated quantitative stratigraphy of the cenomanian-turonian bridge creek limestone member using evolutive harmonic analysis and stratigraphic modeling. *Journal of Sedimentary Research*, 71(4):628–644.

Middelburg, J. J. (1989). A simple rate model for organic matter decomposition in marine sediments. *Geochimica et Cosmochimica Acta*, 53(7):1577–1581.

Middelburg, J. J. and Meysman, F. J. R. (2007). OCEAN SCIENCE: burial at sea. *Science*, 316(5829):1294–1295.

Middelburg, J. J., Soetaert, K., and Herman, P. M. (1997). Empirical relationships for use in global diagenetic models. *Deep Sea Research Part I: Oceanographic Research Papers*, 44(2):327–344.

Middelburg, J. J., Vlug, T., Jaco, F., and van der Nat, W. (1993). Organic matter mineralization in marine systems. *Global and Planetary Change*, 8(1–2):47–58.

Mitchell, J., Johns, T., Gregory, J., and Tett, S. (1995). *Climate response to increasing levels of greenhouse gases and sulphate aerosols*, volume 376.

Monteiro, F. M., Pancost, R. D., Ridgwell, A., and Donnadieu, Y. (2012). Nutrients as the dominant control on the spread of anoxia and euxinia across the cenomanian-turonian oceanic anoxic event (OAE2): model-data comparison. *Paleoceanography*, 27(4).

Moodley, L., Middelburg, J. J., Herman, P. M. J., Soetaert, K., and Lange, G. J. d. (2005). Oxygenation and organic-matter preservation in marine sediments: Direct experimental evidence from ancient organic carbon-rich deposits. *Geology*, 33(11):889–892.

Ozaki, K., Tajima, S., and Tajika, E. (2011). Conditions required for oceanic anoxia/euxinia: Constraints from a one-dimensional ocean biogeochemical cycle model. *Earth and Planetary Science Letters*, 304(1–2):270–279.

Paropkari, A. L., Prakash Babu, C., and Mascarenhas, A. (1992). A critical evaluation of depositional parameters controlling the variability of organic carbon in arabian sea sediments. *Marine Geology*, 107(3):213–226.

Pedersen, T. F. and Calvert, S. E. (1990). Anoxia vs. productivity: What controls the formation of organic-carbon-rich sediments and sedimentary rocks? (1). *AAPG Bulletin*, 74(4):454–466.

Petit, J.-R., Jouzel, J., Raynaud, D., Barkov, N., Barnola, J., Basile, I., Bender, M., Chappellaz, J., Davis, M., Delaygue, G., et al. (1999). Climate and atmospheric history of the past 420,000 years from the vostok ice core, antarctica. *Nature*, 399(6735):429–436.

Pogge von Strandmann, P. A. E., Jenkyns, H. C., and Woodfine, R. G. (2013). Lithium isotope evidence for enhanced weathering during oceanic anoxic event 2. *Nature Geoscience*, 6(8):668–672.

Poulsen, C. J., Barron, E. J., Arthur, M. A., and Peterson, W. H. (2001). Response of the mid-cretaceous global oceanic circulation to tectonic and CO2 forcings. *Paleoceanography*, 16(6):576–592.

Räisänen, J. (2007). How reliable are climate models? *Tellus A*, 59(1):2–29. Cited by 0168.

Randall, D. A., Wood, R. A., Bony, S., Colman, R., Fichefet, T., Fyfe, J., Kattsov, V., Pitman, A., Shukla, J., Srinivasan, J., et al. (2007). Climate models and their evaluation. *Climate change*, 323.

Regnier, P., Dale, A., Arndt, S., LaRowe, D., Mogollon, J., and Van Cappellen, P. (2011). Quantitative analysis of anaerobic oxidation of methane (AOM) in marine sediments: A modeling perspective. *Earth-Science Reviews*, 106(1–2):105–130.

Reimers, C. E. (1998). Carbon cycle: Feedbacks from the sea floor. *Nature*, 391(6667):536–537.

Reimers, C. E., Jahnke, R. A., and McCorkle, D. C. (1992). Carbon fluxes and burial rates over the continental slope and rise off central california with implications for the global carbon cycle. *Global Biogeochemical Cycles*, 6(2):199–224.

Ridgwell, A. (2011). Evolution of the ocean's "biological pump". *Proceedings of the National Academy of Sciences*, 108(40):16485–16486.

Ridgwell, A. and Hargreaves, J. C. (2007). Regulation of atmospheric CO2 by deep-sea sediments in an earth system model. *Global Biogeochemical Cycles*, 21(2).

Ridgwell, A., Hargreaves, J. C., Edwards, N. R., Annan, J. D., Lenton, T. M., Marsh, R., Yool, A., and Watson, A. (2007). Marine geochemical data assimilation in an efficient earth system model of global biogeochemical cycling. *Biogeosciences*, 4(1):87–104.

Ridgwell, A. and Zeebe, R. E. (2005). The role of the global carbonate cycle in the regulation and evolution of the earth system. *Earth and Planetary Science Letters*, 234(3–4):299–315.

Sabine, C. L., Feely, R. A., Gruber, N., Key, R. M., Lee, K., Bullister, J. L., Wanninkhof, R., Wong, C. S., Wallace, D. W. R., Tilbrook, B., Millero, F. J., Peng, T.-H., Kozyr, A., Ono, T., and Rios, A. F. (2004). The oceanic sink for anthropogenic CO2. *Science*, 305(5682):367–371.

Sageman, B. B., Murphy, A. E., Werne, J. P., Ver Straeten, C. A., Hollander, D. J., and Lyons, T. W. (2003). A tale of shales: the relative roles of production, decomposition, and dilution in the accumulation of organic-rich strata, Middle-Upper Devonian, Appalachian basin. *Chemical Geology*, 195(1–4):229–273.

Sarmiento, J., Dunne, J., and Armstrong, R. (2004). Do we now understand the ocean's biological pump? *US JGOFS News*, 12(4):1–5.

Sarmiento, J. and Toggweiler, J. (1984). A new model for the role of the oceans in determining atmospheric pco 2. *Nature*, 308(5960):621–624.

Sarmiento, J. L. and Gruber, N. (2006). *Ocean biogeochemical dynamics*, volume 1015. Princeton University Press Princeton.

Sarmiento, J. L., Herbert, T. D., and Toggweiler, J. R. (1988). Causes of anoxia in the world ocean. *Global Biogeochemical Cycles*, 2(2):115–128.

Schlanger, S., Jenkyns, H., et al. (1976). Cretaceous oceanic anoxic events: causes and consequences. *Geologie en mijnbouw*, 55(3-4):179–184.

Schlanger, S. O., Arthur, M. A., Jenkyns, H. C., and Scholle, P. A. (1987). The cenomanian-turonian oceanic anoxic event, i. stratigraphy and distribution of organic carbon-rich beds and the marine Î´13C excursion. *Geological Society, London, Special Publications*, 26(1):371–399.

Scholle, P. A. and Arthur, M. A. (1980). Carbon isotope fluctuations in cretaceous pelagic limestones: Potential stratigraphic and petroleum exploration tool. *Am. Assoc. Pet. Geol. Bull.; (United States)*, 64:1.

Siegenthaler, U. and Sarmiento, J. (1993). Atmospheric carbon dioxide and the ocean. *Nature*, 365(6442):119–125.

Sigman, D. and Haug, G. (2003). The biological pump in the past. In *Treatise on Geochemistry*, pages 491–528. Elsevier.

Sigman, D. M. and Boyle, E. A. (2000). Glacial/interglacial variations in atmospheric carbon dioxide. *Nature*, 407(6806):859–869.

Sinninghe Damsté, J. S. and De Leeuw, J. W. (1990). Analysis, structure and geochemical significance of organically-bound sulphur in the geosphere: State of the art and future research. *Organic Geochemistry*, 16(4–6):1077–1101.

Sinninghe Damsté, J. S., Eglinton, T. I., De Leeuw, J. W., and Schenck, P. (1989a). Organic sulphur in macromolecular sedimentary organic matter: I. structure and origin of sulphur-containing moieties in kerogen, asphaltenes and coal as revealed by flash pyrolysis. *Geochimica et Cosmochimica Acta*, 53(4):873–889.

Sinninghe Damsté, J. S., Kok, M. D., Köster, J., and Schouten, S. (1998). Sulfurized carbohydrates: an important sedimentary sink for organic carbon? *Earth and Planetary Science Letters*, 164(1–2):7–13.

Sinninghe Damsté, J. S. and Köster, J. (1998). A euxinic southern north atlantic ocean during the Cenomanian/Turonian oceanic anoxic event. *Earth and Planetary Science Letters*, 158(3–4):165–173.

Sinninghe Damsté, J. S., Rijpstra, W. C., Kock-van Dalen, A., De Leeuw, J. W., and Schenck, P. (1989b). Quenching of labile functionalised lipids by inorganic sulphur species: Evidence for the formation of sedimentary organic sulphur compounds at the early stages of diagenesis. *Geochimica et Cosmochimica Acta*, 53(6):1343–1355.

Slomp, C., Malschaert, J., and Van Raaphorst, W. (1998). The role of adsorption in sediment-water exchange of phosphate in north sea continental margin sediments. *Limnology and Oceanography*, 43(5):832–846.

Slomp, C. P., Epping, E. H. G., Helder, W., and Raaphorst, W. V. (1996). A key role for iron-bound phosphorus in authigenic apatite formation in north atlantic continental platform sediments. *Journal of Marine Research*, 54(6):1179–1205.

Smith, S. (1984). Phosphorus versus nitrogen limitation in the marine environment. *LIMNOLOGY*.

Solomon, S., Qin, D., Manning, M., Chen, Z., Marquis, M., Averyt, K., Tignor, M., and Miller, H. (2007). Climate change 2007: The physical science basis. *Contribution of working group I to the fourth assessment report of the intergovernmental panel on climate change*.

Stein, R., Rullkotter, J., and Welte, D. (1986). Accumulation of organic-carbon-rich sediments in the late jurassic and cretaceous atlantic-ocean - a synthesis. *Chemical Geology*, 56(1–2):1–32.

Stone, P. H. and Risbey, J. S. (1990). On the limitations of general circulation climate models. *Geophysical Research Letters*, 17(12):2173–2176.

Thullner, M., Dale, A. W., and Regnier, P. (2009). Global-scale quantification of mineralization pathways in marine sediments: A reaction-transport modeling approach. *Geochemistry, Geophysics, Geosystems*, 10(10).

Toth, D. J. and Lerman, A. (1977). Organic matter reactivity and sedimentation rates in the ocean. *American Journal of Science*, 277(4):465–485.

Trabucho-Alexandre, J., Tuenter, E., Henstra, G. A., van der Zwan, K. J., van de Wal, R. S. W., Dijkstra, H. A., and de Boer, P. L. (2010). The mid-cretaceous north atlantic nutrient trap: Black shales and OAEs. *Paleoceanography*, 25.

Tromp, T., Van Cappellen, P., and Key, R. (1995). A global model for the early diagenesis of organic carbon and organic phosphorus in marine sediments. *Geochimica et Cosmochimica Acta*, 59(7):1259–1284.

Tyson, R. (2001). Sedimentation rate, dilution, preservation and total organic carbon: some results of a modelling study. *Organic Geochemistry*, 32(2):333–339.

Tyson, R. V. and Pearson, T. H. (1991). Modern and ancient continental shelf anoxia: an overview. *Geological Society, London, Special Publications*, 58(1):1–24.

Valdes, P. (2011). Built for stability. *Nature Geoscience*, 4(7):414–416.

Volk, T. and Hoffert, M. I. (1985). Ocean carbon pumps: Analysis of relative strengths and efficiencies in ocean-driven atmospheric co2 changes. *The Carbon Cycle and Atmospheric CO2: Natural Variations Archean to Present, Geophys. Monogr. Ser*, 32:99–110.

Wagner, T., Wallmann, K., Herrle, J. O., Hofmann, P., and Stuesser, I. (2007). Consequences of moderate similar to 25,000 yr lasting emission of light CO2 into the mid-cretaceous ocean. *Earth and Planetary Science Letters*, 259(1–2):200–211. WOS:000248637700017.

Wallmann, K., Aloisi, G., Haeckel, M., Obzhirov, A., Pavlova, G., and Tishchenko, P. (2006). Kinetics of organic matter degradation, microbial methane generation, and gas hydrate formation in anoxic marine sediments. *Geochimica et Cosmochimica Acta*, 70(15):3905–3927.

Werne, J. P., Hollander, D. J., Behrens, A., Schaeffer, P., Albrecht, P., and Sinninghe Damste, J. S. (2000). Timing of early diagenetic sulfurization of organic matter: a precursor-product relationship in holocene sediments of the anoxic cariaco basin, venezuela. *Geochimica et Cosmochimica Acta*, 64(10):1741–1751.

Werne, J. P., Lyons, T. W., Hollander, D. J., Schouten, S., Hopmans, E. C., and Sinninghe Damste, J. S. (2008). Investigating pathways of diagenetic organic matter sulfurization using compound-specific sulfur isotope analysis. *Geochimica et Cosmochimica Acta*, 72(14):3489–3502.

Wilson, P. A. and Norris, R. D. (2001). Warm tropical ocean surface and global anoxia during the mid-cretaceous period. *Nature*, 412(6845):425–429.

Zeebe, R. E. (2011). Where are you heading earth? *Nature Geoscience*, 4(7):416–417.

# Appendix

## A OM sulphurization

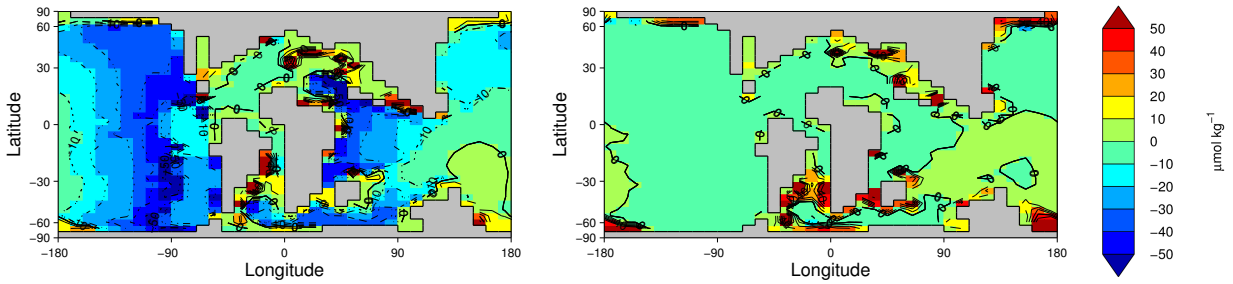


(a) (b)

Figure A.1: Anomaly plots of bottom water $O_2$ concentration as discussed in Section 3.1.2. SULPHURIZATION minus REFERENZ scenario for before (a) and during (b) OAE2. All values in $\mu mol\ kg^{-1}$.

# B Benthic Model

The differential equations for organic matter, oxygen, sulfate and hydrogen sulfide in the different sediment layers, the boundary conditions and the general solution.

## B.1 Organic matter

We model two fractions of OM ($C_{0i}$, (i=1,2) POC concentration at SWI) with different degradation rate constants ($k_i$) and we consider a bioturbation depth ($z_{bio}$), hence we need to implement two conservation equations.

Steady-state advection-diffusion-reaction (ADR) diagenetic equations (for $i = 1, 2$)

$$\frac{\partial C_{1i}}{\partial t} = DC\frac{\partial^2 C_{1i}}{\partial z^2} - w\frac{\partial C_{1i}}{\partial z} - k_i C_{1i} \qquad \text{1. Layer: } (z < z_{bio}) \tag{3}$$

$$\frac{\partial C_{2i}}{\partial t} = -w\frac{\partial C_{2i}}{\partial z} - k_i C_{2i} \qquad \text{2. Layer: } (z \geqq z_{bio}) \tag{4}$$

The ODEs (3, 4) have the following general solutions:

$$\begin{aligned} C_{1i}(z) &= A_{1i} \cdot exp(a_{1i}z) + B_{1i} \cdot exp(b_{1i}z) && \text{1. Layer: } (z < z_{bio}) \\ &\overset{(8)}{=} A_{1i} \cdot [exp(a_{1i}z) - exp(b_{1i}z)] + C_{0i} \cdot exp(b_{1i}z) && (5) \end{aligned}$$

$$C_{2i}(z) = A_{2i} \cdot exp(a_{2i}z) \qquad \text{2. Layer: } (z \geqq z_{bio}) \tag{6}$$

where

$$a_{1i} = \frac{w - \sqrt{w^2 + 4DC \cdot k_i}}{2DC}, \quad b_{1i} = \frac{w + \sqrt{w^2 + 4DC \cdot k_i}}{2DC}, \quad a_{2i} = \frac{-k_i}{w} \tag{7}$$

The integration constants $A_{1i},\ B_{1i},\ A_{2i}$ are derived by assuming the following **boundary conditions**:

1. Known concentration at the sediment-water interface ($z = 0$):

$$C_{0i} = A_{1i} + B_{1i} \iff B_{1i} = C_{0i} - A_{1i} \tag{8}$$

2. Concentrations are the same at boundary depth $z = z_{bio}$:

$$\begin{aligned} C_{1i}(z_{bio}) &= C_{2i}(z_{bio}) \\ A_{1i} \cdot exp(a_{1i}z_{bio}) + B_{1i} \cdot exp(b_{1i}z_{bio}) &= A_{2i} \cdot exp(a_{2i}z_{bio}) \\ A_{2i} &= \frac{A_{1i} \cdot exp(a_{1i}z_{bio}) + B_{1i} \cdot exp(b_{1i}z_{bio})}{exp(a_{2i}z_{bio})} \\ &= \frac{A_{1i} \cdot (exp(a_{1i}z_{bio}) - exp(b_{1i}z_{bio})) + C_{0i} \cdot exp(b_{1i}z_{bio})}{exp(a_{2i}z_{bio})} \end{aligned}$$

3. Diffusive term is zero at boundary depth $z = z_{bio}$:

$$DC \cdot \frac{\partial C_{1i}}{\partial z}(z_{bio}) = 0$$
$$A_{1i}a_{1i} \cdot exp(a_{1i}z_{bio}) + B_{1i}b_{1i} \cdot exp(b_{1i}z_{bio}) = 0$$
$$A_{1i} = -\frac{(C_{01}b_{1i} \cdot exp(b_{1i}z_{bio}))}{(a_{1i} \cdot exp(a_{1i}z_{bio}) - b_{1i} \cdot exp(b_{1i}z_{bio}))}$$

## B.2 Oxygen

### 1. Case ($z_{ox} < z_{bio}$):

**Oxic layer:** The oxygen diagenetic equation (where $i = 1, 2$ are the two TOC fractions). Organic matter mineralization consumes oxygen, with a fixed O:C ratio (3rd term), and the nitrification of 1 mol ammonium consumes 2 mol of oxygen (4th term):

$$\begin{aligned}
\frac{\partial O_2}{\partial t} &= D^1_{O_2}\frac{\partial^2 O_2}{\partial z^2} - w\frac{\partial O_2}{\partial z} - \frac{1-\phi}{\phi}OC \cdot \sum_i k_i C_{1i}(z) - 2 \cdot \gamma_{NH_4}\frac{1-\phi}{\phi} \cdot \sum_i NC_i k_i C_{1i}(z) \\
&= D^1_{O_2}\frac{\partial^2 O_2}{\partial z^2} - w\frac{\partial O_2}{\partial z} - \frac{1-\phi}{\phi}\sum_i k_i \cdot [OC + 2\gamma NC_i] \cdot C_{1i}(z) \\
&\overset{(3)}{=} D^1_{O_2}\frac{\partial^2 O_2}{\partial z^2} - w\frac{\partial O_2}{\partial z} - \frac{1-\phi}{\phi}\sum_i k_i \cdot [OC + 2\gamma NC_i] \cdot \Big(A_{1i} \cdot [exp(a_{1i}z) - exp(b_{1i}z)] + C_{0i} \cdot exp(b_{1i}z)\Big) \\
&= D^1_{O_2}\frac{\partial^2 O_2}{\partial z^2} - w\frac{\partial O_2}{\partial z} - \frac{1-\phi}{\phi}\sum_i k_i \cdot [OC + 2\gamma NC_i] \cdot \Big(A_{1i} \cdot exp(a_{1i}z) - A_{1i} \cdot exp(b_{1i}z)] + C_{0i} \cdot exp(b_{1i}z)\Big)
\end{aligned} \tag{9}$$

For the diagenetic equation (9) the general solution is given by:

$$\begin{aligned}
O_2(z) \quad &= A_{O_2} + B_{O_2} \cdot \exp(b_{O_2}z) + \frac{1-\phi}{\phi}\sum_i \frac{k_i \cdot (OC + 2\gamma NC_i) \cdot A_{1i}}{D^1_{O_2}(-a_{1i})^2 - w \cdot (-a_{1i})} \cdot \exp(a_{1i}z) \\
&\quad - \frac{1-\phi}{\phi}\sum_i \frac{k_i \cdot (OC + 2\gamma NC_i) \cdot A_{1i}}{D^1_{O_2}(-b_{1i})^2 - w \cdot (-b_{1i})} \cdot \exp(b_{1i}z) \\
&\quad + \frac{1-\phi}{\phi}\sum_i \frac{k_i \cdot (OC + 2\gamma NC_i) \cdot C_{0i}}{D^1_{O_2}(-b_{1i})^2 - w \cdot (-b_{1i})} \cdot \exp(b_{1i}z) \\
&:= A_{O_2} + B_{O_2} \cdot \exp(b_{O_2}z) + \sum_i \Phi^I_{1,i} \cdot \exp(a_{1i}z) + \sum_i \Phi^{II}_{1,i} \cdot \exp(b_{1i}z) + \sum_i \Phi^{III}_{1,i} \cdot \exp(b_{1i}z)
\end{aligned} \tag{10}$$

where

$$b_{O_2} = \frac{w + \sqrt{w^2 + 4D^1_{O_2} \cdot k_{O_2}}}{2D^1_{O_2}} = \frac{w}{D^1_{O_2}}$$

$$\Phi^I_{1,i} = \frac{1-\phi}{\phi} \cdot \frac{k_i \cdot (OC + 2\gamma NC_i) \cdot A_{1i}}{D^1_{O_2}(-a_{1i})^2 - w \cdot (-a_{1i})} \tag{11}$$

$$\Phi^{II}_{1,i} = -\frac{1-\phi}{\phi} \cdot \frac{k_i \cdot (OC + 2\gamma NC_i) \cdot A_{1i}}{D^1_{O_2}(-b_{1i})^2 - w \cdot (-b_{1i})} \tag{12}$$

$$\Phi^{III}_{1,i} = \frac{1-\phi}{\phi} \cdot \frac{k_i \cdot (OC + 2\gamma NC_i) \cdot C_{0i}}{D^1_{O_2}(-b_{1i})^2 - w \cdot (-b_{1i})} \tag{13}$$

The integration constants $A_{O_2},\ B_{O_2}$ can be determined using the **boundary conditions**:

1. Oxygen concentration at SWI is $O_2^0$:

$$\begin{aligned} O_2^0 &= O_2(0) \\ O_2^0 &\overset{(10)}{=} A_{O_2} + B_{O_2} + \sum_i \Phi_{1,i}^I + \sum_i \Phi_{1,i}^{II} + \sum_i \Phi_{1,i}^{III} \\ A_{O_2} &= O_2^0 - B_{O_2} - \Big( \sum_i \Phi_{1,i}^I + \sum_i \Phi_{1,i}^{II} + \sum_i \Phi_{1,i}^{III} \Big) \end{aligned} \tag{14}$$

2. Oxygen concentration at oxic-anoxic boundary ($z_{ox}$) is zero:

$$0 \overset{(10)}{=} A_{O_2} + B_{O_2} \cdot \exp(b_{O_2} z_{ox}) + \sum_i \Phi_{1,i}^I \cdot \exp(a_{1i} z_{ox}) + \sum_i \Phi_{1,i}^{II} \cdot \exp(b_{1i} z_{ox}) + \sum_i \Phi_{1,i}^{III} \cdot \exp(b_{1i} z_{ox}) \tag{15}$$

using (14) and regrouping the equation gives:

$$\begin{aligned} B_{O_2} = \Big( -O_2^0 + \sum_i \Big( \Phi_{1,i}^I + \Phi_{1,i}^{II} + \Phi_{1,i}^{III} \Big) \\ - \Big( \sum_i \Phi_{1,i}^I \cdot \exp(a_{1i} z_{ox}) + \sum_i \Phi_{1,i}^{II} \cdot \exp(b_{1i} z_{ox}) + \sum_i \Phi_{1,i}^{III} \cdot \exp(b_{1i} z_{ox}) \Big) \Big) \frac{1}{\exp(b_{O_2} z_{ox}) - 1} \end{aligned} \tag{16}$$

In order to evaluate equation (16) one has to calculate the oxygen penetration depth ($z_{ox}$) using the following boundary condition:

3. **Find oxygen penetration depth:** At $z = z_{ox}$ the reduced substances produced during mineralization in the anoxic layer below diffuse into the oxic layer and are re-oxidised at the oxic-anoxic interface. Therefore finding the root of the following equation gives us $z_{ox}$:

$$- D_{O_2}^1 \frac{\partial O_2}{\partial z}(z_{ox}) = F_{O_2}(z_{ox}) \tag{17}$$

For a first calculation of $z_{ox}$ we assume $z_{ox} < z_{bio}$ and can therefore use (10) to get

$$\begin{aligned} - D_{O_2}^1 \Big( B_{O_2} b_{O_2} \cdot \exp(b_{O_2} z_{ox}) + \sum_i a_{1i} \Phi_{1,i}^I \cdot \exp(a_{1i} z_{ox}) + \sum_i b_{1i} \Phi_{1,i}^{II} \cdot \exp(b_{1i} z_{ox}) + \sum_i b_{1i} \Phi_{1,i}^{III} \cdot \exp(b_{1i} z_{ox}) \Big) \\ = F_{O_2}(z_{ox}) \end{aligned} \tag{18}$$

As we assume $z_{ox} < z_{bio}$ the magnitude of oxygen-flux at the oxic-anoxic boundary layer ($F_{O_2}(z_{ox})$) due to diffusive flux of reduced substances from the anoxic layer can be expressed as

$$F_{O_2}(z_{ox}) = \frac{1-\phi}{\phi} \int_{z_{ox}}^{z_{bio}} \sum_i k_i (OC + 2\gamma NC_i) \cdot C_{1i}(z) dz + \frac{1-\phi}{\phi} \int_{z_{bio}}^{\infty} \sum_i k_i (OC + 2\gamma NC_i) \cdot C_{2i}(z) dz \tag{19}$$

substituting this into (18) gives us

$$
\begin{aligned}
&- D^1_{O_2}\left(B_{O_2}b_{O_2}\cdot\exp(b_{O_2}z_{ox}) + \sum_i a_{1i}\Phi^I_{1,i}\cdot\exp(a_{1i}z_{ox}) + \sum_i b_{1i}\Phi^{II}_{1,i}\cdot\exp(b_{1i}z_{ox}) + \sum_i b_{1i}\Phi^{III}_{1,i}\cdot\exp(b_{1i}z_{ox})\right)\\
&= \frac{1-\phi}{\phi}\int_{z_{ox}}^{z_{bio}}\sum_i k_i(OC+2\gamma NC_i)\cdot C_{1i}(z)dz + \frac{1-\phi}{\phi}\int_{z_{bio}}^{\infty}\sum_i k_i(OC+2\gamma NC_i)\cdot C_{2i}(z)dz
\end{aligned}
\tag{20}
$$

We can evaluate $z_{ox}$ as the root of equation (20) by using (16), (5) and (6) to substitute $B_{O_2}$, $C_{1i}(z)$ and $C_{2i}(z)$ and by calculating the value of the integrals.

**2. Case ($z_{bio} \leq z_{ox}$):**

Steady-state advection-diffusion-reaction (ADR) diagenetic equations:

$$
\frac{\partial O_2^I}{\partial t} = D^1_{O_2}\frac{\partial^2 O_2^I}{\partial z^2} - w\frac{\partial O_2^I}{\partial z} - \frac{1-\phi}{\phi}\sum_i k_i\cdot[OC+2\gamma NC_i]\cdot C_{1i}(z) \qquad \text{1. Layer } (z \leq z_{bio}) \tag{21}
$$

$$
\frac{\partial O_2^{II}}{\partial t} = D^2_{O_2}\frac{\partial^2 O_2^{II}}{\partial z^2} - w\frac{\partial O_2^{II}}{\partial z} - \frac{1-\phi}{\phi}\sum_i k_i\cdot[OC+2\gamma NC_i]\cdot C_{2i}(z) \qquad \text{2. Layer } (z_{bio} < z < z_{ox}) \tag{22}
$$

The general solutions are given by

1. Layer ($z \leq z_{bio}$): (with $\Phi^I_{1,i},\ \Phi^{II}_{1,i},\ \Phi^{III}_{1,i}$ defined as (11)-(13))

$$
O_2^I(z) = A^1_{O_2} + B^1_{O_2}\cdot\exp(b^1_{O_2}z) + \sum_i \Phi^I_{1,i}\cdot\exp(a_{1i}z) + \sum_i \Phi^{II}_{1,i}\cdot\exp(b_{1i}z) + \sum_i \Phi^{III}_{1,i}\cdot\exp(b_{1i}z) \tag{23}
$$

2. Layer ($z_{bio} < z < z_{ox}$)

$$
O_2^{II}(z) = A^2_{O_2} + B^2_{O_2}\cdot\exp(b^2_{O_2}z) + \sum_i \Phi^I_{i,2}\cdot\exp(a_{2i}z) \tag{24}
$$

where

$$
\Phi^I_{i,2} := \frac{1-\phi}{\phi}\cdot\frac{k_i\cdot(OC+2\gamma NC_i)\cdot A_{2i}}{D^2_{O_2}(-a_{2i})^2 - w\cdot(-a_{2i})} \qquad \text{, analogue to (9) - (10)} \tag{25}
$$

with $b^1_{O_2} = \frac{w}{D^1_{O_2}}$ and $b^2_{O_2} = \frac{w}{D^2_{O_2}}$.

The four integration constants can be determined using the following **boundary conditions**:

1. Oxygen concentration at SWI is $O_2^0$:

$$
O_2^I(0) = O_2^0
$$

2. Oxygen concentration at $z_{bio}$ boundary is equal:

$$O_2^I(z_{bio}) = O_2^{II}(z_{bio})$$

3. Diffusive flux at $z_{bio}$ boundary is equal:

$$D_{O_2}^1 \cdot \frac{\partial O_2^I}{\partial z}(z_{bio}) = D_{O_2}^2 \cdot \frac{\partial O_2^{II}}{\partial z}(z_{bio})$$

4. Oxygen concentration at $z_{ox}$ is zero:

$$O_2^{II}(z_{ox}) = 0$$

5. Recalculate oxygen penetration depth!
   analogue to 1. Case

**Anoxic layer:**

$$O_2(z) = 0 \tag{26}$$

## B.3 Sulfate ($SO_4$)

**Special Case 0 ($z_{ox} = z_{bio} = z_{NO_3} = 0$):**

Steady-state advection-diffusion-reaction (ADR) diagenetic equations:

$$\begin{aligned} \frac{\partial SO_4^I}{\partial t} &= D_{SO_4}^2 \frac{\partial^2 SO_4^I}{\partial z^2} - w\frac{\partial SO_4^I}{\partial z} - \frac{1-\phi}{\phi}\sum_i SO_4C \cdot k_i \cdot C_{2i}(z) \qquad \text{1. Layer } (0 < z \leq z_{SO_4}) \\ &= D_{SO_4}^2 \frac{\partial^2 SO_4^I}{\partial z^2} - w\frac{\partial SO_4^I}{\partial z} - \frac{1-\phi}{\phi}\sum_i SO_4C \cdot k_i \cdot A_{2i} \cdot exp(a_{2i}z) \end{aligned} \tag{27}$$

**The general solution is**
1. Layer $(0 < z \leq z_{SO_4})$:

$$SO_4^I(z) = A_{SO_4} + B_{SO_4} \cdot \exp(b_{SO_4}z) + \frac{1-\phi}{\phi}\sum_i \frac{SO_4C \cdot k_i \cdot A_{2i}}{D_{SO_4}^2(-a_{2i})^2 - w \cdot (-a_{2i})} \cdot \exp(a_{2i}z) \tag{28}$$

with

$$b_{SO_4} = \frac{w}{D_{SO_4}^2}$$

The integration constants $A_{SO_4}$, $B_{SO_4}$ can be determined using the following **boundary conditions**:

1. Sulfate concentration at SWI is $SO_4^0$:

$$SO_4^I(0) = SO_4^0$$

2. Sulfate concentration at $z_{SO_4}$ is zero (or saturation constant $Sat_{SO_4}$):

$$SO_4^I(z_{SO_4}) = Sat_{SO_4}$$

3. Calculate $z_{SO_4}$: At $z_{SO_4}$ methane produced in layer below gets re-oxidised, hence must equal the diffusive flux of $SO_4$:

$$-D^2_{SO_4}\frac{\partial SO_4^I}{\partial z}(z_{SO_4}) = F_{SO_4}(z_{SO_4}) = \frac{1-\phi}{\phi}\int_{z_{SO_4}}^{\infty}\sum_i k_i \cdot MC_i \cdot C_{2i}(z)dz$$

**Case 1 ($z_{ox} < z_{bio}$):**

**Subcase $z_{bio} < z_{NO_3}$:**

Steady-state advection-diffusion-reaction (ADR) diagenetic equations:

$$\frac{\partial SO_4^I}{\partial t} = D^1_{SO_4}\frac{\partial^2 SO_4^I}{\partial z^2} - w\frac{\partial SO_4^I}{\partial z} \qquad \text{1. Layer } (z \le z_{ox}) \tag{29}$$

$$\frac{\partial SO_4^{II}}{\partial t} = D^1_{SO_4}\frac{\partial^2 SO_4^{II}}{\partial z^2} - w\frac{\partial SO_4^{II}}{\partial z} \qquad \text{2. Layer } (z_{ox} < z \le z_{bio}) \tag{30}$$

$$\frac{\partial SO_4^{III}}{\partial t} = D^2_{SO_4}\frac{\partial^2 SO_4^{III}}{\partial z^2} - w\frac{\partial SO_4^{III}}{\partial z} \qquad \text{3. Layer } (z_{bio} < z \le z_{NO_3}) \tag{31}$$

$$\begin{aligned}\frac{\partial SO_4^{IV}}{\partial t} &= D^2_{SO_4}\frac{\partial^2 SO_4^{IV}}{\partial z^2} - w\frac{\partial SO_4^{IV}}{\partial z} - \frac{1-\phi}{\phi}\sum_i SO_4C \cdot k_i \cdot C_{2i}(z) \qquad \text{4. Layer } (z_{NO_3} < z)\\ &= D^2_{SO_4}\frac{\partial^2 SO_4^{IV}}{\partial z^2} - w\frac{\partial SO_4^{IV}}{\partial z} - \frac{1-\phi}{\phi}\sum_i SO_4C \cdot k_i \cdot A_{2i} \cdot exp(a_{2i}z)\end{aligned} \tag{32}$$

**The general solutions are**

1. Layer ($z \le z_{ox}$):

$$SO_4^I(z) = A^1_{SO_4} + B^1_{SO_4} \cdot \exp(b^1_{SO_4}z) \tag{33}$$

2. Layer ($z_{ox} < z \le z_{bio}$):

$$SO_4^{II}(z) = A^2_{SO_4} + B^2_{SO_4} \cdot \exp(b^2_{SO_4}z) \tag{34}$$

3. Layer ($z_{bio} < z \le z_{NO_3}$)

$$SO_4^{III}(z) = A^3_{SO_4} + B^3_{SO_4} \cdot \exp(b^3_{SO_4}z) \tag{35}$$

4. Layer ($z_{NO_3} < z$)

$$SO_4^{IV}(z) = A^4_{SO_4} + B^4_{SO_4} \cdot \exp(b^4_{SO_4}z) + \frac{1-\phi}{\phi}\sum_i \frac{SO_4C \cdot k_i \cdot A_{2i}}{D^2_{SO_4}(-a_{2i})^2 - w \cdot (-a_{2i})} \cdot \exp(a_{2i}z) \tag{36}$$

with

$$b^1_{SO_4} = \frac{w}{D^1_{SO_4}}, \quad b^2_{SO_4} = \frac{w}{D^1_{SO_4}}, \quad b^3_{SO_4} = \frac{w}{D^2_{SO_4}}, \quad b^4_{SO_4} = \frac{w}{D^2_{SO_4}}. \tag{37}$$

The eight integration constants $A^j_{SO_4},\ B^j_{SO_4}$ $(j \in \{1,2,3,4\})$ can be determined using the following **boundary conditions**:

1. Sulfate concentration at SWI is $SO_4^0$:

$$SO_4^I(0) = SO_4^0$$

2. Sulfate concentration at $z_{ox}$ boundary is equal:

$$SO_4^I(z_{ox}) = SO_4^{II}(z_{ox})$$

3. Diffusive flux at $z_{ox}$ boundary is equal, considering the flux of reduced substances ($H_2S$) from $z_{NO_3} \leq z \leq z_{SO_4}$:

$$-D^1_{SO_4} \cdot \frac{\partial SO_4^I}{\partial z}(z_{ox}) + \frac{\gamma_{H_2S}}{\phi} \cdot F_{H_2S} = -D^1_{SO_4} \cdot \frac{\partial SO_4^{II}}{\partial z}(z_{ox})$$

where

$$F_{H_2S} = \frac{1-\phi}{\phi} \int_{z_{NO_3}}^{z_{SO_4}} \sum_i k_i \cdot SO_4C \cdot C_{2i}(z)dz$$

4. Sulfate concentration at $z_{bio}$ boundary is equal:

$$SO_4^{II}(z_{bio}) = SO_4^{III}(z_{bio})$$

5. Diffusive flux at $z_{bio}$ boundary is equal:

$$D^1_{SO_4} \cdot \frac{\partial SO_4^{II}}{\partial z}(z_{bio}) = D^2_{SO_4} \cdot \frac{\partial SO_4^{III}}{\partial z}(z_{bio})$$

6. Sulfate concentration at $z_{NO_3}$ boundary is equal:

$$SO_4^{III}(z_{NO_3}) = SO_4^{IV}(z_{NO_3})$$

7. Diffusive flux at $z_{NO_3}$ boundary is equal:

$$D^2_{SO_4} \cdot \frac{\partial SO_4^{III}}{\partial z}(z_{NO_3}) = D^2_{SO_4} \cdot \frac{\partial SO_4^{IV}}{\partial z}(z_{NO_3})$$

8. Sulfate concentration at $z_{SO_4}$ is zero (or saturation constant $Sat_{SO_4}$):

$$SO_4^{IV}(z_{SO_4}) = Sat_{SO_4}$$

9. Calculate $z_{SO_4}$: At $z_{SO_4}$ methane produced in layer below gets re-oxidised, hence must equal the diffusive flux of $SO_4$:

$$-D^2_{SO_4} \frac{\partial SO_4^{IV}}{\partial z}(z_{SO_4}) = F_{SO_4}(z_{SO_4}) = \frac{1-\phi}{\phi} \int_{z_{SO_4}}^{\infty} \sum_i k_i \cdot MC_i \cdot C_{2i}(z)dz$$

**Subcase $z_{NO_3} < z_{bio}$:**

Steady-state advection-diffusion-reaction (ADR) diagenetic equations:

1. Layer ($z \leq z_{ox}$)

$$\frac{\partial SO_4^I}{\partial t} = D^1_{SO_4}\frac{\partial^2 SO_4^I}{\partial z^2} - w\frac{\partial SO_4^I}{\partial z} \tag{38}$$

2. Layer ($z_{ox} < z \leq z_{NO_3} < z_{bio}$)

$$\frac{\partial SO_4^{II}}{\partial t} = D^1_{SO_4}\frac{\partial^2 SO_4^{II}}{\partial z^2} - w\frac{\partial SO_4^{II}}{\partial z} \tag{39}$$

3. Layer ($z_{NO_3} < z \leq z_{bio}$)

$$\begin{aligned}\frac{\partial SO_4^{III}}{\partial t} =& D^1_{SO_4}\frac{\partial^2 SO_4^{III}}{\partial z^2} - w\frac{\partial SO_4^{III}}{\partial z} - \frac{1-\phi}{\phi}\sum_i SO_4C \cdot k_i \cdot C_{1i}(z) \\ =& D^1_{SO_4}\frac{\partial^2 SO_4^{III}}{\partial z^2} - w\frac{\partial SO_4^{III}}{\partial z} \\ & - \frac{1-\phi}{\phi}\sum_i SO_4C \cdot k_i \cdot \Big(A_{1i} \cdot [exp(a_{1i}z) - exp(b_{1i}z)] + C_{0i} \cdot exp(b_{1i}z)\Big)\end{aligned} \tag{40}$$

4. Layer ($z_{bio} < z$)

$$\begin{aligned}\frac{\partial SO_4^{IV}}{\partial t} =& D^2_{SO_4}\frac{\partial^2 SO_4^{IV}}{\partial z^2} - w\frac{\partial SO_4^{IV}}{\partial z} - \frac{1-\phi}{\phi}\sum_i SO_4C \cdot k_i \cdot C_{2i}(z) \\ =& D^2_{SO_4}\frac{\partial^2 SO_4^{IV}}{\partial z^2} - w\frac{\partial SO_4^{IV}}{\partial z} - \frac{1-\phi}{\phi}\sum_i SO_4C \cdot k_i \cdot A_{2i} \cdot exp(a_{2i}z)\end{aligned} \tag{41}$$

**The general solutions are**

1. Layer ($z \leq z_{ox}$):

$$SO_4^I(z) \quad = A^1_{SO_4} + B^1_{SO_4} \cdot \exp(b^1_{SO_4}z) \tag{42}$$

2. Layer ($z_{ox} < z \leq z_{NO_3} < z_{bio}$):

$$SO_4^{II}(z) \quad = A^2_{SO_4} + B^2_{SO_4} \cdot \exp(b^2_{SO_4}z) \tag{43}$$

3. Layer ($z_{NO_3} < z \leq z_{bio}$)

$$\begin{aligned} SO_4^{III}(z) \quad &= A^3_{SO_4} + B^3_{SO_4} \cdot \exp(b^3_{SO_4} z) + \frac{1-\phi}{\phi} \sum_i \frac{SO_4C \cdot k_i \cdot A_{1i}}{D^1_{SO_4}(-a_{1i})^2 - w \cdot (-a_{1i})} \cdot \exp(a_{1i} z) \\ &- \frac{1-\phi}{\phi} \sum_i \frac{SO_4C \cdot k_i \cdot A_{1i}}{D^1_{SO_4}(-b_{1i})^2 - w \cdot (-b_{1i})} \cdot \exp(b_{1i} z) \\ &+ \frac{1-\phi}{\phi} \sum_i \frac{SO_4C \cdot k_i \cdot C_{0i}}{D^1_{SO_4}(-b_{1i})^2 - w \cdot (-b_{1i})} \cdot \exp(b_{1i} z) \end{aligned}$$

4. Layer ($z_{bio} < z$)

$$SO_4^{IV}(z) \quad = A^4_{SO_4} + B^4_{SO_4} \cdot \exp(b^4_{SO_4} z) + \frac{1-\phi}{\phi} \sum_i \frac{SO_4C \cdot k_i \cdot A_{2i}}{D^2_{SO_4}(-a_{2i})^2 - w \cdot (-a_{2i})} \cdot \exp(a_{2i} z) \tag{44}$$

with

$$b^1_{SO_4} = \frac{w}{D^1_{SO_4}}, \quad b^2_{SO_4} = \frac{w}{D^1_{SO_4}}, \quad b^3_{SO_4} = \frac{w}{D^1_{SO_4}}, \quad b^4_{SO_4} = \frac{w}{D^2_{SO_4}}. \tag{45}$$

The eight integration constants $A^j_{SO_4}$, $B^j_{SO_4}$ ($j \in \{1,2,3,4\}$) can be determined using the following **boundary conditions**:

1. Sulfate concentration at SWI is $SO_4^0$:

$$SO_4^I(0) = SO_4^0$$

2. Sulfate concentration at $z_{ox}$ boundary is equal:

$$SO_4^I(z_{ox}) = SO_4^{II}(z_{ox})$$

3. Diffusive flux at $z_{ox}$ boundary is equal, considering the flux of reduced substances ($H_2S$) from $z_{NO_3} \leq z \leq z_{SO_4}$:

$$-D^1_{SO_4} \cdot \frac{\partial SO_4^I}{\partial z}(z_{ox}) + \frac{\gamma_{H_2S}}{\phi} \cdot F_{H_2S} = -D^1_{SO_4} \cdot \frac{\partial SO_4^{II}}{\partial z}(z_{ox})$$

where

$$F_{H_2S} = \frac{1-\phi}{\phi} \int_{z_{NO_3}}^{z_{bio}} \sum_i k_i \cdot SO_4C \cdot C_{1i}(z)dz + \frac{1-\phi}{\phi} \int_{z_{bio}}^{z_{z_{SO_4}}} \sum_i k_i \cdot SO_4C \cdot C_{2i}(z)dz$$

4. Sulfate concentration at $z_{bio}$ boundary is equal:

$$SO_4^{III}(z_{bio}) = SO_4^{IV}(z_{bio})$$

5. Diffusive flux at $z_{bio}$ boundary is equal:

$$D^1_{SO_4} \cdot \frac{\partial SO_4^{III}}{\partial z}(z_{bio}) = D^2_{SO_4} \cdot \frac{\partial SO_4^{IV}}{\partial z}(z_{bio})$$

6. Sulfate concentration at $z_{NO_3}$ boundary is equal:

$$SO_4^{II}(z_{NO_3}) = SO_4^{III}(z_{NO_3})$$

7. Diffusive flux at $z_{NO_3}$ boundary is equal:

$$D^1_{SO_4} \cdot \frac{\partial SO_4^{II}}{\partial z}(z_{NO_3}) = D^1_{SO_4} \cdot \frac{\partial SO_4^{III}}{\partial z}(z_{NO_3})$$

8. Sulfate concentration at $z_{SO_4}$ is zero (or saturation constant $Sat_{SO_4}$):

$$SO_4^{IV}(z_{SO_4}) = Sat_{SO_4}$$

9. Calculate $z_{SO_4}$: At $z_{SO_4}$ methane produced in layer below gets re-oxidised, hence must equal the diffusive flux of $SO_4$:

$$-D^2_{SO_4}\frac{\partial SO_4^{IV}}{\partial z}(z_{SO_4}) = F_{SO_4}(z_{SO_4}) = \frac{1-\phi}{\phi}\int_{z_{SO_4}}^{\infty}\sum_i k_i \cdot MC_i \cdot C_{2i}(z)dz$$

**Case 2 ($z_{bio} < z_{ox}$):**

Steady-state advection-diffusion-reaction (ADR) diagenetic equations:

$$\frac{\partial SO_4^I}{\partial t} = D^1_{SO_4}\frac{\partial^2 SO_4^I}{\partial z^2} - w\frac{\partial SO_4^I}{\partial z} \qquad \text{1. Layer } (z \le z_{bio}) \tag{46}$$

$$\frac{\partial SO_4^{II}}{\partial t} = D^2_{SO_4}\frac{\partial^2 SO_4^{II}}{\partial z^2} - w\frac{\partial SO_4^{II}}{\partial z} \qquad \text{2. Layer } (z_{bio} < z \le z_{ox}) \tag{47}$$

$$\frac{\partial SO_4^{III}}{\partial t} = D^2_{SO_4}\frac{\partial^2 SO_4^{III}}{\partial z^2} - w\frac{\partial SO_4^{III}}{\partial z} \qquad \text{3. Layer } (z_{bio} < z_{ox} < z \le z_{NO_3}) \tag{48}$$

$$\begin{aligned}\frac{\partial SO_4^{IV}}{\partial t} &= D^2_{SO_4}\frac{\partial^2 SO_4^{IV}}{\partial z^2} - w\frac{\partial SO_4^{IV}}{\partial z} - \frac{1-\phi}{\phi}\sum_i SO_4C \cdot k_i \cdot C_{2i}(z) \qquad \text{4. Layer } (z_{NO_3} < z)\\ &= D^2_{SO_4}\frac{\partial^2 SO_4^{IV}}{\partial z^2} - w\frac{\partial SO_4^{IV}}{\partial z} - \frac{1-\phi}{\phi}\sum_i SO_4C \cdot k_i \cdot A_{2i} \cdot exp(a_{2i}z)\end{aligned} \tag{49}$$

**The general solutions are**

1. Layer ($z \le z_{bio}$):

$$SO_4^I(z) = A^1_{SO_4} + B^1_{SO_4} \cdot \exp(b^1_{SO_4}z) \tag{50}$$

2. Layer ($z_{bio} < z \le z_{ox}$):

$$SO_4^{II}(z) = A^2_{SO_4} + B^2_{SO_4} \cdot \exp(b^2_{SO_4}z) \tag{51}$$

3. Layer ($z_{bio} < z_{ox} < z \leq z_{NO_3}$)

$$SO_4^{III}(z) = A^3_{SO_4} + B^3_{SO_4} \cdot \exp(b^3_{SO_4} z) \tag{52}$$

4. Layer ($z_{NO_3} < z$)

$$SO_4^{IV}(z) = A^4_{SO_4} + B^4_{SO_4} \cdot \exp(b^4_{SO_4} z) + \frac{1-\phi}{\phi} \sum_i \frac{SO_4C \cdot k_i \cdot A_{2i}}{D^2_{SO_4}(-a_{2i})^2 - w \cdot (-a_{2i})} \cdot \exp(a_{2i} z) \tag{53}$$

with

$$b^1_{SO_4} = \frac{w}{D^1_{SO_4}}, \quad b^2_{SO_4} = \frac{w}{D^2_{SO_4}}, \quad b^3_{SO_4} = \frac{w}{D^2_{SO_4}}, \quad b^4_{SO_4} = \frac{w}{D^2_{SO_4}}. \tag{54}$$

The eight integration constants $A^j_{SO_4}$, $B^j_{SO_4}$ ($j \in \{1,2,3,4\}$) can be determined using the following **boundary conditions**:

1. Sulfate concentration at SWI is $SO_4^0$:

$$SO_4^I(0) = SO_4^0$$

2. Sulfate concentration at $z_{bio}$ boundary is equal:

$$SO_4^I(z_{bio}) = SO_4^{II}(z_{bio})$$

3. Diffusive flux at $z_{bio}$ boundary is equal:

$$D^1_{SO_4} \cdot \frac{\partial SO_4^I}{\partial z}(z_{bio}) = D^2_{SO_4} \cdot \frac{\partial SO_4^{II}}{\partial z}(z_{bio})$$

4. Sulfate concentration at $z_{ox}$ boundary is equal:

$$SO_4^{II}(z_{ox}) = SO_4^{III}(z_{ox})$$

5. Diffusive flux at $z_{ox}$ boundary is equal, considering the flux of reduced substances ($H_2S$) from $z_{NO_3} \leq z \leq z_{SO_4}$:

$$-D^2_{SO_4} \cdot \frac{\partial SO_4^{II}}{\partial z}(z_{ox}) + \frac{\gamma_{H_2S}}{\phi} \cdot F_{H_2S} = -D^2_{SO_4} \cdot \frac{\partial SO_4^{III}}{\partial z}(z_{ox})$$

where

$$F_{H_2S} = \frac{1-\phi}{\phi} \int_{z_{NO_3}}^{z_{SO_4}} \sum_i k_i \cdot SO_4C \cdot C_{2i}(z) dz$$

6. Sulfate concentration at $z_{NO_3}$ boundary is equal:

$$SO_4^{III}(z_{NO_3}) = SO_4^{IV}(z_{NO_3})$$

7. Diffusive flux at $z_{NO_3}$ boundary is equal:

$$D^2_{SO_4} \cdot \frac{\partial SO_4^{III}}{\partial z}(z_{NO_3}) = D^2_{SO_4} \cdot \frac{\partial SO_4^{IV}}{\partial z}(z_{NO_3})$$

8. Sulfate concentration at $z_{SO_4}$ is zero (or saturation constant $Sat_{SO_4}$):

$$SO_4^{IV}(z_{SO_4}) = Sat_{SO_4}$$

9. Calculate $z_{SO_4}$: At $z_{SO_4}$ methane produced in layer below gets re-oxidised, hence must equal the diffusive flux of $SO_4$:

$$-D_{SO_4}^2 \frac{\partial SO_4^{IV}}{\partial z}(z_{SO_4}) = F_{SO_4}(z_{SO_4}) = \frac{1-\phi}{\phi} \int_{z_{SO_4}}^{\infty} \sum_i k_i \cdot MC_i \cdot C_{2i}(z) dz$$

## B.4 Hydrogen sulfide ($H_2S$)

**Special Case 0 ($z_{ox} = z_{bio} = z_{NO_3} = 0$):**

Steady-state advection-diffusion-reaction (ADR) diagenetic equations:

$$\begin{aligned} \frac{\partial H_2S^I}{\partial t} &= D_{H_2S}^2 \frac{\partial^2 H_2S^I}{\partial z^2} - w\frac{\partial H_2S^I}{\partial z} + \frac{1-\phi}{\phi}\sum_i SO_4C \cdot k_i \cdot C_{2i}(z) \qquad \text{1. Layer } (0 < z \leq z_{SO_4}) \\ &= D_{H_2S}^2 \frac{\partial^2 H_2S^I}{\partial z^2} - w\frac{\partial H_2S^I}{\partial z} + \frac{1-\phi}{\phi}\sum_i SO_4C \cdot k_i \cdot A_{2i} \cdot exp(a_{2i}z) \qquad (55) \\ \frac{\partial H_2S^{II}}{\partial t} &= D_{H_2S}^2 \frac{\partial^2 H_2S^{II}}{\partial z^2} - w\frac{\partial H_2S^{II}}{\partial z} \qquad \text{2. Layer } (z_{SO_4} < z \leq z_{inf}) \\ & \qquad (56) \end{aligned}$$

**The general solutions are**

1. Layer $(0 < z \leq z_{SO_4})$:

$$H_2S^I(z) = A_{H_2S}^I + B_{H_2S}^I \cdot \exp(b_{H_2S}z) - \frac{1-\phi}{\phi}\sum_i \frac{SO_4C \cdot k_i \cdot A_{2i}}{D_{H_2S}^2(-a_{2i})^2 - w \cdot (-a_{2i})} \cdot \exp(a_{2i}z) \qquad (57)$$

$$H_2S^{II}(z) = A_{H_2S}^{II} + B_{H_2S}^{II} \cdot \exp(b_{H_2S}z) \qquad (58)$$

with

$$b_{H_2S} = \frac{w}{D_{H_2S}^2}$$

The integration constants $A_{H_2S}^I,\ B_{H_2S}^I, A_{H_2S}^{II},\ B_{H_2S}^{II}$ can be determined using the following **boundary conditions**:

1. Sulfide concentration at SWI is $H_2S^0$:

$$H_2S^I(0) = H_2S^0$$

2. Sulfide concentration at $z_{SO_4}$ boundary is equal:

$$H_2S^I(z_{SO_4}) = H_2S^{II}(z_{SO_4})$$

3. Diffusive flux at $z_{SO_4}$ boundary is equal:

$$D_{H_2S}^2 \cdot \frac{\partial H_2S^I}{\partial z}(z_{SO_4}) = D_{H_2S}^2 \cdot \frac{\partial H_2S^{II}}{\partial z}(z_{SO_4})$$

4. Change in Sulfide flux at $z = \infty$ is zero:

$$\frac{\partial H_2S^{II}}{\partial z}(z) = 0$$

**Case 1 ($z_{ox} < z_{bio}$):**

**Subcase 1** $z_{ox} < z_{bio} < z_{NO_3}$**:**

Steady-state advection-diffusion-reaction (ADR) diagenetic equations:

$$\frac{\partial H_2S^I}{\partial t} = D^1_{H_2S}\frac{\partial^2 H_2S^I}{\partial z^2} - w\frac{\partial H_2S^I}{\partial z} \qquad \text{1. Layer } (z \le z_{ox}) \tag{59}$$

$$\frac{\partial H_2S^{II}}{\partial t} = D^1_{H_2S}\frac{\partial^2 H_2S^{II}}{\partial z^2} - w\frac{\partial H_2S^{II}}{\partial z} \qquad \text{2. Layer } (z_{ox} < z \le z_{bio}) \tag{60}$$

$$\frac{\partial H_2S^{III}}{\partial t} = D^2_{H_2S}\frac{\partial^2 H_2S^{III}}{\partial z^2} - w\frac{\partial H_2S^{III}}{\partial z} \qquad \text{3. Layer } (z_{bio} < z \le z_{NO_3}) \tag{61}$$

$$\begin{aligned}\frac{\partial H_2S^{IV}}{\partial t} &= D^2_{H_2S}\frac{\partial^2 H_2S^{IV}}{\partial z^2} - w\frac{\partial H_2S^{IV}}{\partial z} + \frac{1-\phi}{\phi}\sum_i SO_4C \cdot k_i \cdot C_{2i}(z) \qquad \text{4. Layer } (z_{NO_3} < z \le z_{SO_4}) \\ &= D^2_{H_2S}\frac{\partial^2 H_2S^{IV}}{\partial z^2} - w\frac{\partial H_2S^{IV}}{\partial z} + \frac{1-\phi}{\phi}\sum_i SO_4C \cdot k_i \cdot A_{2i} \cdot exp(a_{2i}z)\end{aligned} \tag{62}$$

$$\frac{\partial H_2S^V}{\partial t} = D^2_{H_2S}\frac{\partial^2 H_2S^V}{\partial z^2} - w\frac{\partial H_2S^V}{\partial z} \qquad \text{5. Layer } (z_{SO_4} < z \le z_{inf}) \tag{63}$$

**The general solutions are**

1. Layer ($z \le z_{ox}$):

$$H_2S^I(z) = A^1_{H_2S} + B^1_{H_2S} \cdot \exp(b^1_{H_2S}z) \tag{64}$$

2. Layer ($z_{ox} < z \le z_{bio}$):

$$H_2S^{II}(z) = A^2_{H_2S} + B^2_{H_2S} \cdot \exp(b^2_{H_2S}z) \tag{65}$$

3. Layer ($z_{bio} < z \le z_{NO_3}$)

$$H_2S^{III}(z) = A^3_{H_2S} + B^3_{H_2S} \cdot \exp(b^3_{H_2S}z) \tag{66}$$

4. Layer ($z_{NO_3} < z \le z_{SO_4}$)

$$H_2S^{IV}(z) = A^4_{H_2S} + B^4_{H_2S} \cdot \exp(b^4_{H_2S}z) - \frac{1-\phi}{\phi}\sum_i \frac{SO_4C \cdot k_i \cdot A_{2i}}{D^2_{H_2S}(-a_{2i})^2 - w \cdot (-a_{2i})} \cdot \exp(a_{2i}z) \tag{67}$$

5. Layer ($z_{SO_4} < z \leq z_{inf}$):

$$H_2S^V(z) = A^5_{H_2S} + B^5_{H_2S} \cdot \exp(b^5_{H_2S} z) \tag{68}$$

with

$$b^1_{H_2S} = \frac{w}{D^1_{H_2S}}, \quad b^2_{H_2S} = \frac{w}{D^1_{H_2S}}, \quad b^3_{H_2S} = \frac{w}{D^2_{H_2S}}, \quad b^4_{H_2S} = \frac{w}{D^2_{H_2S}}, \quad b^5_{H_2S} = \frac{w}{D^2_{H_2S}}. \tag{69}$$

The ten integration constants $A^j_{H_2S},\ B^j_{H_2S}$ ($j \in \{1,2,3,4,5\}$) can be determined using the following **boundary conditions**:

1. Sulfide concentration at SWI is $H_2S^0$:

$$H_2S^I(0) = H_2S^0$$

2. Sulfide concentration at $z_{ox}$ boundary is equal:

$$H_2S^I(z_{ox}) = H_2S^{II}(z_{ox})$$

3. Diffusive flux at $z_{ox}$ boundary is equal, considering the flux of reduced substances ($H_2S$) from $z_{NO_3} \leq z \leq z_{SO_4}$:

$$-D^1_{H_2S} \cdot \frac{\partial H_2S^I}{\partial z}(z_{ox}) - \frac{\gamma_{H_2S}}{\phi} \cdot F_{H_2S} = -D^1_{H_2S} \cdot \frac{\partial H_2S^{II}}{\partial z}(z_{ox})$$

   where

$$F_{H_2S} = \frac{1-\phi}{\phi} \int_{z_{NO_3}}^{z_{SO_4}} \sum_i k_i \cdot SO_4C \cdot C_{2i}(z) dz$$

4. Sulfide concentration at $z_{bio}$ boundary is equal:

$$H_2S^{II}(z_{bio}) = H_2S^{III}(z_{bio})$$

5. Diffusive flux at $z_{bio}$ boundary is equal:

$$D^1_{H_2S} \cdot \frac{\partial H_2S^{II}}{\partial z}(z_{bio}) = D^2_{H_2S} \cdot \frac{\partial H_2S^{III}}{\partial z}(z_{bio})$$

6. Sulfide concentration at $z_{NO_3}$ boundary is equal:

$$H_2S^{III}(z_{NO_3}) = H_2S^{IV}(z_{NO_3})$$

7. Diffusive flux at $z_{NO_3}$ boundary is equal:

$$D^2_{H_2S} \cdot \frac{\partial H_2S^{III}}{\partial z}(z_{NO_3}) = D^2_{H_2S} \cdot \frac{\partial H_2S^{IV}}{\partial z}(z_{NO_3})$$

8. Sulfide concentration at $z_{SO_4}$ boundary is equal:

$$H_2S^{IV}(z_{SO_4}) = H_2S^V(z_{SO_4})$$

9. Diffusive flux at $z_{SO_4}$ boundary is equal:

$$D^2_{H_2S} \cdot \frac{\partial H_2S^{IV}}{\partial z}(z_{SO_4}) = D^2_{H_2S} \cdot \frac{\partial H_2S^{V}}{\partial z}(z_{SO_4})$$

10. Change in Sulfide flux at $z = \infty$ is zero:

$$\frac{\partial H_2S^{V}}{\partial z}(z) = 0$$

**Subcase 2** $z_{NO_3} < z_{bio}$**:**

Steady-state advection-diffusion-reaction (ADR) diagenetic equations:

1. Layer $(z \leq z_{ox})$

$$\frac{\partial H_2S^{I}}{\partial t} = D^1_{H_2S}\frac{\partial^2 H_2S^{I}}{\partial z^2} - w\frac{\partial H_2S^{I}}{\partial z} \tag{70}$$

2. Layer $(z_{ox} < z \leq z_{NO_3} < z_{bio})$

$$\frac{\partial H_2S^{II}}{\partial t} = D^1_{H_2S}\frac{\partial^2 H_2S^{II}}{\partial z^2} - w\frac{\partial H_2S^{II}}{\partial z} \tag{71}$$

3. Layer $(z_{NO_3} < z \leq z_{bio})$

$$\begin{aligned}\frac{\partial H_2S^{III}}{\partial t} =& D^1_{H_2S}\frac{\partial^2 H_2S^{III}}{\partial z^2} - w\frac{\partial H_2S^{III}}{\partial z} + \frac{1-\phi}{\phi}\sum_i SO_4C \cdot k_i \cdot C_{1i}(z) \\ =& D^1_{H_2S}\frac{\partial^2 H_2S^{III}}{\partial z^2} - w\frac{\partial H_2S^{III}}{\partial z} \\ &+ \frac{1-\phi}{\phi}\sum_i SO_4C \cdot k_i \cdot \Big( A_{1i} \cdot [exp(a_{1i}z) - exp(b_{1i}z)] + C_{0i} \cdot exp(b_{1i}z) \Big)\end{aligned} \tag{72}$$

4. Layer $(z_{bio} < z \leq z_{SO_4})$

$$\begin{aligned}\frac{\partial H_2S^{IV}}{\partial t} =& D^2_{H_2S}\frac{\partial^2 H_2S^{IV}}{\partial z^2} - w\frac{\partial H_2S^{IV}}{\partial z} + \frac{1-\phi}{\phi}\sum_i SO_4C \cdot k_i \cdot C_{2i}(z) \\ =& D^2_{H_2S}\frac{\partial^2 H_2S^{IV}}{\partial z^2} - w\frac{\partial H_2S^{IV}}{\partial z} + \frac{1-\phi}{\phi}\sum_i SO_4C \cdot k_i \cdot A_{2i} \cdot exp(a_{2i}z)\end{aligned} \tag{73}$$

5. Layer $(z_{SO_4} < z \leq z_{inf})$

$$\frac{\partial H_2S^{V}}{\partial t} = D^2_{H_2S}\frac{\partial^2 H_2S^{V}}{\partial z^2} - w\frac{\partial H_2S^{V}}{\partial z} \tag{74}$$

**The general solutions are**

1. Layer ($z \leq z_{ox}$):

$$H_2S^I(z) \quad = A^1_{H_2S} + B^1_{H_2S} \cdot \exp(b^1_{H_2S} z) \tag{75}$$

2. Layer ($z_{ox} < z \leq z_{NO_3} < z_{bio}$):

$$H_2S^{II}(z) \quad = A^2_{H_2S} + B^2_{H_2S} \cdot \exp(b^2_{H_2S} z) \tag{76}$$

3. Layer ($z_{NO_3} < z \leq z_{bio}$)

$$\begin{aligned} H_2S^{III}(z) \quad = A^3_{H_2S} + B^3_{H_2S} \cdot \exp(b^3_{H_2S} z) &- \frac{1-\phi}{\phi} \sum_i \frac{SO_4C \cdot k_i \cdot A_{1i}}{D^1_{H_2S}(-a_{1i})^2 - w \cdot (-a_{1i})} \cdot \exp(a_{1i} z) \\ &+ \frac{1-\phi}{\phi} \sum_i \frac{SO_4C \cdot k_i \cdot A_{1i}}{D^1_{H_2S}(-b_{1i})^2 - w \cdot (-b_{1i})} \cdot \exp(b_{1i} z) \\ &- \frac{1-\phi}{\phi} \sum_i \frac{SO_4C \cdot k_i \cdot C_{0i}}{D^1_{H_2S}(-b_{1i})^2 - w \cdot (-b_{1i})} \cdot \exp(b_{1i} z) \end{aligned}$$

4. Layer ($z_{bio} < z \leq z_{SO_4}$)

$$H_2S^{IV}(z) \quad = A^4_{H_2S} + B^4_{H_2S} \cdot \exp(b^4_{H_2S} z) - \frac{1-\phi}{\phi} \sum_i \frac{SO_4C \cdot k_i \cdot A_{2i}}{D^2_{H_2S}(-a_{2i})^2 - w \cdot (-a_{2i})} \cdot \exp(a_{2i} z) \tag{77}$$

5. Layer ($z_{SO_4} < z \leq z_{inf}$):

$$H_2S^V(z) \quad = A^5_{H_2S} + B^5_{H_2S} \cdot \exp(b^5_{H_2S} z) \tag{78}$$

with

$$b^1_{H_2S} = \frac{w}{D^1_{H_2S}}, \quad b^2_{H_2S} = \frac{w}{D^1_{H_2S}}, \quad b^3_{H_2S} = \frac{w}{D^1_{H_2S}}, \quad b^4_{H_2S} = \frac{w}{D^2_{H_2S}}, \quad b^5_{H_2S} = \frac{w}{D^2_{H_2S}}. \tag{79}$$

The ten integration constants $A^j_{H_2S},\ B^j_{H_2S}$ ($j \in \{1,2,3,4,5\}$) can be determined using the following **boundary conditions**:

1. Sulfide concentration at SWI is $H_2S^0$:

$$H_2S^I(0) = H_2S^0$$

2. Sulfide concentration at $z_{ox}$ boundary is equal:

$$H_2S^I(z_{ox}) = H_2S^{II}(z_{ox})$$

3. Diffusive flux at $z_{ox}$ boundary is equal, considering the flux of reduced substances ($H_2S$) from $z_{NO_3} \leq z \leq z_{H_2S}$:

$$-D^1_{H_2S} \cdot \frac{\partial H_2S^I}{\partial z}(z_{ox}) - \frac{\gamma_{H_2S}}{\phi} \cdot F_{H_2S} = -D^1_{H_2S} \cdot \frac{\partial H_2S^{II}}{\partial z}(z_{ox})$$

where

$$F_{H_2S} = \frac{1-\phi}{\phi}\int_{z_{NO_3}}^{z_{bio}} \sum_i k_i \cdot SO_4C \cdot C_{1i}(z)dz + \frac{1-\phi}{\phi}\int_{z_{bio}}^{z_{SO_4}} \sum_i k_i \cdot SO_4C \cdot C_{2i}(z)dz$$

4. Sulfide concentration at $z_{bio}$ boundary is equal:

$$H_2S^{III}(z_{bio}) = H_2S^{IV}(z_{bio})$$

5. Diffusive flux at $z_{bio}$ boundary is equal:

$$D^1_{H_2S} \cdot \frac{\partial H_2S^{III}}{\partial z}(z_{bio}) = D^2_{H_2S} \cdot \frac{\partial H_2S^{IV}}{\partial z}(z_{bio})$$

6. Sulfide concentration at $z_{NO_3}$ boundary is equal:

$$H_2S^{II}(z_{NO_3}) = H_2S^{III}(z_{NO_3})$$

7. Diffusive flux at $z_{NO_3}$ boundary is equal:

$$D^1_{H_2S} \cdot \frac{\partial H_2S^{II}}{\partial z}(z_{NO_3}) = D^1_{H_2S} \cdot \frac{\partial H_2S^{III}}{\partial z}(z_{NO_3})$$

8. Sulfide concentration at $z_{SO_4}$ boundary is equal:

$$H_2S^{IV}(z_{SO_4}) = H_2S^{V}(z_{SO_4})$$

9. Diffusive flux at $z_{SO_4}$ boundary is equal:

$$D^2_{H_2S} \cdot \frac{\partial H_2S^{IV}}{\partial z}(z_{SO_4}) = D^2_{H_2S} \cdot \frac{\partial H_2S^{V}}{\partial z}(z_{SO_4})$$

10. Change in Sulfide flux at $z = \infty$ is zero:

$$\frac{\partial H_2S^{V}}{\partial z}(z) = 0$$

**Case 2 ($z_{bio} < z_{ox} < z_{NO3} < z_{SO4}$):**

Steady-state advection-diffusion-reaction (ADR) diagenetic equations:

1. Layer ($z \leq z_{bio}$)

$$\frac{\partial H_2S^I}{\partial t} = D^1_{H_2S}\frac{\partial^2 H_2S^I}{\partial z^2} - w\frac{\partial H_2S^I}{\partial z} \tag{80}$$

2. Layer ($z_{bio} < z \leq z_{ox}$)

$$\frac{\partial H_2S^{II}}{\partial t} = D^2_{H_2S}\frac{\partial^2 H_2S^{II}}{\partial z^2} - w\frac{\partial H_2S^{II}}{\partial z} \tag{81}$$

3. Layer ($z_{bio} < z_{ox} < z \leq z_{NO_3}$)

$$\frac{\partial H_2S^{III}}{\partial t} = D^2_{H_2S}\frac{\partial^2 H_2S^{III}}{\partial z^2} - w\frac{\partial H_2S^{III}}{\partial z} \tag{82}$$

4. Layer ($z_{NO_3} < z \leq z_{SO_4}$)

$$\begin{aligned}\frac{\partial H_2S^{IV}}{\partial t} &= D^2_{H_2S}\frac{\partial^2 H_2S^{IV}}{\partial z^2} - w\frac{\partial H_2S^{IV}}{\partial z} + \frac{1-\phi}{\phi}\sum_i SO_4C \cdot k_i \cdot C_{2i}(z) \\ &= D^2_{H_2S}\frac{\partial^2 H_2S^{IV}}{\partial z^2} - w\frac{\partial H_2S^{IV}}{\partial z} + \frac{1-\phi}{\phi}\sum_i SO_4C \cdot k_i \cdot A_{2i} \cdot exp(a_{2i}z)\end{aligned} \tag{83}$$

5. Layer ($z_{SO_4} < z \leq z_{inf}$)

$$\frac{\partial H_2S^{V}}{\partial t} = D^2_{H_2S}\frac{\partial^2 H_2S^{V}}{\partial z^2} - w\frac{\partial H_2S^{V}}{\partial z} \tag{84}$$

**The general solutions are**

1. Layer ($z \leq z_{bio}$):

$$H_2S^I(z) = A^1_{H_2S} + B^1_{H_2S} \cdot \exp(b^1_{H_2S}z) \tag{85}$$

2. Layer ($z_{bio} < z \leq z_{ox}$):

$$H_2S^{II}(z) = A^2_{H_2S} + B^2_{H_2S} \cdot \exp(b^2_{H_2S}z) \tag{86}$$

3. Layer ($z_{bio} < z_{ox} < z \leq z_{NO_3}$)

$$H_2S^{III}(z) = A^3_{H_2S} + B^3_{H_2S} \cdot \exp(b^3_{H_2S}z) \tag{87}$$

4. Layer ($z_{NO_3} < z \leq z_{SO_4}$)

$$H_2S^{IV}(z) = A^4_{H_2S} + B^4_{H_2S} \cdot \exp(b^4_{H_2S}z) - \frac{1-\phi}{\phi}\sum_i \frac{SO_4C \cdot k_i \cdot A_{2i}}{D^2_{H_2S}(-a_{2i})^2 - w \cdot (-a_{2i})} \cdot \exp(a_{2i}z) \tag{88}$$

5. Layer ($z_{SO_4} < z \leq z_{inf}$):

$$H_2S^V(z) = A^5_{H_2S} + B^5_{H_2S} \cdot \exp(b^5_{H_2S}z) \tag{89}$$

with

$$b^1_{H_2S} = \frac{w}{D^1_{H_2S}}, \quad b^2_{H_2S} = \frac{w}{D^2_{H_2S}}, \quad b^3_{H_2S} = \frac{w}{D^2_{H_2S}}, \quad b^4_{H_2S} = \frac{w}{D^2_{H_2S}}, \quad b^5_{H_2S} = \frac{w}{D^2_{H_2S}}. \tag{90}$$

The ten integration constants $A^j_{H_2S},\ B^j_{H_2S}$ ($j \in \{1,2,3,4,5\}$) can be determined using the following **boundary conditions**:

1. Sulfide concentration at SWI is $H_2S^0$:

$$H_2S^I(0) = H_2S^0$$

2. Sulfide concentration at $z_{bio}$ boundary is equal:

$$H_2S^I(z_{bio}) = H_2S^{II}(z_{bio})$$

3. Diffusive flux at $z_{bio}$ boundary is equal:

$$D^1_{H_2S} \cdot \frac{\partial H_2S^I}{\partial z}(z_{bio}) = D^2_{H_2S} \cdot \frac{\partial H_2S^{II}}{\partial z}(z_{bio})$$

4. Sulfide concentration at $z_{ox}$ boundary is equal:

$$H_2S^{II}(z_{ox}) = H_2S^{III}(z_{ox})$$

5. Diffusive flux at $z_{ox}$ boundary is equal, considering the flux of reduced substances ($H_2S$) from $z_{NO_3} \leq z \leq z_{H_2S}$:

$$-D^2_{H_2S} \cdot \frac{\partial H_2S^{II}}{\partial z}(z_{ox}) - \frac{\gamma_{H_2S}}{\phi} \cdot F_{H_2S} = -D^2_{H_2S} \cdot \frac{\partial H_2S^{III}}{\partial z}(z_{ox})$$

where

$$F_{H_2S} = \frac{1-\phi}{\phi} \int_{z_{NO_3}}^{z_{SO_4}} \sum_i k_i \cdot SO_4C \cdot C_{2i}(z)dz$$

6. Sulfide concentration at $z_{NO_3}$ boundary is equal:

$$H_2S^{III}(z_{NO_3}) = H_2S^{IV}(z_{NO_3})$$

7. Diffusive flux at $z_{NO_3}$ boundary is equal:

$$D^2_{H_2S} \cdot \frac{\partial H_2S^{III}}{\partial z}(z_{NO_3}) = D^2_{H_2S} \cdot \frac{\partial H_2S^{IV}}{\partial z}(z_{NO_3})$$

8. Sulfide concentration at $z_{SO_4}$ boundary is equal:

$$H_2S^{IV}(z_{SO_4}) = H_2S^{V}(z_{SO_4})$$

9. Diffusive flux at $z_{SO_4}$ boundary is equal:

$$D^2_{H_2S} \cdot \frac{\partial H_2S^{IV}}{\partial z}(z_{SO_4}) = D^2_{H_2S} \cdot \frac{\partial H_2S^{V}}{\partial z}(z_{SO_4})$$

10. Change in Sulfide flux at $z = \infty$ is zero:

$$\frac{\partial H_2S^V}{\partial z}(z) = 0$$

## B.5 $PO_4$ profiles

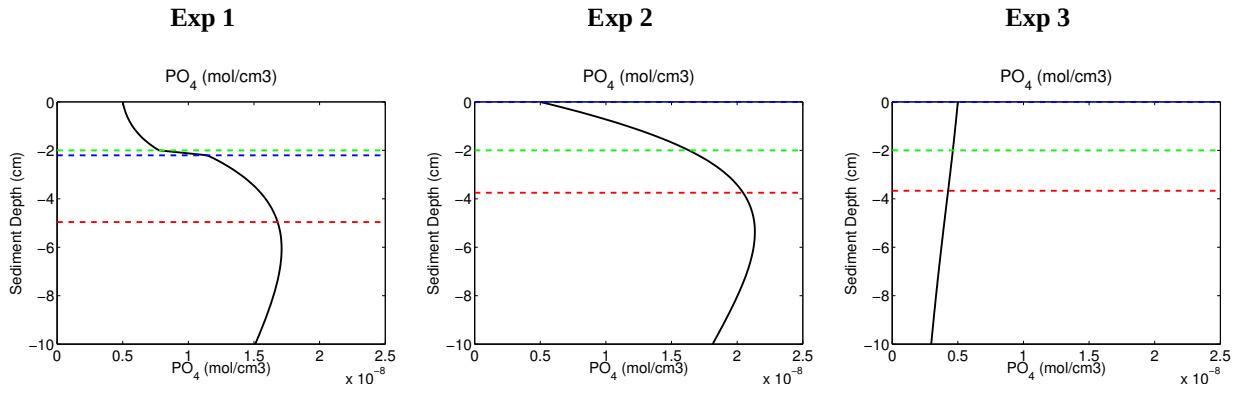


Figure B.1: Comparison of $PO_4$ profiles generated by our new analytic model under different organic matter loadings and oxygenation of the overlying bottom water. For the Experiment setup see Table 5. Dashed horizontal lines representing the different penetration depths ($z_{bio}$, $z_{ox}$ and $z_{SO_4}$).

## B.6 Parameter Table

Table 9: Variables and parameters

| Parameter/Variable | Unit | Value | Description |
|---|---|---|---|
| **sediment characteristics and transport parameters** | | | |
| $\rho_{sed}$ | $g/cm^3$ | 2.5 | sediment density |
| $w$ | $cm/yr$ | 0.03 | burial velocity/ sediment accumulation rate |
| $z_{bio}$ | cm | depending on water depth see Middelburg et al. (1997) | bioturbation depth |
| $D_{bio}$ | $cm^2/yr$ | 3 | bioturbation coefficient |
| $\phi$ | - | 0.8 | porosity |
| F | - | 3.0 | tortuosity |
| irrF | - | 1 | irrigation factor |
| dispF | - | $irrF \cdot \phi^{F-1.0}$ | dispersion factor |
| **bottom water concentrations** | | | |
| T | $°C$ | GENIE | Temperature |
| $C_{01}$ | $mol/cm^3$ | GENIE | frac 1 TOC concentration at SWI |
| $C_{02}$ | $mol/cm^3$ | GENIE | frac 2 TOC concentration at SWI |
| $O_2^0$ | $mol/cm^3$ | GENIE | $O_2$ concentration at SWI |
| $SO_4^0$ | $mol/cm^3$ | GENIE | $SO_4$ concentration at SWI |
| $H_2S^0$ | $mol/cm^3$ | GENIE | $H_2S$ concentration at SWI |
| **diffusion coefficients** | | | |
| DC | $cm^2/yr$ | $D_{bio}$ | POC diffusion coefficient |
| $qdispO_2$ | $cm^2/yr$ | 348.5750 | $O_2$ diffusion coefficient in water |
| $adispO_2$ | $cm^2/yr/°C$ | 14.0890 | $O_2$ linear coefficient for temp. dependence |
| $D^1_{O_2}$ | $cm^2/yr$ | $(qdispO_2 + adispO_2 \cdot T) \cdot dispF + Dbio$ | $O_2$ diffusion coefficient in bioturbated layer |
| $D^2_{O_2}$ | $cm^2/yr$ | $(qdispO_2 + adispO_2 \cdot T) \cdot dispF$ | $O_2$ diffusion coefficient in non-bioturbated layer |
| $qdispX$ | $cm^2/yr$ | 309.0528 | diffusion coefficient in water for $X \in \{SO_4,\ H_2S,\ PO_4\}$ |
| $adispX$ | $cm^2/yr/°C$ | 12.2640 | linear coefficient for temp. dependence for $X \in \{SO_4,\ H_2S,\ PO_4\}$ |
| $D^1_X$ | $cm^2/yr$ | $(qdispX + adispX \cdot T) \cdot dispF + Dbio$ | diffusion coefficient in bioturbated layer for $X \in \{SO_4,\ H_2S,\ PO_4\}$ |
| $D^2_X$ | $cm^2/yr$ | $(qdispX + adispX \cdot T) \cdot dispF$ | diffusion coefficient in non-bioturbated layer for $X \in \{SO_4,\ H_2S,\ PO_4\}$ |
| **rate constants** | | | |
| $k_1$ | $1/yr$ | GENIE | POC degradation rate constant refractory fraction |
| $k_2$ | $1/yr$ | GENIE | POC degradation rate constant labile fraction |